NASA Technical Memorandum 87623

Research and Technology

1985 Annual Report of the Langley Research Center

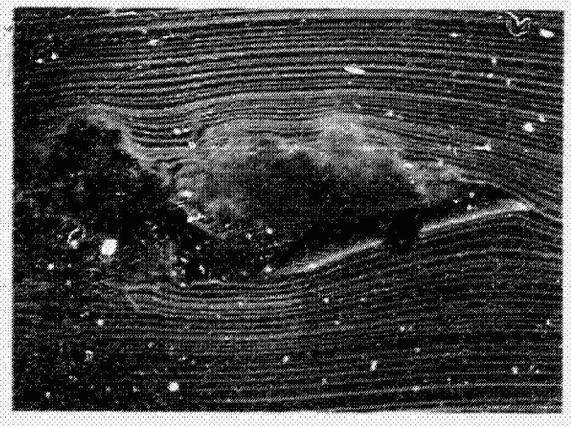

National Aeronautics and
Space Administration

NASA Technical Memorandum 87623

Research and Technology

1985 Annual Report of the Langley Research Center

NASA

National Aeronautics and
Space Administration

Langley Research Center
Hampton, Virginia 23665-5225

1985

Foreword

The role of the Langley Research Center is to engage in the basic and applied research necessary for the advancement of aeronautics and space flight, to generate new and advanced concepts for the accomplishment of related national goals, and to provide research advice, technological support, and assistance to other NASA installations, other government agencies, and industry. This Langley Research Center 1985 Annual Report on Research and Technology contains highlights of our major accomplishments and applications made during the past year. The highlights illustrate both the broad range of the research and technology activities at the Langley Research Center and the contributions of this work toward maintaining United States leadership in aeronautics and space research. For further information about the report contact Jerry C. South, Chief Scientist, Mail Stop 103, Langley Research Center, Hampton, Virginia 23665, (804) 865-3316.

Richard H. Petersen
Director

Availability Information

The NASA program office and the corresponding Agency-wide Research and Technology Objectives and Plans (RTOP) work breakdown structure are listed for each research and technology accomplishment in the Contents. OAST designates the Office of Aeronautics and Space Technology; OSSA designates the Office of Space Science and Applications; AA designates the Associate Administrator; OCE designates the Office of the Chief Engineer; OCP designates the Office of Commercial Programs; and OSF designates the Office of Space Flight.

For additional information on any summary, contact the individual identified with the highlight. This individual is generally either a member or a leader of the research group submitting the highlight. Commercial telephone users may dial the listed extension preceded by (804) 865. Telephone users with access to the Federal Telecommunications System (FTS) may dial the extension preceded by 928.

Contents

Electronics Directorate

Flight Systems Directorate

Space Directorate

Structures Directorate

Projects Directorate

Systems Engineering and Operations Directorate

Technology Utilization Program

Aeronautics Directorate

The Aeronautics Directorate is composed of approximately 300 scientists and engineers engaged in basic and applied research in the various aeronautics disciplines. The directorate is organized into three research divisions, which conduct aeronautical research to advance the state of the art throughout the complete aerodynamic speed range.

The Low-Speed Aerodynamics Division conducts research in the areas of basic fluid mechanics, low-speed aerodynamics, flight dynamics and flight management, aircraft operations, aviation safety, laminar flow control, and improved test methods. The division develops and validates theoretical aerodynamic methods for subsonic conditions and design methodology required to improve subsonic aerodynamic performance, stall/spin behavior, handling qualities, and takeoff and landing performance.

The Transonic Aerodynamics Division conducts research to advance the state of the art of transonic aircraft technology in the areas of fundamental aerodynamics, with particular emphasis on Reynolds number effects, laminar-flow concepts, stability and control, performance analysis, configuration concepts, and related aerodynamic phenomena. Particular areas of emphasis include improving the efficiency and reducing the fuel consumption of conventional jet transports, developing the technology for advanced military combat aircraft, developing theoretical and analytical methods for predicting aerodynamic characteristics in separated and transonic flows, developing advanced airfoils for low-speed and transonic aircraft and helicopters, and developing advanced experimental techniques, including advanced wall concepts, for transonic wind tunnels, cryogenic wind tunnel technology, and magnetic suspension and balance systems.

The High-Speed Aerodynamics Division conducts research to advance the state of the art for supersonic aircraft, hypersonic aircraft, and missiles, and to support the development of high-performance military aircraft, advanced cruise and tactical missiles, the Space Shuttle, and follow-on advanced space transportation systems. New analytical methods for design and analysis are derived and applied to advanced high-speed aircraft and missile concepts. Key experiments are conducted to validate the analytical methods, explore the potential of advanced concepts, and provide a data base for use by industry design teams. Conceptual designs for advanced high-speed vehicles are conceived and analyzed in order to determine the performance payoff from the application of advanced research results.

Reynolds Number Effects on F-106B Aircraft Vortex System

The purpose of this experiment was to use a vapor screen technique to determine the effect of Reynolds number on the vortex system generated from an F-106B aircraft. An onboard seeding system was developed to enable visualization of the vortex system without the interference of atmospheric water vapor. Techniques for utilization of this system as well as the light sheet and video systems also developed were refined in the Langley 30- by 60-Foot Tunnel on a half-airplane model of the F-106. The general arrangement of the system components on the aircraft is shown in the figure.

Two different types of maneuvers were performed in this flight program, 1-*g* constant altitude flight and 5-*g* spiral descent. Both types of night maneuvers showed that there were measurable Reynolds number effects on the vortex system details regarding core location and inner extent of the envelope. Reynolds number differences of only 7×10^6 for 1-*g* flight were sufficient to cause the delay of leading-edge vortex formation on this round-edged cambered wing from 17° to 19 ° angle of attack. (Note that lower Reynolds numbers occur at the higher altitudes.)

Comparison of the 5-*g* transonic maneuver and 1-*g* constant altitude flights at an angle of attack of 19° at 25,000 ft showed that the transonic maneuver produced a more inboard vortex system.

(John E. Lamar, 2601)

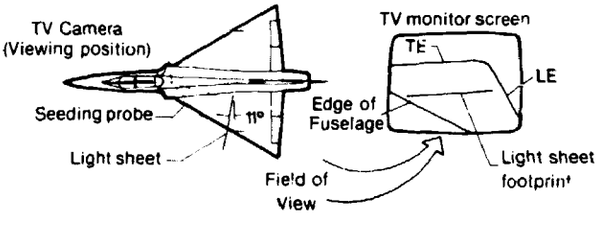

In-flight leading-edge vortex flow visualization on F-106B.

Computational Method for Transonic Wings

The availability of a new generation of supercomputers, coupled with recent advances in numerical algorithms, has opened up the possibility of computing transonic viscous flows over aircraft components of practical interest. Based on recent experience gained through two-dimensional viscous and three-dimensional inviscid flow calculations, a multistage Runge-Kutta type time-stepping scheme appears to be quite attractive. An effort has been initiated at Langley to extend this scheme to solve three-dimensional high Reynolds number viscous flows. Reynolds averaged thin-layer Navier-Stokes (TLNS) equations are used to describe the basic flow field, and turbulence closure is provided via an eddy viscosity model. Since the main emphasis is to obtain steady-state solutions for adiabatic flows, convergence is accelerated by the use of local time stepping and enthalpy damping. The computer code has been vectorized to achieve further computational efficiency.

An isolated ONERA M6 wing was selected as a test case to check the accuracy of present solutions. The computed pressure distributions at 45- and 65-percent spanwise locations are shown here along with the experimental data. Both the inviscid and viscous solutions were obtained on the same surface mesh with the same code. However, much finer normal spacing was employed in the viscous calculations to resolve extremely thin turbulent boundary layers developing on the wing surface.

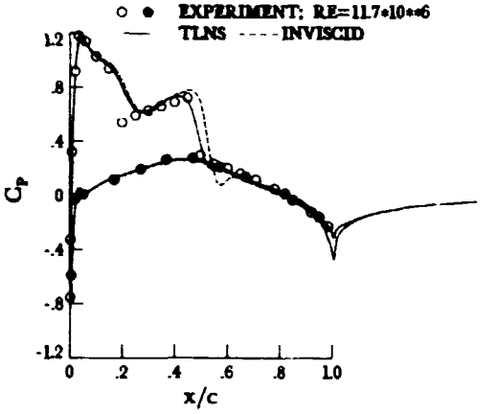

Measured and predicted chordwise (x/c) wing pressures (C_p) at $\alpha = 3.06$.

From the results shown here, it appears that although inviscid analysis can be used to predict the surface pressures qualitatively, viscous analysis must be used to predict the correct shock locations even at such small angles of attack.
(Veer N. Vatsa, 2627)

Vortex Breakdown Simulation Based on Nonlinear Inviscid Model

The phenomenon of vortex breakdown has been known for some time. Numerical simulation based on steady axisymmetric Navier-Stokes equations is in good agreement with experimental results. There are, however, some theoretical investigations based on inviscid models. In this work, it is shown that the inviscid (Euler) equations admit solutions with a vortex breakdown structure qualitatively similar to that observed experimentally. A stream function formulation is used to reduce the conservation of mass, momentum, and energy to a single second-order elliptic equation in the form of a nonlinear eigenvalue problem. Two numerical algorithms are adopted. In the first approach, the equation is discretized with central differences on a Cartesian grid. The resulting algebraic system of equations (with a free-swirl velocity parameter) is solved by a multigrid method that uses a standard relaxation procedure as a smoothing operator. The second approach is applicable, however, for any prescribed swirl velocity parameter and is based on a least-squares formulation. The same solution can be obtained with either method. As expected, the multigrid calculation is, of course, more efficient. The numerical results clearly demonstrate the existence of solutions with a closed region of recirculating flow.
(M.D. Salas, 2627)

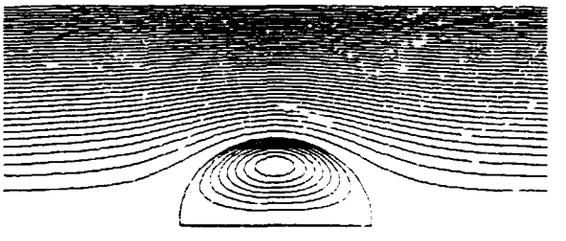

Calculated streamlines depicting recirculation bubble.

Numerical Simulation of Finite-Length Taylor-Couette Flow

Taylor-Couette flow (the flow between two concentric cylinders induced by rotating one cylinder with respect to the other) has been investigated for almost a century as a model for the instability of curved and rotating shear flows. In the case in which the concentric cylinders are very long compared to the gap between them, there is a critical rotation speed of the inner cylinder with respect to the stationary outer cylinder at which regularly sized axisymmetric annular vortices rapidly fill the entire gap. This occurrence was analyzed mathematically in 1923 by G.I. Taylor in a landmark paper on flow stability. At higher rotation speeds, these Taylor vortices lose their axial symmetry in regular azimuthal waves and eventually show contained bursts of turbulence.

The situation in which the length of the cylinders is of the same order as the gap width, however, shows far more complicated behavior in its axisymmetric states. Two Taylor vortices appear near the stationary end plates, even at low rotation rates. As the rotation rate goes up, state bifurcations occur, with the number of vortices increasing (and sometimes decreasing) in pairs, depending on the length-to-gap ratio. So-called "anomalous" modes can also appear, in which the number of vortices is odd, or they rotate in a direction opposite to that normally seen, depending on how the state is approached. This complicated and sensitive behavior makes the finite-length Taylor-Couette flow a prime test problem for the study of stability of viscous flow. A computer code that uses spectral methods to accurately solve the Navier-Stokes equations has been developed at Langley to simulate this flow. Axisymmetric bifurcations are currently under study and the method is easily extendable to full three-dimensional simulations of higher rotation-rate states and eventually to simulations of the contained transition occurrences.

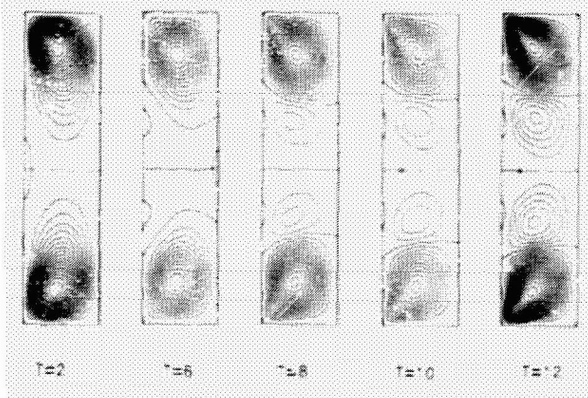

Time evolution of Taylor-Couette flow.

The figure shows contours of stream function in the cross-sectional plane of a vertical cylinder geometry with a length-to-gap ratio of 3.25. The inner, rotating cylinder lies at the left boundary of the cross sections. The plots show the transition from the two- to four-cell state as the rotation rate is increased. Agreement with well-documented experiments for this case is good.

(Craig L. Streett, 2627)

New Design Procedure for Hypersonic Wind Tunnel Nozzles

A new procedure has been developed to design high-temperature hypersonic wind tunnel nozzles that blend smoothly into the end section of an existing facility. The new nozzle contours are generated with respect to geometrical constraints that include the axial location and radius of the subsonic entrance to the nozzle, the axial location of the throat, and the axial location at which the new nozzle blends with the existing end section of the nozzle. Because of the high-temperature flow in the tunnel, foreign gas used for transpiration cooling in the nozzle throats must be accounted for. Furthermore, the large static temperature variation in the nozzles leads to a significant variation in gas properties, and these variations must be properly modeled.

The new iterative design procedure couples several Langley developed codes, an Euler code, a method-of-characteristics code, and a boundary layer code. A Navier-Stokes code is used to check the flow quality in the final design. All codes include real-gas chemistry packages that are consistent with each other. In addition, the Navier-Stokes and boundary layer codes can account for transpiration cooling with foreign gas injection.

The new technique was applied to the design of alternate Mach 4 and 5 nozzles for the Langley 8-Foot High-Temperature Tunnel. These nozzles were required to merge smoothly with the last 200 in. of the current Mach 7 nozzle. The exit Mach number distribution for the Mach 5 nozzle as obtained from

the Navier-Stokes code is shown in the figure on a scale of 0 to 5. It has a maximum deviation of 0.1 about its mean value over more than 70 percent of the test section radius. This small variation was within the constraints imposed on the final flow quality.
(Gordon Erlebacher, 3171)

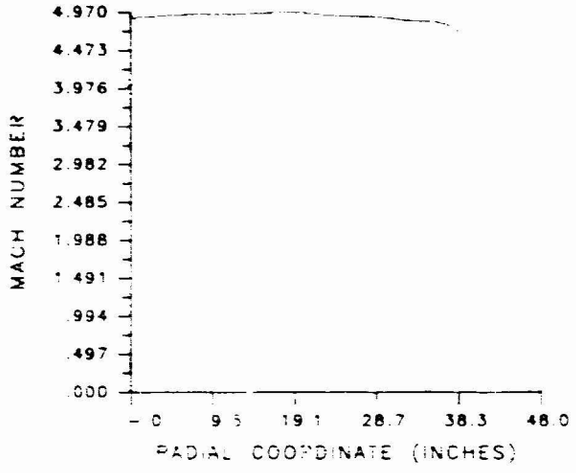

Exit plane Mach number profile in newly designed alternate Mach 5 nozzle for Langley 8-Foot High-Temperature Tunnel.

Passive Device for Flow Separation Control at Supersonic Speeds

A passive technique has been developed for flow separation control in shock boundary layer interactions. Such interactions commonly occur in high-speed internal and external flows. Impinging shocks of sufficient strength can cause boundary layer separation and can seriously degrade the performance of components such as inlets, diffusers, combustors, and lifting surfaces. Most previous attempts to control or eliminate the shock-induced separation have involved active systems such as suction, blowing, or wall cooling, which result in increased weight and complexity.

The present system uses a sharp plate parallel to the wall on which the original shock boundary layer interaction is taking place. The control plate is placed so that the interaction shock is intercepted and reflected by this small plate, and the original thick, easily separated boundary layer is thus protected from the severe pressure gradient of the shock wave.

Experimental data pertaining to this device were obtained in the 20-Inch Mach 6 Tunnel on a flat plate with a turbulent boundary layer intersected by a 22.7° shock (15° shock generator). The figure shows data obtained from a control plate at a height of about one boundary layer thickness off the wall. The pressure rise moves from the separated case (no control plate) toward the inviscid pressure distribution due to the control plate. Other data indicate that longer plates placed further from the surface are more effective. This may be simply the result of the remaining disturbance field being moved further from the original thick, easily separated boundary layer. Oil flow results indicated elimination of separation for some configurations, and numerical simulations have indicated that control plates can eliminate separation even for laminar boundary layers. This research is especially applicable to optimization of supersonic inlets.
(E. Leon Morrisette, 3302)

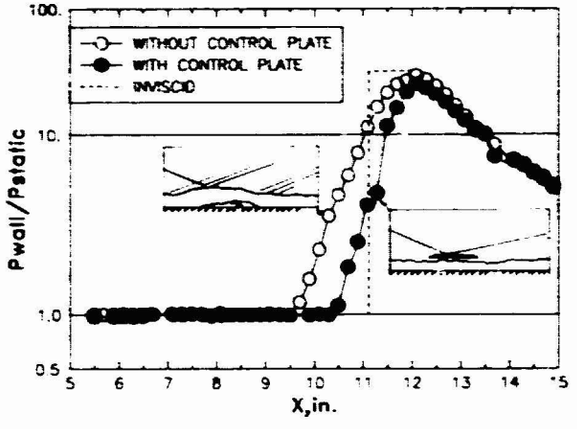

Effect of control plate on pressure distribution (p_{wall}/p_{static}).

Effect of Acoustic Excitation on Flow Over Low Reynolds Number Airfoil

Acoustic excitation has been known to significantly influence the performance of a low Reynolds number airfoil by affecting the laminar separation

bubble as well as the structure of the turbulent wake. Langley has initiated an experimental study to provide a basic understanding of this phenomenon and to develop a sufficient data base for empirical prediction schemes.

The experiment was performed in a small wind tunnel with a 1.5- by 1-ft test section. A 4-in.-chord airfoil (LRN 1007) was used for the study. The excitation was imparted by an acoustic driver attached to the side of the test section which utilized the tunnel resonance frequencies. The amplitude of the sound wave was monitored by a microphone mounted flush on the test section wall. Lift, drag, and hot-wire spectra measurements were made at varying frequencies and amplitudes of excitation at chord Reynolds numbers of 40,000 and 100,000.

A systematic set of data has been gathered, including documentation of the acoustic and flow fields. Sample flow visualization photographs shown in the figure demonstrate the effect of excitation. The separation control at $\alpha = 8°$ and the profound effect on the wake structure at $\alpha = 15°$ can be readily observed. The lift-to-drag ratio has been found to increase several fold for specific cases of excitation. Estimates show that the most pronounced effect at $\alpha = 15°$ occurs when the excitation frequency approximately matches the maximally unstable frequency of the separated, laminar shear layer on the upper surface. The collected data are currently being analyzed. Attempts are being made to correlate these data with stability analyses of the boundary layer and the separated shear layer for different angles of attack.
(W.D. Harvey, 2631)

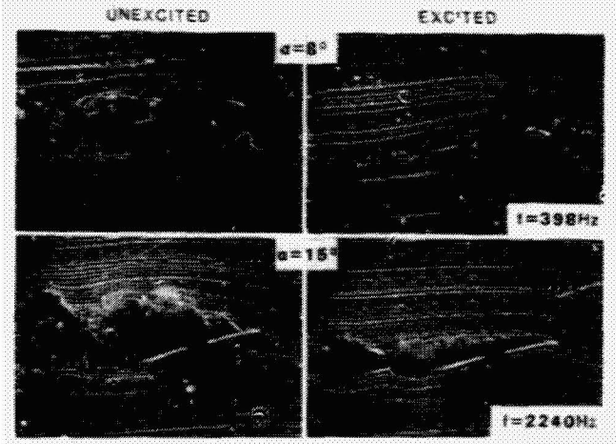

Flow visualization photographs.

Measured Characteristics of Laminar Separation Bubbles

Laser velocimetry was used to study the nature of a laminar separation bubble in the concave region of an airfoil model in the Langley Low-Turbulence Pressure Tunnel. Coincident three-component velocity measurements were employed to determine histograms of particle velocity, mean velocity profiles, turbulence intensities, and Reynolds stresses within the shear layer. The locations of laminar separation, transition, and turbulent reattachment were then ascertained from these data.

The concave test region of the airfoil extended from 17 to 25 percent chord. The boundary layer was laminar and attached up to 19 percent chord, and transition in the separated region occurred in the region from 21.5 to 22.5 percent chord. Reverse flow was noticeable at a height of 0.027 percent chord above the model surface at 21.5 percent chord, was most pronounced at 22.5 percent chord, and was practically absent at 23 percent chord. There was no reverse flow at 23.5 and 25 percent chord, which indicated boundary layer reattachment. The maximum height of the laminar separation bubble was about 0.22 percent chord. The length of the laminar part of the bubble was 3 percent chord and transition and turbulent reattachment were completed within 1.5 percent chord. The separating streamline was at an angle of approximately 1.6° to the surface. A comparison of test results with existing empirical relations showed good agreement. Further, the present experiment indicates that the laser velocimeter is a very powerful nonintrusive tool that can be used to study the laminar characteristics of separation bubbles.
(J. Ray Dagenhart, 2631)

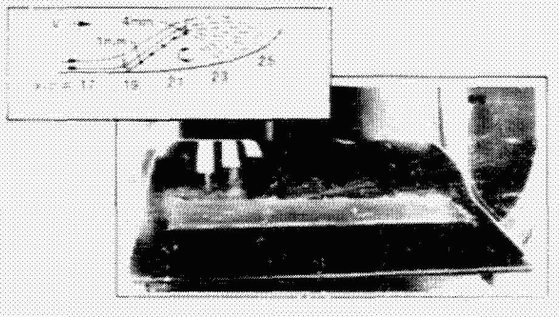

Laminar separation bubble studied with laser velocimetry.

Application of Natural Laminar Airfoil to Light General Aviation Airplane

Airfoils for general aviation applications have received considerable attention at Langley over the past decade, with emphasis on the design and experimental verification of conceptual turbulent-flow airfoils. The overall objective involved in developing such a series of airfoils included the following performance requirements: low cruise drag, high climb lift-drag ratios, high maximum lift, and practical, docile stall behavior. Although these airfoils did achieve improved climb performance and higher maximum lift coefficients compared with the characteristics of the earlier NASA four- and five-digit airfoils, the cruise drag coefficients were about the same. Accordingly, recent emphasis has been shifted toward natural laminar flow (NLF) airfoils in an attempt to obtain lower cruise drag yet retain the high lift coefficients of the NASA airfoils.

A low-speed 14-percent-thick NLF airfoil has been designed with 0.70*c* laminar flow on both surfaces, a lift coefficient of 0.4, a chord Reynolds number of 10×10^6, and a Mach number of 0.4. This airfoil is designated NLF(1)-0414F and has a 12.5-percent chord cruise flap. Tests were conducted in the Langley Low-Turbulence Pressure Tunnel (LTPT) to verify its performance. Extensive NLF was maintained over both surfaces at design conditions, and the profile drag was reduced by 33 percent compared to that previously obtained on NLF airfoils.

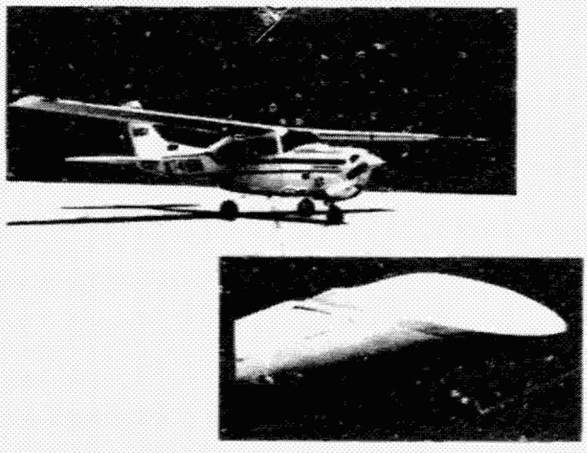

L-85-9172

Flight test airplane and airfoil profile.

A wide low-drag lift coefficient range was achieved by deflection of the trailing-edge flap. An airfoil lift-drag ratio of 245 was verified at the design Reynolds number, which represents a significant gain in airfoil performance compared with previously documented results. Excellent stall characteristics that exceeded those expected for NLF airfoils were demonstrated by the achievement of maximum lift coefficients with either zero flap or with a split flap deflected 60°. The application of roughness trips near the leading edge caused fully turbulent flow over the airfoil and decreased the maximum lift coefficient achieved with NLF by only about 0.04.

The Cessna Aircraft Corporation has recently incorporated a wing with this airfoil on a Cessna 210 airplane. The flight results indicated a speed increase of 12 knots over that of the baseline aircraft, and the pilot reported gentle stall characteristics.

(R.J. McGhee, 4516)

Swept Supercritical Laminar Flow Control Airfoil Technology

Rather large decreases in friction drag can be realized on airfoils or wings if a laminar boundary layer can be maintained either by passive natural laminar flow (NLF), which is controlled through geometric shaping, or by active laminar flow control (LFC), which usually combines both shaping and local mass transfer through the surface. A large chord-swept LFC airfoil has been designed and constructed, and a test program was recently completed in the Langley 8-Foot Transonic Pressure Tunnel to evaluate the combination of surface suction control laminarization with discrete spanwise slots and supercritical technology at conditions typical of high-performance transports. Requirements for this test also included modifications of the wind tunnel to achieve the desired flow quality and test section wall contouring to stimulate free air flow about an infinite yawed model at transonic speeds.

Performance testing with the LFC experiment installed in the tunnel has been ongoing since September 1982. This research has involved the development of systems operational procedures and performance documentation of the LFC airfoil, suction system, and wind tunnel liner. Results indicate that full-chord suction laminarization can be maintained on moderately swept supercritical airfoils with shock-

less flow up to high speeds and Reynolds numbers. Correspondingly, very low drag can be achieved when both the drag penalty due to suction and the wake are accounted for. Suction laminarization over an extensive supercritical zone can also be obtained at high chord Reynolds numbers with low drag. The present LFC results indicate performance comparable to that of typical high-performance turbulent supercritical airfoils but with a decrease in drag of almost an order of magnitude.
(W.D. Harvey, 2631)

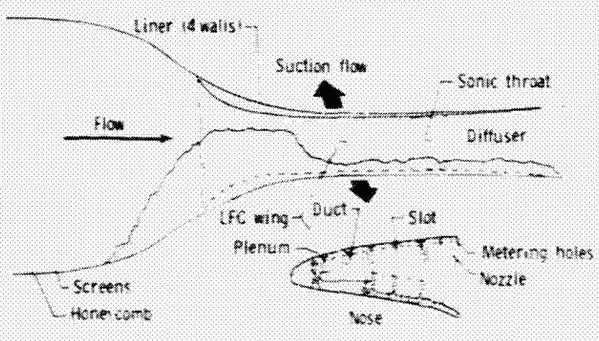

Test setup in 8-Foot Transonic Pressure Tunnel.

quite effective for boundary layer excitation and control. The experimental results obtained in air are also well described and predicted by the analysis.
(Lucio Maestrello, 2631)

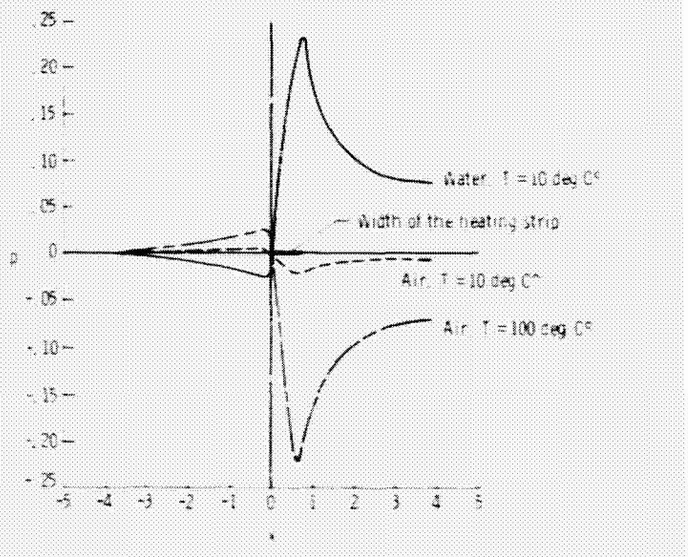

Wall pressure p *due to single heating strip in water and in air.*

Analysis of Active Control by Surface Heating

Investigation into the interaction of surface heating with boundary layer is of interest from the point of view of controlling transition and turbulence. It has been demonstrated that surface heating can excite boundary layer disturbances, which in turn can be used to cancel or enhance instability waves. A theoretical analysis that relates the disturbances in the flow field to the surface heating has been developed. The problem is analyzed by the method of matched asymptotic expansions as an unsteady problem to relate temperature, velocity, and pressure disturbances to the local surface heating.

The wall pressure variation due to a single heating strip in water and in air is shown. In air, the effect of surface temperature variation is of opposite sign to that of the water. In addition, heating in air requires 10 times the temperature needed to achieve an equivalent pressure amplitude in water. The analysis confirms experimental results and shows that heating is

Amplitude Control and Nonlinear Stability of Compressible Flows

It has been demonstrated by numerical solution that either heating or cooling can be used to effectively reduce the level of disturbances propagating in a boundary layer. The simulations are based on the solution of two-dimensional compressible time-dependent Navier-Stokes equations on a flat plate. The method of solution is an explicit predictor-corrector technique which is fourth-order accurate in space and second-order in time.

Starting from the steady state, perturbations in the form of the Orr-Sommerfeld solution are superimposed at the inflow to obtain the uncontrolled growth of disturbances. For control, the temperature boundary condition is modified locally with the use of a steady and an unsteady component with phase. The figure shows the effect of active control on the growth of disturbance amplitude for a Mach number of 0.4 and a free-stream Reynolds number per foot of

3×10^5. The disturbance growth is plotted in terms of the rms (root mean square) of mass flux versus Reynolds number, based on the local displacement thickness. The amplitude growths for the uncontrolled and controlled cases are compared for both heating and cooling. The figure shows a reduction in the amplitude growth for both heating and cooling compared to the uncontrolled case. A reduction of about 6 percent is indicated for heating with an overheat of 1000°F, and a 12-percent reduction is indicated with cooling for a temperature difference of 300°F.
(Lucio Maestrello, 2631)

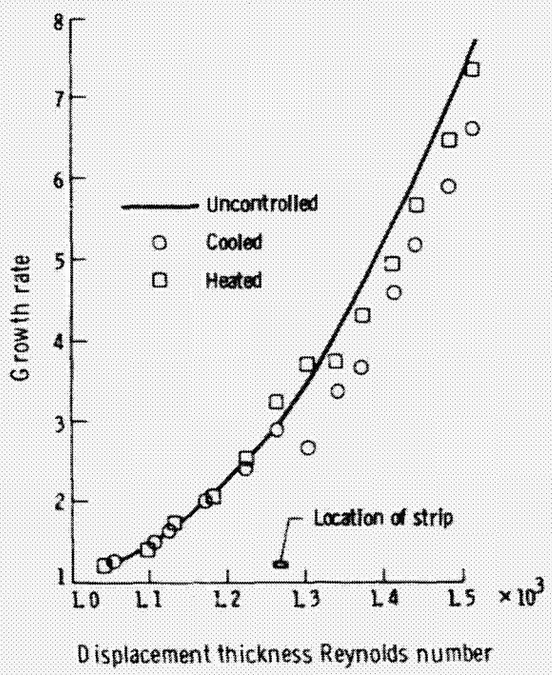

Effect of control on rms amplitude growth.

Computational Design of Natural Laminar Flow Glove

An integrated two-dimensional/three-dimensional computational design process developed at Langley used state-of-the-art transonic flow computational techniques to design a natural laminar flow (NLF) glove for the outer panel of an F-14 aircraft. This design work was done in conjunction with the Variable Sweep Transition Flight Experiment (VSTFE). The objective of the VSTFE is to obtain data for various combinations of favorable pressure gradients, Reynolds numbers, and sweep angles to assist in identifying and quantifying the influence of the interaction of cross flow and Tollmien-Schlichting disturbances on wing boundary layer transition.

Since the glove was to be designed for the actual operational environment of the aircraft ($M = 0.7$, altitude = 35,000 ft), three-dimensional computer codes were used to model the highly swept inboard strake region of the wing and the fuselage. In addition, physical constraints were imposed on the design. The modified region could extend from the leading edge to 60 percent chord on the upper surface and 10 percent chord on the lower surface, and the glove thickness was required to be a minimum of 0.65 in. with a maximum thickness at the spoiler hinge line of less than 1.0 in. Because the flight test experiment was to be conducted in an asymmetric configuration, the design also had a rolling-moment constraint of less than 0.01 over the test envelope.

The glove design has been successfully completed for the VSTFE. Physical and aerodynamic constraints were met for the design, and analysis of the final design yielded favorable upper surface pressure gradients over 50 percent of the wing chord for a wide range of flight conditions. The figure shows a midspan section contour and pressure distribution at the design condition.
(Edgar G. Waggoner, 2601)

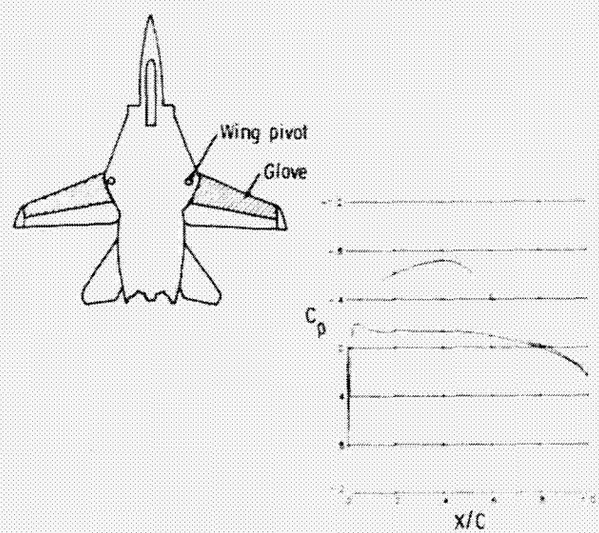

VSTFE glove design and wing pressure distribution (C_p).

Optimization of Canard and Wing Flap Deflections at Supersonic Speeds

The projected requirements for future fighter aircraft to cruise and maneuver at supersonic speeds while maintaining good subsonic and transonic aerodynamic characteristics have resulted in increased interest in the use of variable wing camber in the form of leading- and trailing-edge flaps. As part of an effort to expand the wing flap data base, an investigation of the experimental and theoretical aerodynamic characteristics of a wing with leading- and trailing-edge flaps operating in the downwash field of a canard at supersonic speeds has been completed. The wing planform, shown in the figure, has a highly swept leading edge on the inboard section for good supersonic performance. The leading-edge flap on this part of the wing was designed to function as a vortex flap at transonic speeds. The sweep on the outboard panel was reduced to improve the subsonic-transonic performance characteristics.

The analytic method used in the study is a linear theory lifting surface program which predicts some of the aerodynamic characteristics of wing-canard configurations in supersonic flow. The method has been modified to include the effects of leading- and trailing-edge flaps. The experimental data exhibited various nonlinear properties, which limited the direct application of the modified linear theory method as an optimization tool. Consequently, the theoretical and experimental characteristics of a variety of combinations of canard and flap deflections were used to devise guidelines and correlation factors to establish a design methodology. This methodology was then used to determine the optimum deflections of canard and wing flaps for best trimmed performance at maneuver lift conditions.

Some of the results from an experimental verification of the design methodology are shown. For the theoretical optimum combination of leading- and trailing-edge flap deflections and a near-optimum canard deflection, a reduction of 7 percent in trimmed drag due to lift was achieved over the canard-alone trimmed drag due to lift.

(Barrett L. Shrout, 3294)

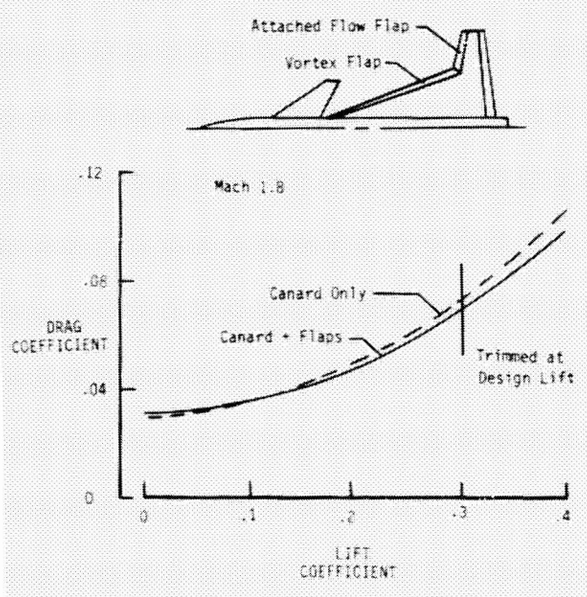

Experimental drag characteristics of configuration.

Supersonic Nonlinear Aerodynamic Wing Design and Analysis

Advanced military aircraft requirements indicate a desirability for sustained supersonic cruise and supersonic maneuverability. Improved numerical aerodynamic prediction techniques are required to support the conceptual design of these aircraft and the optimization of their performance to achieve these goals. Linearized design methods are currently widely used, although the restrictions of linear theory may severely limit significant advancements in supersonic aerodynamic performance. Nonlinear effects due to embedded shock systems, flow separation, and transonic edge conditions have been neglected, and the result has been less than expected performance at the maneuver point. Nonlinear analysis is required for shock capture and pressure gradient management to maximize the extent of attached flow over the configuration.

Nonlinear potential analysis methods are now mature enough to allow a timely, economical analysis (when coupled with new, high-speed computers) which can impact conceptual aircraft design. A joint effort between Langley and the Rockwell International Corporation was undertaken to demonstrate the use of a potential analysis technique for aerodynamic wing design at supersonic cruise and maneuver conditions (NASA CR-172507). The configuration used in the study is a Rockwell concept developed

and sized to meet modern fighter requirements. It consists of a blended wingbody with widely spaced underslung nacelles and twin vertical tails.

The applicability of nonlinear theoretical techniques was investigated through the aerodynamic design of two outboard wing panels for the fighter model. A 55° sweep maneuver point Mach 1.6 design and a multi-operating point 48° sweep design were developed and tested in the Langley Unitary Plan Wind Tunnel. Experimental force and pressure data were obtained and used to assess the wing designs through comparisons with their pretest performance estimates.

A preliminary comparison between the experimental surface pressure data on the 55 ° point design wing and an analysis of the 55° configuration with the supersonic full potential code is shown. Theory and experiment agree quite well on the lower surface of the wing and the agreement is good over most of the upper surface of the wing. For the upper surface, the theoretical results presently overpredict the pressure distribution near the leading edge, particularly at the two outboard stations. The predicted full-potential results compare very well with the experimental data and provide an improved estimate of the vehicle's performance over that available with the linear analysis. The routine use of nonlinear analysis techniques in the early design process is suggested since this is where they can have the greatest impact on subsequent system development.
(Noel A. Talcott, Jr., 3294)

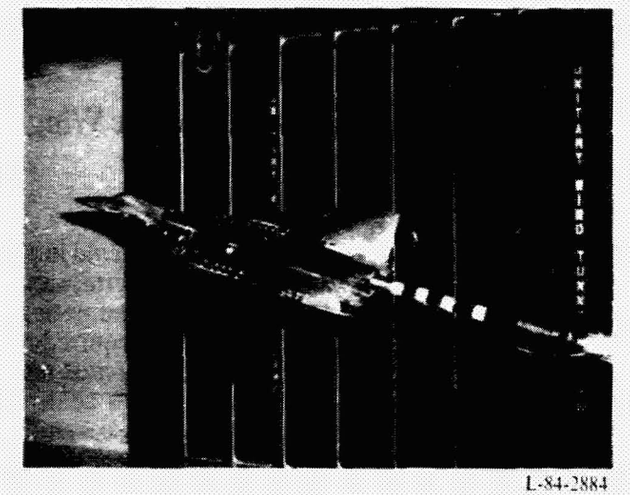

L-84-2884

Mach 1.6 55° leading-edge sweep point design configuration.

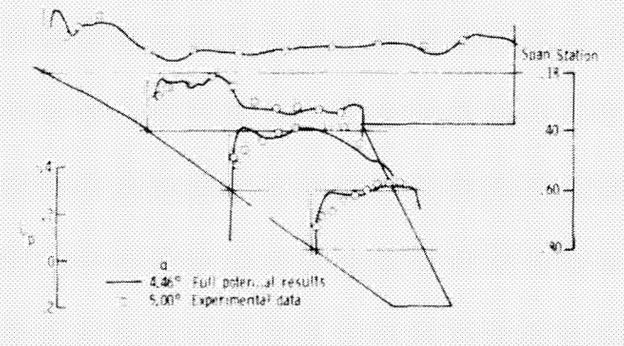

Measured and predicted surface pressure data (C_p).

Thrust Vectoring Control Effectiveness at High Angle of Attack

Modern air combat requires the aircraft to maneuver effectively at high-angle-of-attack conditions. However, the angle-of-attack envelope of current fighters is limited by a combination of degraded stability characteristics and inadequate control effectiveness. One promising means of providing large control moments that are not dependent on angle of attack and dynamic pressure, as are aerodynamic controls, is vectoring the engine exhaust. To explore this potential, an investigation of control effectiveness from both thrust vectoring and horizontal tails has recently been made in the Langley 16-Foot Transonic Tunnel. Tests were conducted on a twin-engine general research model with two-dimensional convergent-divergent (2-D C-D) nozzles at Mach numbers (M) from 0.15 to 0.90, angles of attack (α) up to 34°, and nozzle pressure ratios (NPR) up to 5.0.

Thrust vectoring (in the pitch plane) and horizontal tail effectiveness are presented as a function of angle of attack at three different Mach numbers for the configuration. Open symbols represent pitch vectoring effectiveness and were determined with tails off for thrust vector angles of 0° and 15°. Solid symbols represent horizontal tail effectiveness and were determined at horizontal tail deflection of 0° and −5°. Data are presented at a typical turbofan NPR for each Mach number. Thrust vectoring effectiveness is nearly independent of angle of attack throughout the entire angle-of-attack range. This is not generally the case for typical aerodynamic control surfaces (solid symbols), especially in angle-of-attack regions where

the horizontal tails may be stalled. Since tail surfaces are generally sized for low-speed control, they are capable of providing large moments at higher Mach numbers (0.6 and 0.9). In fact, they provide more pitch capability than needed. At low speeds (M = 0.15), thrust vectoring is three times more effective (per degree of deflection) than the horizontal tails at producing pitching moment.
(Francis J. Capone, 2673)

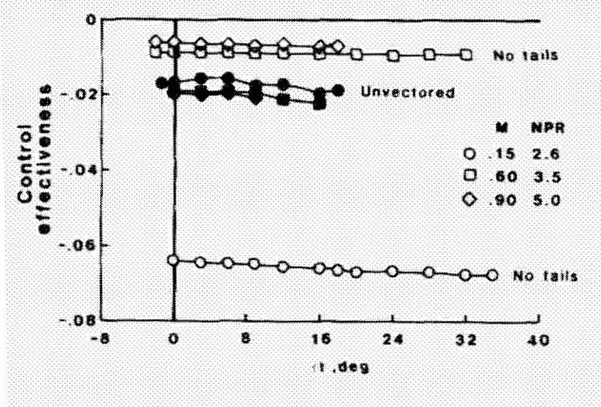

Vectoring and horizontal tail effectiveness.

Navier-Stokes Code for Predicting Performance of Two-Dimensional Thrust Reversing Nozzles

A Navier-Stokes code has been developed by Robert MacCormack at the University of Washington under contract to NASA. This code is capable of solving the flow field in two-dimensional nozzles with up to three exhaust ports. The code solves the finite-volume form of the Navier-Stokes equations with either MacCormack's explicit-implicit scheme or a Gauss-Seidel line relaxation. Each of these schemes is combined with flux vector splitting. Turbulence is modeled with the Baldwin-Lomax eddy viscosity model. The code has been applied to a variety of nozzle configurations. The flow fields in fully deployed thrust reversers, partially deployed thrust reversers, single-expansion ramp nozzles, and convergent-divergent nozzles have been successfully predicted with this Navier-Stokes code.

Comparisons of the predicted flow fields and the predicted thrust and mass flow characteristics with experimental measurements for a variety of nozzle geometries have shown that the code provides predictions of two-dimensional nozzle flows to within 0.5 percent. Even though the code is two-dimensional, these comparisons have shown that the code can be used with good results for rectangular nozzles with straight parallel sidewalls.
(Lawrence E. Putnam, 2673)

Multiaxis Thrust Vectoring System for Axisymmetric Nozzles

A multiaxis thrust vectoring system for axisymmetric nozzles has been tested at static conditions (no external flow). This thrust vectoring system consisted of either three or four vectoring vanes located downstream of the nozzle exit. In addition to the number of vanes, other test variables included vane curvature and vane location relative to the nozzle exit. Nozzle pressure was varied from 1 to 6 atmospheres. High-pressure air was used to simulate the jet exhaust and a six-component strain gauge balance was used to measure forces and moments about all three model axes.

For the range of variables tested, the effects of vane curvature and vane location on measured turning angles were small. A double-curvature ("spoon" shaped) vane generally produced about 1° to 2° higher turning angles than a single-curvature (airfoil shaped) vane. The effect of vane location on turning angle was also limited to about 2°. The geometric parameter with the largest effect on measured turning angles was the number of vectoring vanes used. The four-vane thrust vectoring system had a much larger thrust vector angle envelope, especially for combined pitch and yaw vector angles, than the three-vane thrust vectoring system. In addition, it was difficult to decouple the pitch and yaw vector functions for the three-vane thrust vectoring system. The thrust vector angle envelope of the four-vane system was sufficiently large to augment both maneuverability and control about all axes for most airplane configurations.
(Bobby L. Berrier, 2673)

Experimental Investigation of Supersonic Store-on-Store Interference Drag

An experimental study has been undertaken to determine the store-on-store interference drag of a series of generic stores mounted in various arrays on a flat plate. The generic stores were cylinders with nose and afterbody shapes consisting of hemispheres, ogives, and flat surfaces. The various arrays consisted of either two or three stores tangent and semisubmerged and mounted in a lateral, tandem, or staggered configuration. A portion of the flat plate was segmented from the plate and is identified as a metric pallet. The metric pallet was mounted on a dedicated one-component drag balance so the top surface of the pallet was flush with the plate surface. One of the generic stores was mounted on the metric pallet and the remaining stores were mounted on the nonmetric flat plate. This arrangement allowed the drag of only one store to be measured as the positions of the other nonmetric stores were varied. This method allows very accurate store drag measurements because the one-component drag balance can be sized to measure the drag of only one store. These tests were conducted at Mach numbers of 1.6, 1.9, 2.16, and 2.86 and a Reynolds number of 2×10^6 per foot.

Typical data for hemispherical nose and afterbody stores mounted in two-store lateral and tandem configurations are shown in the figure. The plots show the drag of the metric store ($C_{D_{\pi}}$) versus the lateral spacing (Y) and tandem spacing (X) nondimensionalized by the store diameter (d). In the figure, the store inside the box identifies the store mounted on the metric pallet. The lateral spacing data show that as two stores are placed close together, the drag of one store is less than the store-alone value and approaches the store-alone value as the stores are separated. The tandem spacing data show that as the stores are separated, the drag of the rearward store is less than half the store-alone value even at a separation distance of three store diameters.

(Floyd J. Wilcox, 4010)

Supersonic Evaluation of Leading-Edge Flaps

Various types of variable-camber wings have been considered in an effort to design aircraft that satisfy the severe aerodynamic requirement of efficient cruise and high-lift flight across the Mach number range. One simple variable-camber device, the leading-edge flap, has typically been designed to improve aircraft performance at subsonic and transonic speeds. Preliminary theoretical studies have indicated that these flap designs may improve the supersonic performance as well. Consequently, an experimental study was conducted to evaluate the supersonic performance of a leading-edge flap design on wings with variations in planform and aspect ratio. The joint experimental investigation between General Dynamics and Langley was conducted in the Langley Unitary Plan Wind Tunnel at Mach numbers from 1.60 to 2.16.

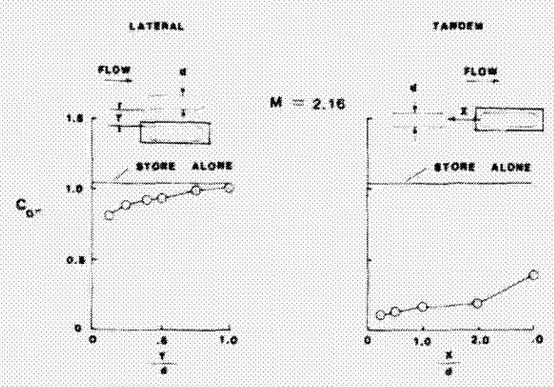

Store-on-store interference drag effects for lateral and tandem spacing.

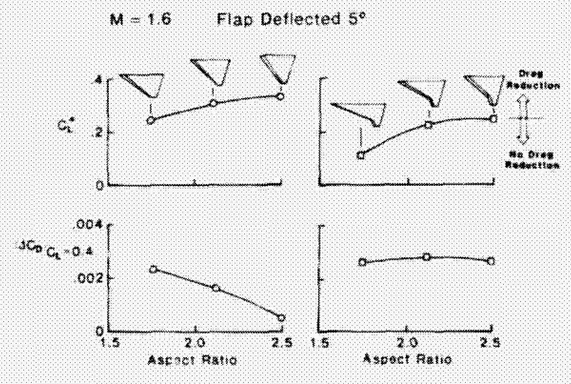

Leading-edge flap effectiveness for supersonic drag reduction.

The wind tunnel results shown in the figure indicate the effectiveness of leading-edge flaps for supersonic drag reduction. Leading-edge flaps provided drag reduction at lift conditions greater than the critical lift coefficient (C_L*). As aspect ratio increases, the critical lift coefficient increases. The drag reduction for a constant lift coefficient of 0.4, $(\Delta C_D)_{C_L} = 0.4$, is also shown in the figure. Generally, the leading-edge flaps yielded greater performance benefits on the double-delta wings than on the delta wings.
(Peter F. Covell, 4008)

Drag of Rectangular Box Cavities at Supersonic Speeds

Several experimental studies have been initiated at Langley to define the aerodynamic characteristics of various cavity configurations. One of these studies consists of detailed pressure measurements in a rectangular box cavity located in a flat-plate wind tunnel model. Cavity variables consisted of length, depth, and width. The rear face of the cavity was a sliding block that could be remotely positioned during tunnel operation to provide wide flexibility in the selection of cavity lengths. The pressure measurement data were used to analyze the cavity flow field and were also integrated to define cavity drag coefficients (C_D).

Typical pressure coefficient (C_P) distributions for the length (L) of the cavity ceiling are shown in the figure. The pressure data are shown for a shallow cavity (L/D = 19) and a deep cavity (L/D = 4). For the shallow cavity, the cavity pressure distributions are indicative of a "closed" cavity flow field. For this case, the approaching shear layer expands over the leading edge, impinges on the cavity ceiling, and exits ahead of the rear face. Large turning angles occur in the local flow field and result in large pressure gradients, as shown by the pressure data. For the deep cavity, the approaching shear layer simply bridges the cavity and results in small turning angles and a relatively uniform pressure distribution. This type of cavity flow is often referred to as an "open" flow field.

The cavity drag coefficients show relatively low drag levels for $L/D \leq 12$. Pressure and schlieren data indicated an "open" flow field for this range of L/D. At L/D = 12, an abrupt increase in C_D occurred which corresponded to the switching of the cavity flow field from "open" to "closed" flow. The increase in drag resulted from both the decrease in pressure over the front face associated with the flow expanding into the cavity and the increase in pressure over the rear face associated with the flow exiting from the cavity. Switching of the flow field occurred at L/D = 12 throughout the test range of Mach number from 1.5 to 2.86.
(Robert L. Stallings, Jr., 4004)

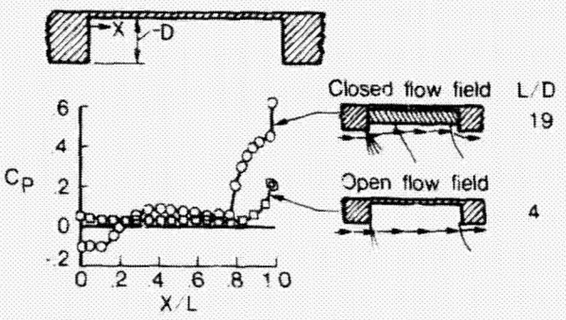

Pressure distributions.

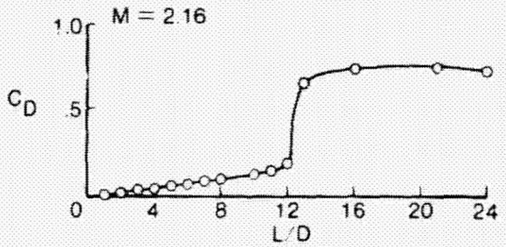

Drag characteristics.

Supersonic Separated-Flow Flap Study

The separated-flow wing design philosophy has been studied extensively at subsonic speeds and has led to the design of several unique leading-edge devices. To evaluate the potential of this wing design approach for Mach numbers greater than 1.0, an experimental investigation of the aerodynamics of a series of sharp-leading-edge flat-upper-surface delta wings has been conducted.

Wing leeside flow characteristics are presented as a function of wing leading-edge deflection angle (δ_F) and wing angle of attack (α) at the left of the figure. Three basic flow types were observed: at low angles of attack and small deflection angles a vortex will be positioned on the flap (shaded area); as flap deflection is increased the dominant separation occurs at the flap hinge line; and as angle of attack is increased the vortex will migrate inboard off the flap. The data suggest that a significant loss in aerodynamic performance would result from hinge line separation and with the migration of the vortex off the flap.

At the right of the figure are the measured drag-due-to-lift characteristics of each wing along with the linear theory flat wing (zero-percent thrust) and optimum cambered wing (100-percent thrust) characteristics. The drag characteristics are presented in the form of the drag-due-to-lift parameter ($\Delta C_D/\beta C_L^2$) plotted as a function of lift coefficient (C_L). The data show that significant drag reductions can be achieved at supersonic speeds with the management of wing leading-edge vortex flows. The data for the 10° and 15° leading-edge deflections show a significant loss in performance due to hinge line separation compared to the 5° leading-edge deflection data, which do not show hinge line separation. However, all flap deflections result in drag reductions compared to the flat wing.

The experimental results indicate that the separated flow wing design concept can be extended to supersonic speeds; however, the large drag reductions achieved are overshadowed by the hinge line separation problem. To develop a better understanding of the hinge line separation phenomenon, a fundamental theoretical and experimental research program has been established.

(Richard M. Wood, 4926)

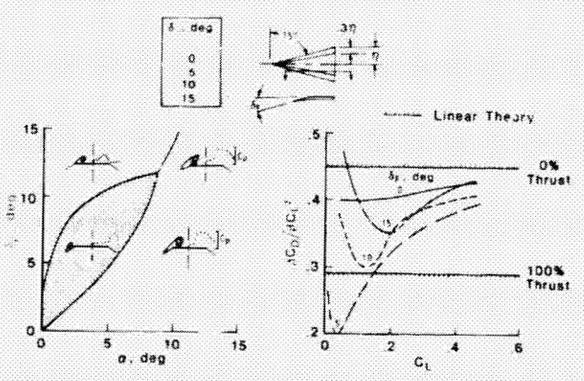

Supersonic test results.

Wind Tunnel Free-Flight Test of EA-6B Configuration

As part of a broad program to improve the cruise maneuverability of the Navy EA-6B electronic countermeasures aircraft, a high-angle-of-attack stability and control investigation was conducted in the Langley 30- by 60-Foot Tunnel and the 12-Foot Low-Speed Tunnel. The EA-6B is an electronic warfare version of the A-6 series aircraft. Although the A-6 and the EA-6B have identical NACA 64-series airfoils, the EA-6B operates routinely at 10,000- to 15,000-lb higher gross weights in fleet use. This higher gross weight has severely constrained the maneuvering capability of the configuration. The investigation consisted of static force tests on a 1/8.5-scale model which was subsequently flown with the free-flight test technique in the 30- by 60-Foot Tunnel. The objective of the test program was to increase the maximum usable lift with an improvement in lateral-directional stability and lateral control near stall.

The investigation revealed that the maneuverability capability of the aircraft was limited because of instability that resulted from an adverse vortex flow at the vertical tail. Several modifications were developed in the test program which can be implemented easily on the fleet aircraft. The modifications consisted of airfoil contour improvements, a glove leading-edge extension, a droop extension on the inboard flap, a fin extension, and use of the speed brakes for lateral control augmentation. The free-flight tests demonstrated that this enhanced maneuver configuration was directionally and laterally stable beyond stall with a 25-percent increase in maximum usable lift over that of the basic design.

(Frank L. Jordan, Jr., 2184)

L-85-8914

EA-6B model in free-flight test in 30- by 60-Foot Tunnel.

Ignition/Flameholding Characteristics of Wedge Injectors

A parametric scramjet engine model has been tested extensively in the Langley Mach 4 Scramjet Test Facility. The most basic configuration for this engine had smooth internal walls with no protruding surfaces. Hydrogen fuel was injected from the combustor sidewalls perpendicular to the air flow and was usually ignited by injection of a pyrophoric fuel mixture (20 percent monosilane/80 percent hydrogen by volume). Ignition of the pyrophoric fuel mixture was not achieved at Mach 4 flight total-temperature conditions (i.e., T_t = 1640°R), and the test gas total temperature had to be increased to about Mach 4.7 conditions to autoignite. Wedges were added at the primary fuel injector location to provide a base region to increase fuel/air residence time. These wedges were effective in lowering the autoignition temperature to below Mach 4 conditions and were also durable.

Because of the lack of visibility within the engine, simple Mach 2 tests of a single wedge injector were conducted with the injector mounted on a flat plate. The photographs show combustion of the silane/hydrogen mixture (injected upstream of the wedge) and the wedge primary hydrogen fuel at a free-stream total temperature of 1700°R at both low and high flow rates of fuel injection. Ignition at a low fuel flow rate occurred only in the recirculation region downstream of the wedge, and in subsequent tests this occurred at total temperatures below Mach 4 conditions. Higher fuel flow rates resulted in interactive burning occurring from the upstream silane/hydrogen injectors and encompassing the entire wedge. These modes of flameholding and burning are believed to be representative of the mode of combustion with the wedges in the scramjet engine.

(Earl H. Andrews, 3772)

L-85-9212

Ignition and burning in wedge base region with low fuel flow rates at T_t = *1700°R.*

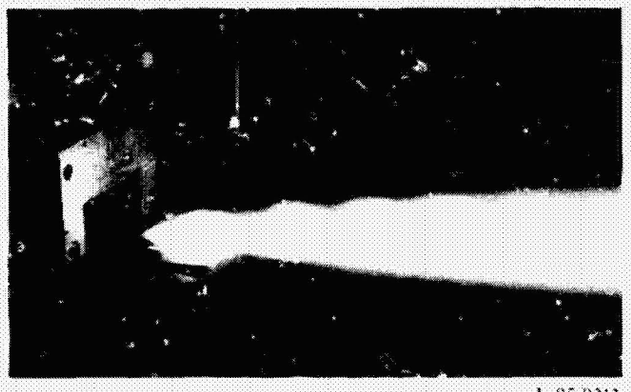

L-85-9213

Ignition and burning in region of upstream boundary layer separation with high fuel flow rates at T_t = *1700°R.*

Numerical Simulation of Flow Through High-Speed Inlets and Nozzles

A computer program has been developed at Langley to analyze the flow through complex inlet and nozzle configurations. It solves the three-dimensional Euler or Navier-Stokes equations in conservation form by MacCormack's explicit or explicit-implicit method. An algebraic eddy viscosity model is used for turbulent-flow calculations. The code is operational on the Control Data VPS-32 computer system at Langley and has been optimized to take maximum advantage of the vector-processing capability of the system. Special attention has been paid in structuring the program to allow the use of as many grid points as possible without the need to exceed the primary memory of the computer. With the currently available 32-million 32-bit word memory, the program can calculate approximately 1.4 million grid points at a computational rate of about 7×10^{-6} sec/grid point/time step.

Since its development, the program has been used to analyze the flow through a variety of high-speed inlet and nozzle configurations. Results for a two-strut scramjet inlet, shown with the cowl plate removed, are presented here at an inflow Mach number of 4.03. A grid of 275,000 points is used in the calculations. The analysis includes the interaction between the high-pressure internal flow and the low-pressure external flow caused by the aft placement of the cowl on the inlet undersurface. The computed pressure distributions on the inlet sidewall and the strut inner surface at mid-inlet height are shown. It can be seen that the computed pressure distributions are in very good agreement with the experimental results.
(Ajay Kumar, 3171)

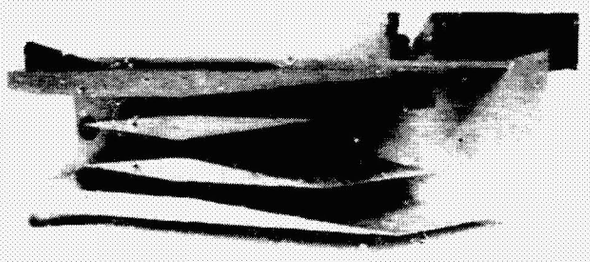

L-85-7231

Two-strut scramjet inlet configuration.

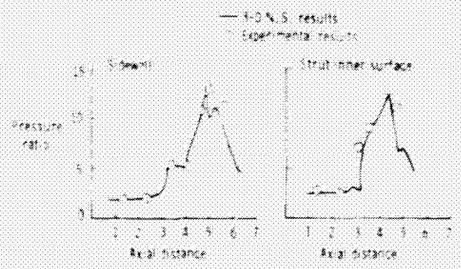

Surface pressure distribution at mid-inlet height.

Airfoil Performance in Simulated Heavy Rain

Tests have been conducted in the Langley 4- by 7-Meter Tunnel to study the effect of heavily water laden airflow on an airfoil's performance. The objective of the study is to determine if there are performance penalties of sufficient magnitude to reduce the safety margin of airplanes flying in rain. Several recent commercial airplane accidents have occurred during severe weather operations when heavy rain was present.

The wind tunnel tests were conducted with a wing model section that was representative of a transport airplane airfoil in a landing configuration. The model was located in the back portion of the tunnel test section and a water spray manifold was located 25 ft upstream of the model in the forward part of the test section. The manifold produced a simulated rain environment of a very heavy rainfall. The tests were run at tunnel speeds of 112 to 159 ft/sec. The data showed that for the extreme rain rates, the maximum lift capability of the model was reduced by 20 percent. Initial attempts to understand the scaling laws involved in this type of tests would suggest that full-size airplanes would experience lift loss at much lower rainfall rates than were simulated in the tunnel tests.
(R. Earl Dunham, Jr., 3274)

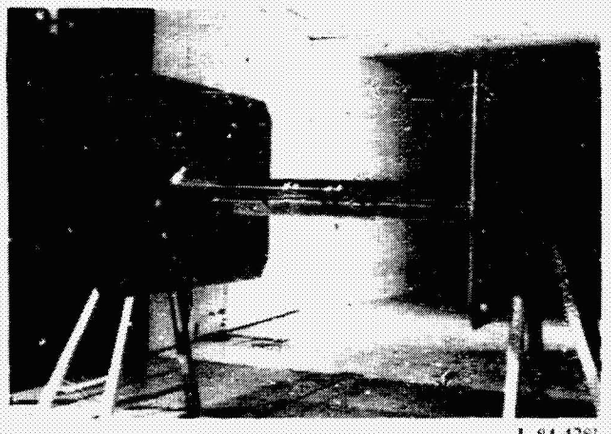

L-84-4281

Model for studying rain effects.

High-Angle-of-Attack Simulation Research on the X-29

The experimental X-29 fighter class airplane brings together for the first time in a single design many different technologies. These include a highly swept forward wing planform, a three-surface pitch

control arrangement (forward-mounted canards, wing flaps, and aft-mounted strake flaps), a high level of static longitudinal instability, and a digital fly-by-wire flight control system, all of which have potentially favorable performance benefits. The high-angle-of-attack aerodynamic characteristics of this configuration have been extensively explored with a variety of wind tunnel test techniques. However, the overall flight characteristics of an aircraft as unstable as this configuration are equally dependent on both the aerodynamic characteristics and the flight control system definition. To explore the high-angle-of-attack potential of the X-29, a simulation program is being conducted in the Differential Maneuvering Simulator facility.

The primary purposes of the simulation effort are to document the stability and control characteristics of the aircraft and identify flight control system features required to ensure an effective yet safe operation up to and beyond stall angle of attack. In the study, various flight control system features are investigated with open-loop and pilot-in-the-loop assessments of the flight dynamics and handling qualities.

The configuration exhibits high levels of pitch control authority and is well stabilized in all axes in the low-angle-of-attack regime ($\alpha < 20°$). At higher angles of attack the handling qualities are severely degraded due to the onset of an undamped large-amplitude oscillation about the roll axis. Enhancement of the roll damping through the use of an artificial stability augmentation scheme along with reduction of the effective roll rate command alleviated this problem. The study also showed that the configuration can be maneuvered into an unrecoverable flat spin. This dangerous flight condition can be successfully avoided through the implementation of a spin prevention system.

(Mark A. Croom, 2184)

L-85-773

X-29 airplane during flight test at Edwards Air Force Base.

Effect of Exhaust Plumes on Shuttle Ascent Configuration Aerodynamic Loads

An investigation was conducted in the Langley 16-Foot Transonic Tunnel to determine the effects of exhaust plumes on the aerodynamic loads of the Shuttle ascent configuration. The 0.01-scale model used in the investigation was tested at Mach numbers from 0.80 to 1.25 at angles of attack from $-6°$ to $2°$. The tests were made at a Reynolds number of about 4×10^6 per foot. In the test, solid bodies were used to simulate the jet exhaust plumes. The basic solid-body plume simulators were designed with the use of two axisymmetric theoretical codes. Perturbations of the basic design were constructed to determine the sensitivity of the Shuttle ascent configuration aerodynamic loads to plume shape. From this experimental matrix of plume shapes it was possible to select a plume shape that produced base pressures on the orbiter and external tank which matched flight measured values.

During the test, measurements of orbiter wing shear, bending moment, and torsion as well as elevon hinge moments were made. The results of the investigation showed that the jet exhaust plumes caused increases in wing shear, bending, torsion, and elevon hinge moments.

(Lawrence E. Putnam, 2673)

L-84-11,204

Scale model of Shuttle ascent configuration.

Shuttle Ascent Wing Loads

Orbiter wing loads determined from strain measurements in flight indicate differences from those predicted by the wind tunnel data. These differences have caused the launch configuration and trajectory parameters to be altered from those desired for optimum performance.

A program of research was undertaken to resolve these differences and better define the orbiter wing loads. Analysis of the original data identified the lack of Reynolds number simulation and uncertainties in exhaust plume simulation as the prominent deficiencies. Several wind tunnel tests were conducted to evaluate these deficiencies. The 0.01-scale model of the ascent configuration is shown installed in the National Transonic Facility (NTF). The model was instrumented with wing and tank pressures, wing and tank thermocouples, and a wing balance. The solid-body exhaust plume simulators were developed in a test conducted in the Langley 16-Foot Transonic Tunnel. Results from the NTF tests indicated that the plume effects (plumes on and off) had a pronounced effect on wing loads.

(Jerry B. Adcock, 2601)

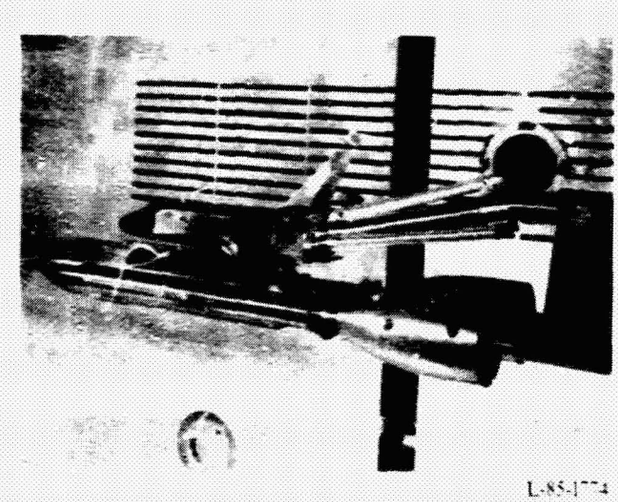

L-85-1774

Scale model of Shuttle ascent configuration mounted in NTF.

Electronics Directorate

The Electronics Directorate is responsible for the planning, direction, and evaluation of research and applications programs in the areas of measurements and computer science which will potentially benefit the Center's aerospace research activities, and for the management of the Center's instrumentation, data acquisition, and data processing resources. The directorate is organized into three divisions with specific support functions.

The Analysis and Computation Division is responsible for the development and application of mathematical and computer theory to the solution of computational problems arising from theoretical and experimental aerospace research activities performed at Langley. Additional responsibilities include conception, design, implementation, and management of advanced centralized data processing systems, flight software systems, and flight simulators, as well as providing consultation on Langley application of computer technology.

The Instrument Research Division provides instrumentation and measurement support for experimental aerospace research activities performed at Langley, with primary responsibility for the instrumentation of ground-based facilities. The division conducts research and development programs in instrument areas where present measurement capabilities are deficient or nonexistent to satisfy both current and future aerospace test program requirements. Additional responsibilities include providing engineering and application expertise to support computer-based data acquisition and control requirements, developing and maintaining measurement standards, calibrating and repairing instruments, and managing an instrument pool.

The Flight Electronics Division is responsible for the development and application of electronic and electro-optical systems for aerospace flight and flight-related projects. The division conducts research and development programs in electronics, optics, lasers, and related disciplines to provide measurement, communication, and data processing systems. Additional responsibilities include design, fabrication, testing, and operation of ground and flight electronic and instrumentation equipment for approved flight projects and applications.

Airborne System Measures Atmospheric Ammonia and Nitric Acid

Although ammonia (NH_3) and nitric acid (HNO_3) are key atmospheric species to an understanding of nitrogen cycle chemistry and photochemistry in the Earth's atmosphere, very little is known about the diurnal, seasonal, and spatial variability and vertical distribution of these species. An airborne system has been developed at Langley which is capable of simultaneous atmospheric measurements of both NH_3 and HNO_3 with sensitivity in the sub-part-per-billion (ppb) range. The system uses hollow collection tubes to preconcentrate NH_3 and HNO_3 by selective adsorption on tungsten oxide coated surfaces. The adsorbed gases are released by controlled application of heat to the collection tube, converted by catalytic reaction to nitric oxide (NO), and detected in an NO chemiluminescent analyzer.

An order of magnitude improvement in measurement time over previous filter techniques was demonstrated. This improvement enabled near real time airborne measurements over the pertinent atmospheric scales. To achieve this sensitivity and response, the collection efficiency and the signal noise response of the detection system were maximized and the effects of gas sample interactions with transfer lines and other surfaces were minimized.

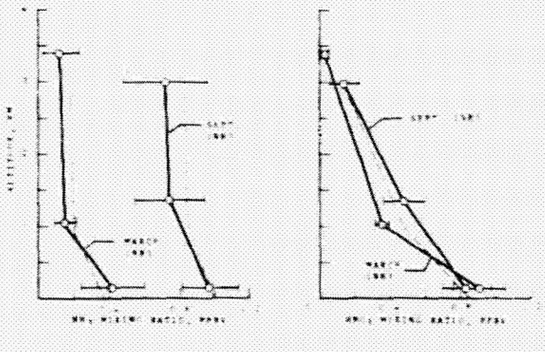

Vertical profiles (left) and seasonal variation (right) of tropospheric ammonia and nitric acid over coastal Virginia and Maryland. Dashed lines are results of photochemical calculations.

With this instrument, the first simultaneous measurements of NH_3 and HNO_3 in the rural troposphere were made from an aircraft over coastal Maryland and Virginia in March and September 1983. These profiles, taken at altitudes from 150 to 3000 m, show NH_3 and HNO_3 mixing ratios that decrease with altitude. Ammonia profiles show substantial seasonal variation, with lower concentrations in March, whereas nitric acid profiles show essentially no seasonal variation. These profiles were analyzed with a one-dimensional photochemical atmospheric model to study loss mechanisms for NH_3 and HNO_3 in the atmosphere.
(Peter J. LeBel, 2818)

Elucidation of Oxygen-Silica Reaction Rates and Mechanisms With Stable Isotope Mass Spectrometry

Thermal insulation for reusable space vehicles such as the Space Shuttle is accomplished by use of ceramic tiles made of 99.8 percent silica, which reduce the heat of reentry because they are partially noncatalytic to atom recombination. A laboratory test was conducted to determine the reaction rate constants of oxygen interactions with silica surfaces. Both catalytic exchange at the surface and exchange with the surface were measured at high temperatures by means of stable isotope mass spectrometry.

Results indicated that both oxygen interactions (catalytic exchange at the surface and exchange with the surface) followed a second-order rate law. The activation energy obtained for amorphous silica was 31.8 kcal and that for quartz was 58 kcal. The proposed mechanism for the reaction with the quartz surface is adsorption of $^{18}O_2$ on the surface, followed by reaction of $^{18}O_2$ with the surface and the adsorbed species to form oxygen with mass 34. The proposed mechanism for reaction with amorphous silica indicates a more complex interaction. A reaction with the surface, which produces exchanged molecular oxygen with mass 34, is followed by a catalytic exchange at the surface, which produces oxygen with mass 34. This oxygen in turn reacts with the surface to produce a labeled surface and gaseous $^{16}O_2$.
(Carmen E. Batten, 2466)

Quantitative Thermal Diffusivity Tensor Measurements for NDE of Composites

A radiometric technique has been developed at Langley to measure the thermal diffusivity tensor components in the plane of a graphite-epoxy composite plate. The technique has been shown to have strong potential as an NDE nondestructive evaluation tool to image broken fiber damage in composites. At present, no satisfactory NDE technique is available for rapid imaging of large composite structures in field settings. This technique has the potential to satisfy these demands with a noncontacting one-sided quantitative measurement of a material property.

The technique utilizes a remote laser heat source and a scanning infrared radiometric detector. A sample is heated and the time evolution of the resulting temperature distribution is measured and recorded. The one-dimensional thermal diffusivity is then extracted from the temperature measurements. The orientation of the source can be changed to measure the prime diffusivity components in the plane of the sample. Since the diffusivity along the fibers is much greater than that perpendicular to the fibers, information about the condition of the fibers can be obtained. The technique has been shown to give quantitative diffusivity measurements that are accurate to within 2 percent for composite materials. Diffusivity measurements have been made which illustrate a factor of 7 change between the components perpendicular and parallel to the fibers in a unidirectional composite. The functional dependence of diffusivity with angle to fiber direction has been shown to agree closely with $\cos(2a)$, where a is the angle to the fiber direction. In addition, diffusivity measurements have been made of a composite sample with cut fiber damage. A 13-percent decrease in diffusivity was observed between the cut fiber region and the intact region.
(D. Michele Heath, 3036)

Development of Ultrasonic Ice Detection System

Icing conditions represent one of the most severe weather hazards encountered during aircraft flight

and one of the hardest weather conditions to forecast accurately. The potential for aircraft icing exists whenever an aircraft encounters liquid moisture at outside temperatures at or below the freezing point. Any exposed surface on an aircraft is subject to icing, with a subsequent change in lift characteristics due to drag forces. A practical ice detection warning system would be useful to warn pilots when icing conditions are encountered.

The feasibility of using a pulsed-echo ultrasonic system to detect ice on an airfoil has been investigated. Initial tests were conducted in a laboratory experiment that used refrigerated ice on an aluminum surface. Tests were conducted with both compressional and shear waves at a test frequency of 5 MHz. The figures show how sound wave reflections are detected at the interface of aluminum and ice and at the interface of ice and air. In each figure, ΔT_1 represents the time required for a compressional wave and a shear wave to travel through a 20-mm-thick type 7075 aluminum, and ΔT_2 represents the time required for a shear wave and a compressional wave to travel through ice 6.1 and 4 mm thick, respectively. From these and other measurements, it was determined that the speed of sound in refrigerated ice was approximately 1.93 mm/μsec for a shear wave and approximately 3.98 mm/μsec for a compressional wave.

Data obtained from these laboratory studies showed that ultrasonics can be used to detect icing on a surface. This technique could be used in the aircraft industry with the incorporation of electronic signal processing to determine the growth rate of ice on an airfoil.

(Alphonse C. Smith, 3036)

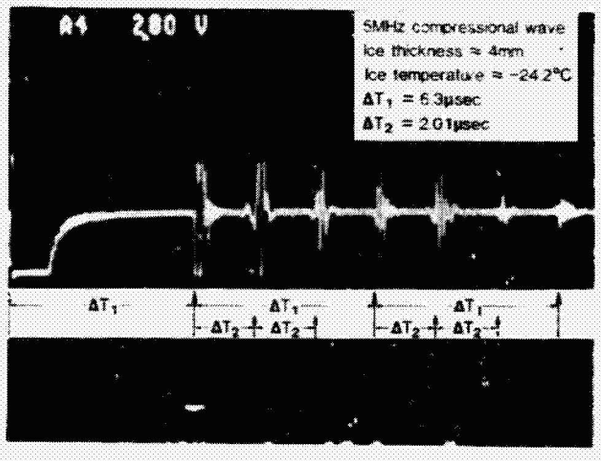

Laboratory test of pulsed-echo ultrasonic system.

Time Gain Compensation Circuit for General Use in NDE and Ultrasonics

A high-frequency time gain compensation circuit was designed and built for a wide variety of applications in nondestructive evaluation (NDE) and ultrasonics measurements. The circuit features a wide signal bandwidth (in excess of 50 MHz) and a large dynamic range (greater than 50 dB). The control bandwidth of 5 MHz assures accuracy to the control signal. The signal-to-noise ratio is 100 dB.

The circuit is presently being used in a number of applications. In one case, its use permits retrieval of more information from ultrasonic signals sent through composite materials, which are highly attenuating. Another application has been in the use of ultrasonics to measure the depth of skin burn in humans. The circuit affords the wide bandwidth necessary for adequate resolution of burn depth while compensating for the large high-frequency ultrasonic attenuation of human skin.

The figure shows a typical pulse echo pattern received after an ultrasonic tone burst has been sent through an aluminum sample. The tone burst patterns decay nearly exponentially. The middle trace is the control signal, which is designed to offset the exponential decay. The bottom trace shows the effect of "removing" the exponential decay.

(W. T. Yost, 3036)

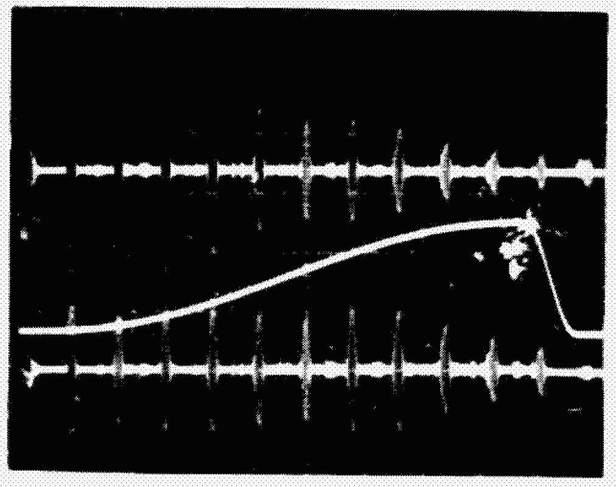

Typical pulse echo pattern.

Laser Transit Anemometer Measurements in Supersonic Boundary Layer

Langley, NASA Lewis Research Center, and the Air Force Arnold Engineering Development Center (AEDC) are participating in a 3-year collaborative research and development program to investigate the laser transit anemometer (LTA) nonintrusive measurement technique and develop an advanced prototype instrument for future aerodynamic research. One of the significant results of the first year's effort has been the completion of a successful joint test program conducted in the AEDC Supersonic Tunnel A with the Langley LTA instrument.

The primary purpose of this test was to explore the potential of the LTA technique to measure supersonic laminar and turbulent boundary layer velocity profiles. A 7° (half angle) sharp-cone model was selected for this experiment. It was tested at Mach 4 with free-stream Reynolds numbers of 0.6 and 3 × 10^6 per foot at zero angle of attack. The cone model was extensively instrumented to measure surface temperature, pressure, and heat transfer distributions. In addition, the LTA measurements were supported with high-precision pitot/total temperature survey rake measurements. The figure shows a comparison of LTA data taken in a laminar boundary layer region with pitot measurements and a theoretical velocity profile. These data clearly show the high spatial resolution and accuracy potential of the LTA nonintrusive measurement technique as well as the undesirable flow disturbance produced by the intrusive pitot pressure probe. This joint experiment represents the first use of the LTA technique for supersonic boundary layer velocity measurements at AEDC.
(William C. Honaker, 2791)

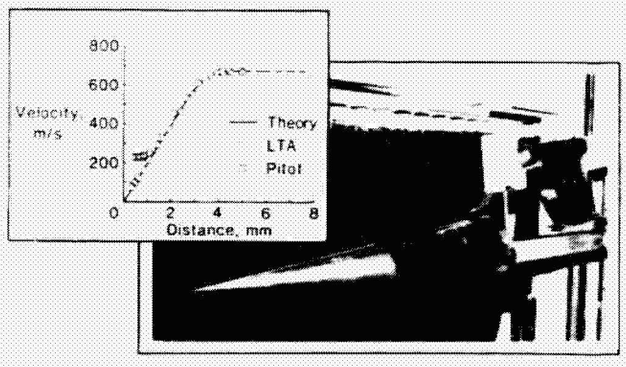

Laser transit anemometry.

Statistical Modeling of Wind Gusts

Three existing statistical techniques have been combined to develop a method for modeling wind gust components. The method uses a statistical approach because of the random nature of the gusts. In the first step of the method, a principal components (PC) analysis is applied to the three gust components. The PC analysis rotates the components to a new axis system, which is aligned with the major variations in the measured gusts and simultaneously removes correlations between the components. An autoregressive integrated moving average (ARIMA) model can then be individually fit to each new component with the use of standard Box-Jenkins methods. It is usually assumed that the residuals remaining from the ARIMA fit have a Gaussian distribution. The new method provides for the use of a generalized probability distribution to model the residuals if their statistical properties are non-Gaussian. To generate simulated gust components, the preceding steps are reversed. Random residuals are generated and input to the three ARIMA component models, and the inverse PC transformation is applied to rotate to the original gust axes.

The new method was tested on gust components measured during flights of an F-106B into severe storm centers. The figure shows one of the horizontal components (U) generated with the statistical model.
(James R. Schiess, 2747)

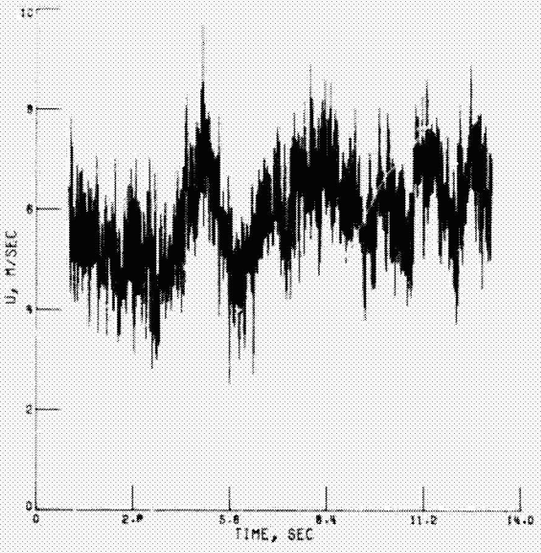

Simulated horizontal wind gust component.

Rational Spline Interpolation of Surface Data

A standard method for interpolating surface data is the bicubic spline function. Unfortunately, if the slope of the data changes drastically, the interpolating surface may exhibit fictitious fluctuations. H. Spath, of the Universität Karlsruhe, developed the interpolating rational spline, which incorporates a single tension parameter for the entire surface. As the tension parameter increases, the interpolating surface increasingly resembles the interpolating bilinear surface.

Recently, an algorithm for a multiple-tension parameter interpolating rational spline surface was developed at Langley. This version of the rational spline provides a distinct tension parameter for each subinterval along the x and y axes; in this way, local behavior of the surface can be controlled. The figure illustrates reduction of the fluctuations of a surface that represents terrain elevations. Tension was applied to only three subintervals parallel to and neighboring the ridge at $x = 1800$.

(James R. Schiess, 2747)

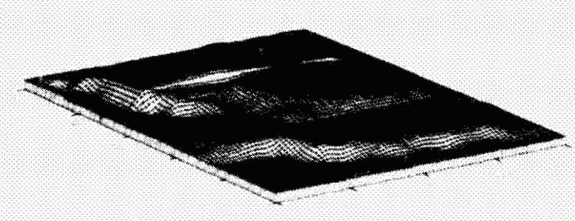

Rational spline interpolation applied to terrain elevations.

Grid Generation for Aerodynamic Applications

An algebraic procedure for the generation of boundary-fitted grids about high-speed aerodynamic configurations has been developed at Langley. An aerodynamic configuration is initially defined in the Langley standard format in terms of cross-sectional coordinates of each component of the configuration (fuselage, wing, and canard, in the present state of development). The cross-sectional data are fitted with cubic splines to determine derivatives at the defining points. Cross section points and derivatives at the points for each component provide data for "coons' patch" descriptions of the components. For high-speed aerodynamic configurations in which the wing and canard are thin, grids are determined in cross sections perpendicular to the x axis.

A distribution of cross sections is chosen and the intersection of planes along the distribution and the patch descriptions of the components are computed to form the inner boundary for the grid. The outer boundary is presently described by circular sections, and the two-boundary technique is used to compute the interior grid with desired concentrations, such as those near the solid surfaces. In the present development, the grid is divided into two parts: a grid above the wing and canard, and a grid below the wing and canard. Supersonic flow field calculations have been made in the fuselage-canard region. The pressure on four surfaces for a Mach 3 solution is shown in the figure.

(Robert E. Smith, Jr., 3978)

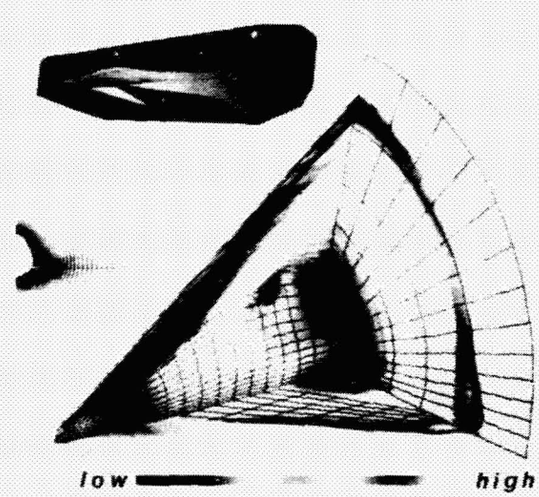

Model, grid cross section, and pressure solution.

Laboratory Technique for Detection of Composite Fiber Damage

A laboratory technique has been developed for detection of fiber damage in graphite-epoxy com-

posites. The technique couples electric current into the graphite fibers and maps the resulting magnetic fields. The technique differs from eddy-current techniques in that the current is coupled directly to the fibers and is not an induced current. Because of this, the "skin effect" does not limit the depth of inspection. The magnetic field is detected with an air gap toroid and a high-gain synchronous amplifier. Since broken fibers appear as disruptions in conductivity paths, detected field gradients are directly related to broken fibers.

This technique has been used to detect back-surface holes 0.25 mm deep and 1 mm in diameter in a 2-mm-thick composite sample. Subsurface defects of various sizes have also been detected. Work is being performed to make this laboratory technique into a practical method of material evaluation.
(Travis N. Blalock, 3036)

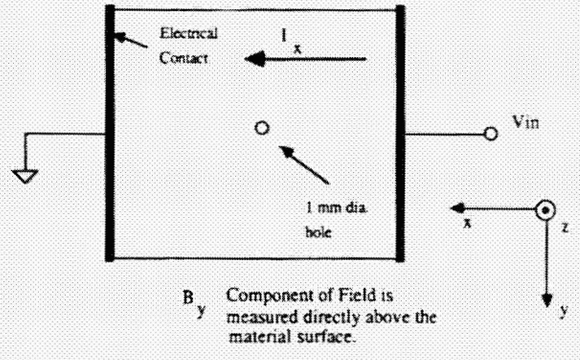

Schematic of magnetic field image.

Magnetic field image of 1-mm-diameter hole.

Correction for Energy Shadowing of Defects in Ultrasonic Scan Data

Conventional ultrasonic investigation of defects in the bulk of complex materials is a common industrial technique. A usual procedure is to scan the specimen in a water bath, where the ultrasonic transducer transmits waves into the investigated material. When the propogating waves reach acoustical discontinuities such as defects, partial reflection occurs. The reflected waves are detected by the transducer, and a graphical representation of the integrity of the specimen is displayed. Some advanced systems even correct for simple attenuation.

However, this method has a major drawback. As the waves continue to propagate through the material, any major reflection causes reduction in the transmitted wave. This effect, which may be even more dominant than the simple attenuation, causes any further reflections to appear weaker than they actually are. This effect thus misrepresents the defects that are "shadowed" by previous defects.

A numerical algorithm developed at Langley enables the correction of such shadowing by digital signal processing. This algorithm is fast and simple enough to be adopted for real-time applications in industry. The figure shows an example of such a correction. Deep reflections, which look very small in the raw data (represented by weak amplitudes, late in time, in the top figure), show up much stronger in the corrected case (bottom figure). Images of material defects with the shadowing corrections permit more quantitative interpretation of the material state.
(Joe Heyman, 3036)

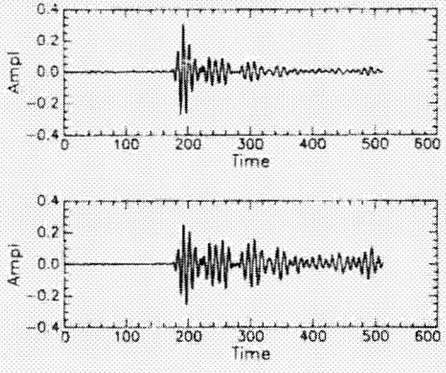

Ultrasonic reflections before (top) and after (bottom) digital signal processing.

Digital Enhancement of Flow Field Images

Significantly enhanced flow visualization has been achieved at Langley by the application of digital image processing techniques to photographs of wind tunnel experiments. The photographs are typically low contrast, and smoke is used to highlight the flow field features. Of particular interest are the size, shape, and location of vortex cores before and after they interact with an airfoil.

The photographs are taken with a 70-mm-film camera and then digitized into a 2048 × 2048 pixel image with an Eikonix 78/99 digitizing camera, which has an eight-bit gray level resolution per pixel. Digitization takes several minutes per photograph. The digital images are then processed with a variety of enhancement techniques to fulfill the objectives of improving the contrast, highlighting key vortex structural features, and producing useful publication quality images. Contrast is improved by the application of linear contrast stretching to use the full range of possible gray levels. Low-pass filtering is used to suppress noise and graininess induced by the digitization process. Selective gray level regions are then mapped to black to produce a contouring effect and highlight structural features within the vortices. Enhanced images can also be displayed as black-on-white contour plots or as pseudo-color images.

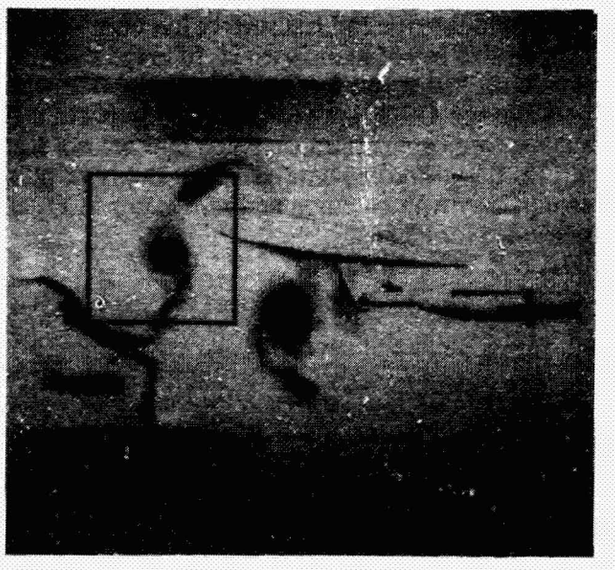

Typical low-contrast flow field photograph.

Previous methods of analyzing this type of data by hand with a digitizing tablet and visual estimation of gray level boundaries were slow and inaccurate given the low contrast of the original images. In contrast, the digital enhancement technique is performed interactively in minutes with a Gould IP8500 image processing system and special software written by Langley personnel. Input and output images can be in the form of negatives, positives, or video tape.
(R.A. Kudlinski, 3434)

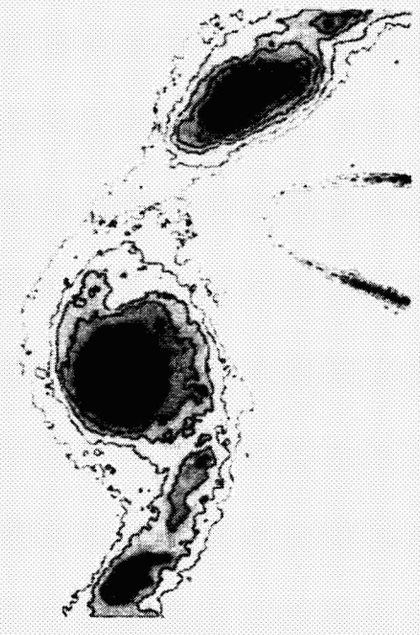

Enhanced digital image of vortex indicated in previous figure.

Tunable Solid-State Laser Materials

Remote sensing of atmospheric constituents by laser detection and ranging (lidar) from spacecraft and airborne platforms requires a laser system that is efficient, tunable, stable, and capable of unattended operation for extended periods of time. A key element of a tunable lidar system with these characteristics is a solid-state material capable of lasing over a broad wavelength range. The absorption and fluorescence characteristics of potential laser ions and materials can be measured over a wide temperature range. The

results of these measurements will yield information directly related to practical laser parameters and basic laser mechanisms. For example, materials that exhibit broad fluorescence emission will also be capable of tunable laser operation over a wide wavelength range. Very low temperature operation permits evaluation of the basic solid-state phonon mechanism for laser tuning.

The absorption and emission of a range of host materials, including titanium dioxide, strontium titanate, and sapphire in combination with the ions of chromium, titanium, iron, and nickel, have been investigated for the first time over a temperature range from 13 K to 580 K. The most promising tunable solid-state laser material to date is titanium doped into sapphire. The figure shows room temperature fluorescence emission spectrum and laser gain as a function of tuning range, predicted from this emission curve. This material will lase continuously over wavelengths ranging from 700 nm to beyond 950 nm. This wavelength range includes important absorption lines of water vapor, which can be used to obtain atmospheric pressure and temperature profiles.
(Charles E. Byvik, 2818)

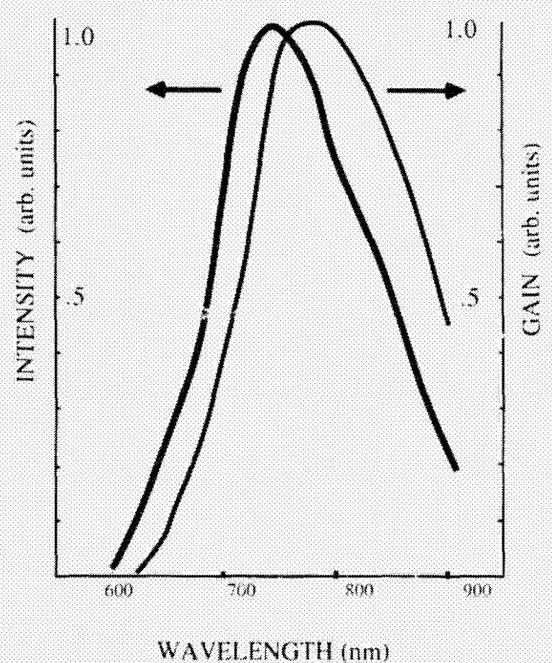

Fluorescence intensity and laser gain plotted against wavelength for titanium doped sapphire at room temperature.

Development of Low-Temperature Catalysts for Long-Lifetime Closed-Cycle CO_2 Laser Operation From Satellites

CO_2 Doppler lidar shows great promise for satellite-based wind velocity measurements. For such application, CO_2 lasers must have long lifetimes, and because of satellite constraints they must be operated closed cycle. However, electric discharge excitation of such lasers causes some dissociation into O_2 and CO, and the resultant O_2^- ions can decrease laser power and lifetime. The concentration of O_2 must be minimized by recombination with CO as rapidly as dissociation occurs. The problem is to develop catalysts for efficient recombination of CO and O_2 which operate at sufficiently low temperatures to minimize catalyst heating.

A platinum dispersed on SnO_2 catalyst has been extensively studied in a laboratory reactor system at Langley and a method of scaling the results to lasers of known properties has been derived. Virtually 100-percent conversion efficiency of CO and O_2 to CO_2 has been achieved in this system at 100°C. Furthermore, recent results have shown that suitable pretreatment of the catalyst with CO increases its efficiency by 75 percent. A corresponding decrease in required catalyst weight is projected. The CO-pretreated catalyst has been tested in the laboratory for 12,000 minutes (equivalent to 7×10^6 pulses in a 10 pulse/sec laser) with minimal loss of efficiency. In related studies, the catalyst surface has been successfully treated by reduction with H_2 followed by oxidation with $^{18}O_2$ to prevent isotope scrambling when rare isotope $C^{18}O_2$ is used. $C^{18}O_2$ is important to enhance atmospheric transmission and aerosol scattering. Long-lifetime catalyst tests in a high-pulse energy laser with common and rare isotope CO_2 are scheduled for FY86.
(David R. Schryer, 2818)

Calibration System for ERBE Instruments

The Earth Radiation Budget Experiment (ERBE) includes a complement of two multichannel radiometers (a nonscanner and a scanner) designed to make highly accurate measurements of the Earth's reflected and emitted radiation and incident solar

radiation. The instruments are being flown aboard two orbiting spacecraft, the Earth Radiation Budget Satellite (ERBS) in a 57° inclination orbit, and the NOAA 9 satellite in a Sun-synchronous orbit.

The nonscanner provides Earth-viewing spectral coverage from 0.2 to 5.0 μm (shortwave) and 0.2 to greater than 50.0 μm (broadband). The solar output monitor is a shuttered version of the Active Cavity Radiometers (ACRs) used in the Earth-viewing channels. The scanner, which covers the shortwave, broadband, and longwave bands, scans across the Earth once every 4 sec.

To accurately calibrate the ERBE instruments, a ground calibration chamber was constructed which contained several unique advanced development concepts in radiation sources. A wide-field blackbody and integrating sphere were designed to mount in the chamber so that accurate measurements of radiation with respect to a reference standard could be made by the instruments in vacuo. The ERBE instruments also contain simila, internal sources which permit calibration checks during orbital operation. In addition to having internal checks on both shortwave and longwave calibration, both instruments regularly view the Sun for a solar calibration. The nonscanner Earth-viewing detectors accomplish this by rotating on a single-beam assembly to view the Sun through four ports that limit the detectors' field of view. The scanner detectors view a unique mirror attenuator mosaic (MAM) designed to diffuse incident solar radiation independently of angle over the MAM field of view.

Calibration of both the nonscanner and the scanner was accomplished to an accuracy of less than 1 percent with a precision of better than 1.0 W m^{-2} with these developments.

(Leonard P. Kopia, 2307)

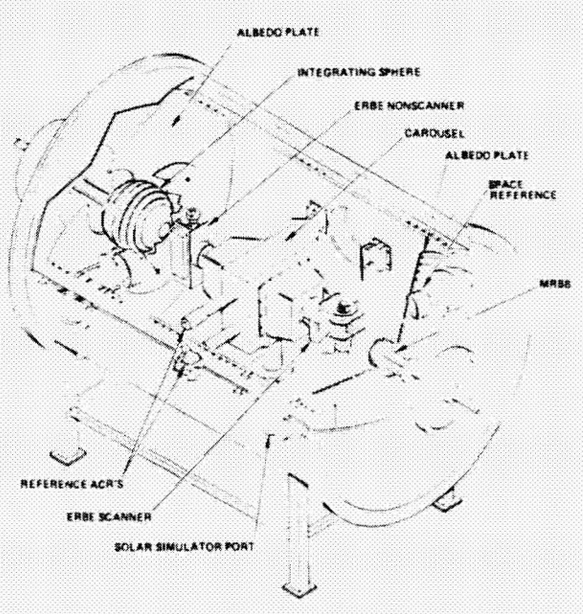

Ground calibration chamber.

Alignment of HALOE Infrared Optical Instrument

HALOE (Halogen Occultation Experiment) is a multispectral absorption radiometer and gas filter correlation radiometer. Orbital measurements of limb absorption profiles can be inverted to give atmospheric gas concentrations when the Sun is tracked during occultation events. These gas concentrations will provide science data for pollution monitoring, weather, and climate studies.

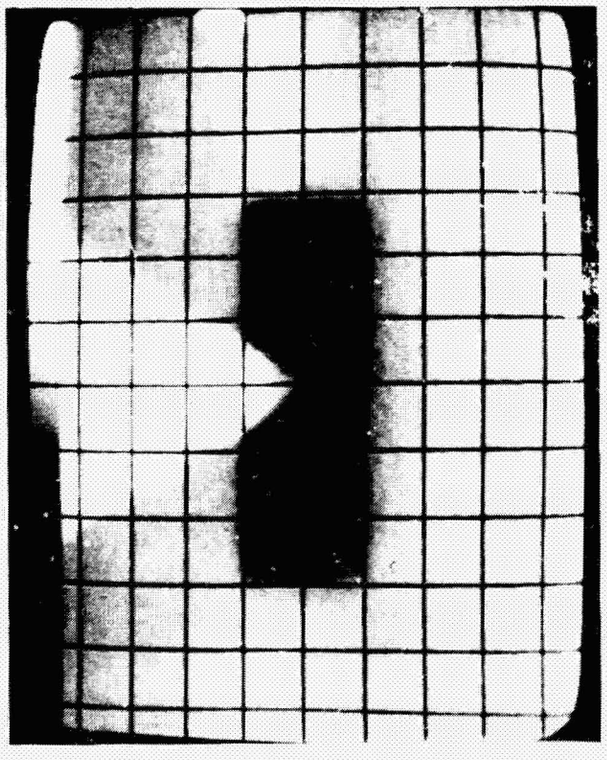

HALOE thermal field stop image (dark rectangle) aligned to mechanical pin (light triangle).

The image-forming optical elements in the HALOE instrument are constructed of visually opaque germanium. Specially modified infrared thermal imaging devices were used to develop techniques to complete the optical alignment of the HALOE instrument. Commercially available and in-house developed infrared lenses were used with an available thermal imaging camera. With this device, thermal images and beams in the 2- to 11-μm spectral region could be viewed on a standard TV monitor. The mechanical image or beam position was established with precise fixtures and reticles, and the thermal imaging device was used to superimpose the thermal image, or beam, at the proper mechanical location. In all cases, the image or beam was located within ± 50 μm. The number of optical elements aligned with this novel technique exceeded 100. The figure shows the instrument's thermal field stop image being aligned to a precisely located mechanical pin.
(Joseph H. Goad, 3761)

Flight Systems Directorate

The Flight Systems Directorate conducts basic research and development in the broad, multidisciplinary area associated with aerospace flight systems. This includes systems hardware and software architecture concepts and design guidelines, validation and verification methods for reliable flight control systems, advanced cockpit interfaces, advanced airborne systems technology, aircraft operating procedures, fundamental electronics research, automation and robotics technology, and aircraft and spacecraft guidance and control system design methods, guidelines, and criteria.

The Advanced Transport Operating Systems Program Office coordinates a wide-scale focused technology research and development effort aimed at developing and improving the technology base for transport aircraft operating systems and the integration of these systems with the current and future air traffic control environments. The office also provides a focus for research and development of improved airborne operations and procedures and operates the NASA Boeing 737 aircraft and associated simulator.

The Information Systems Division conducts research to provide an advanced technology base for future spacecraft and aircraft systems. Specifically, the division performs research in the areas of robotics and automation, fault-tolerant systems validation, reliable software, system architectures, electronic/optical subsystem technology, and software engineering. The scope of activities is broad and encompasses both the highest level systems considerations and the investigation of solid-state physics phenomena.

The Guidance and Control Division conducts generic and applied research on aircraft and spacecraft guidance, control, and antenna systems. The research is directed toward the development of a technology base for advanced aircraft and spacecraft systems analysis and design methods, including validation and verification demonstrations of advanced concepts. The division also develops multidisciplinary computer-based tools and techniques which allow appropriate guidance, control, and antenna design issues to be considered through all stages of aircraft and spacecraft design.

The Flight Management Division conducts research to provide a viable technology base for future aircraft and spacecraft flight management systems. Specifically, the division provides technologies required by designers of crew station systems; defines and evaluates improved guidance and control procedures; and studies advanced airborne systems technology, traffic control strategies, and operating procedures for improving the efficiency of air traffic control operations. In addition, the division provides methodologies and criteria for measuring crew workload and stress.

Controls/Structures Interaction Study for Proposed Space Station Configurations

A study was made to investigate the dynamic response of two proposed space station configurations subjected to several expected external and active controller disturbances. The objective of the study was to obtain controls/structures interaction comparisons between the 9- and 15-ft bay models of the 75-kW power tower space station configuration. The finite-element models used in the analysis included the first 100 natural vibration modes and frequencies for each configuration. The disturbance conditions investigated were crew motion, orbit reboost, shuttle dock, and attitude control commands.

DISTURBANCE	CONFIGURATION	PEAK DISPLACEMENTS, IN.			PEAK ACCELERATIONS, g's($\times 10^{-3}$)		
		EXPERIMENT MODULE	SOLAR ARRAY TIP	CMG LOCATION	EXPERIMENT MODULE	SOLAR ARRAY TIP	CMG LOCATION
SHUTTLE DOCK	15 foot	.05	.80	.08	151.	984.	272.
	9 foot	.10	1.05	.10	162.	362.	80.
CREW ROTATION	15 foot	.0021	.0119	.0025	12.5	14.2	9.47
	9 foot	.0072	.060	.0046	18.2	31.8	5.73
ORBIT REBOOST	15 foot	.34	2.06	.21	191.	1110.	928.
	9 foot	.33	3.68	.24	6.8.	2780.	576.
1° ATTITUDE COMMAND	15 foot	.0002	.014	.0018	.856	9.47	4.74
	9 foot	.0085	.018	.0022	.997	10.90	4.91

Dynamic responses for 9- and 15-ft bay models.

Typical results from the study are given in the table. Shown are peak displacements and accelerations at the experiment module, the solar array tip, and the control moment gyro location for both space station models. Peak deflections were generally larger for the 9-ft model. No consistent trend existed to distinguish between the two models based on peak accelerations. With the exception of the attitude command maneuver, the $10^{-5}g$ requirement proposed for micro-g experiments was violated at the experimental module for all disturbances. No significant controls/structures interactions were found for either model when control moment gyros were used for attitude control because the rigid body control frequency was low compared to the fundamental structural frequencies. Reboost maneuvers resulted in controls/structures interactions but no instability in structural deflection was observed.
(John W. Young, 4591)

Vectorization of Equilibrium Air Chemistry Code

An equilibrium air chemistry code that is widely used within NASA and the university community has been vectorized to run efficiently on the VPS-32 vector computer at Langley. The original subroutine was developed by Dr. John Tannehill of Iowa State University and consists of a series of curve fits to determine pressure and sound speed over 15 regions of density and internal energy.

This type of computation is serial in nature and executes only at scalar speeds on the VPS-32. This subroutine has been rewritten to make it amenable to vector computation. The vectorization approach has been to make a single call to the new subroutine with the density and internal energy at each of the N grid points, sort the N points into 15 groups, one group for each region, do the vector computation for each group, and finally re-sort the results back into the order of the input.

The speedup over the scalar code depends on the average vector length used, which in this case is approximately N/NG where $NG \leq 15$ is the number of regions containing points. The efficiency, therefore, increases with N and is higher when the points fall in only a few regions. To further increase the efficiency, the serial subroutine is called by the vector subroutine whenever a region has only a few points. Limited experience indicates that for $N > 1000$, a speedup by a factor of 5 to 15 can be achieved, depending on the distribution of points.
(Jules J. Lambiotte, Jr., 4612)

Efficient Estimation of Nonlinear Airplane Parameters From Flight Data

Parameter estimation techniques used to determine aircraft stability and control parameters from flight data are well established for linear flight regimes. In the nonlinear regimes, as in high-angle-of-attack conditions, the aerodynamic model can be a complex function of states and control inputs. In the nonlinear case two different but closely coupled problems occur. First, the best mathematical representation (model structure) must be determined. Second, model parameters (aerodynamic derivatives) must be estimated for the chosen model structure. Model structure and model parameters may change rapidly throughout the nonlinear flight regimes, and as a result, substantial computational effort is required to obtain unbiased minimum-variance parameter estimates. A commonly used estimation technique is maximum likelihood (ML) in conjunction with a modified Newton-Raphson (MNR) optimization. This approach requires that a large set of sensitivity equations be analytically derived in advance for each new model structure and integrated at each iteration.

An algorithm for efficient maximum likelihood (ML) estimation has been developed at Langley which relies on a new optimization method referred to as a modified Newton-Raphson with estimated sensitivities (MNRES). MNRES capitalizes on an efficient method of approximating the sensitivities. The sensitivities are determined with slope information from local surface approximations of each output variable in parameter space. The fitted surface allows sensitivity information to be updated at each iteration with less computational effort than either a finite-difference method or integration of the analytically determined sensitivity equations. Because MNRES eliminates sensitivity equations, algorithm reformulation is eliminated for each new model and a flexibility is provided to use model equations in any format. The accuracy of ML/MNRES is equivalent to that of ML/MNR. The greater speed of ML/MNRES compared to that of ML/MNR is shown in the figure by a comparison of convergence

criterion and central processing unit (CPU) time. ML/MNRES has been found to be very effective in aircraft parameter estimation and flight data compatability analysis.
(Patrick C. Murphy, 4681)

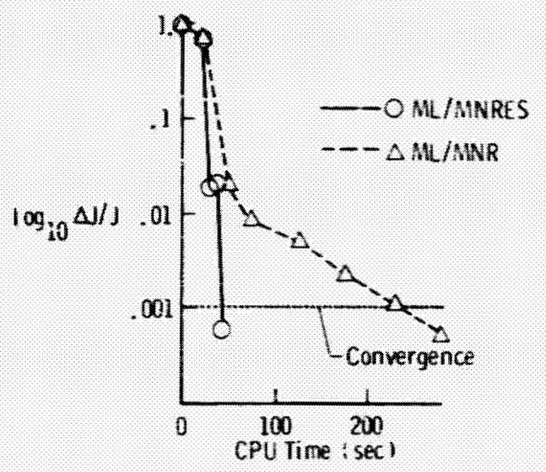

Convergence criterion ($\log_{10} \Delta J/J$) versus CPU time for two maximum likelihood estimation algorithms for modified Newton-Raphson (MNR) and modified Newton-Raphson with estimated sensitivities (MNRES) optimization schemes. Each is applied to flight data from an advanced twin-engine fighter.

model which spontaneously entered large uncontrolled lateral oscillations during a flight in which control inputs were designed according to results from static and oscillatory wind tunnel tests. The recorded data from that flight were provided to Langley researchers to aid in determining the cause of the instability that led to the oscillations.

The flight data were analyzed with the Langley developed stepwise regression and data partitioning methodology. That methodology partitions the entire data set into smaller subsets that span limited angle-of-attack ranges and then uses a modified stepwise regression algorithm to determine an adequate mathematical aerodynamic model in terms of stability and control derivatives. The figure indicates the results obtained for the damping in roll derivative C_{l_p} from the flight data compared with results from both oscillatory and rotary balance wind tunnel tests. The flight test analysis indicates a total loss of roll damping in the test region. Subsequent rotary tests tended to verify this loss of damping. Hence, the proper analysis of model flight test data can indicate regions of departure instability which are not predicted in standard oscillatory wind tunnel tests and thus contributes to control law design and enhanced safety of the flight vehicle. This particular study led to an intensive wind tunnel investigation of the region of indicated instability.
(James G. Batterson, 4591)

Parameter Estimation Applied to Data From Free-Flight Research Model at High Angles of Attack

Control of modern high-speed aircraft and in particular prevention of departure from controlled flight is accomplished with the aid of computerized flight control systems (FCS). The control laws programmed into the FCS must be based on a correct mathematical model of the aerodynamic forces and moments throughout the aircraft's operating envelope.

Historically, these control laws were designed from results of wind tunnel tests and theoretical predictions. However, such data may be inadequate to predict potentially catastrophic dynamic behavior of a vehicle in flight. This was vividly demonstrated by a Royal Aircraft Establishment free-flight research

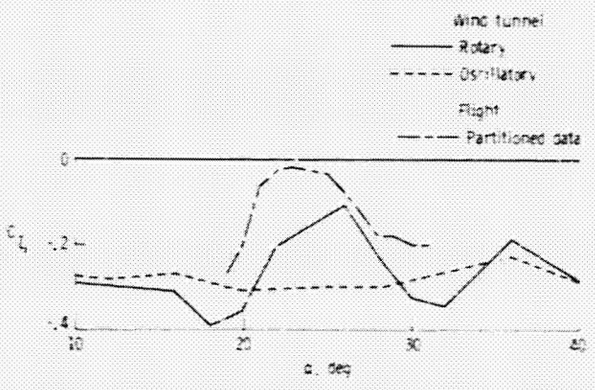

Damping in roll derivative C_{l_p} estimated from flight data compared with rotary and oscillatory wind tunnel derived values.

Unified Analysis Methods for Fault-Tolerant Redundant Strapdown Inertial Measurement Unit

Considerable attention is being given to the use of a redundant strapdown inertial measurement unit (RSDIMU) for aircraft as a source of sensor information vital to the flight control, display, and navigation systems. Safety, performance, and reliability considerations for these flight-crucial sensors dictate a high level of redundancy, which an RSDIMU with an optimal array of sensors and efficient redundancy management algorithms can satisfy. Failure detection and isolation (FDI) algorithms have been developed to ensure the transfer of valid information to the elements of the integrated avionics system in an environment that includes vehicle maneuvers and turbulence.

A unified analysis to identify and assess critical areas of reliability and fault-tolerant performance for the RSDIMU has been developed. A 27-state Markov reliability evaluation model defined in terms of the operational states of the RSDIMU has been developed to assess the correct and incorrect decisions of the FDI system with regard to detection and isolation of failures, false alarms, missed detections, failure rates, damage, and mission time.

An indication of the usefulness of this analysis tool is shown in the figure. The plots indicate the need for sensitivity to sensor failure and coverage in the FDI system. The results indicate the advantage of the development of FDI techniques with improved reliability as the product.

(Frederick R. Morrell, 3291)

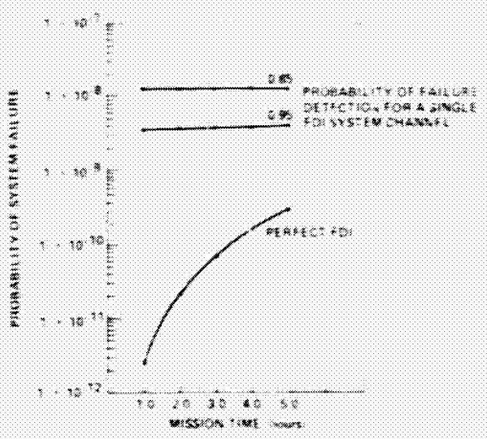

Probability of system failure vs mission time.

Model for Analyzing Effects of Coincident Errors on Multiversion Fault-Tolerant Software

The application of redundancy has long been established as an effective method of increasing the reliability of hardware systems. Dissimilar redundancy applied to software, known as fault-tolerant software, is a relatively new and untested technology motivated largely by the need for high reliability in life-critical applications such as flight control. Under the assumption that software errors will occur randomly in independently designed replicate software codes, existing models project large gains in reliability as the level of redundancy increases. However, empirical evidence suggests that joint errors among software components, referred to as coincident errors, are not randomly distributed, and thus there is a clear need for alternatives to models which assume independent failures of the component versions.

A model was recently developed at Langley to study the failure probability of multiversion software systems in which the component versions give rise to coincident errors. The model directly links certain basic quantities with the experimental process of testing software components and thus provides a probabilistic framework for empirically evaluating the strategy of software redundancy. Moreover, the

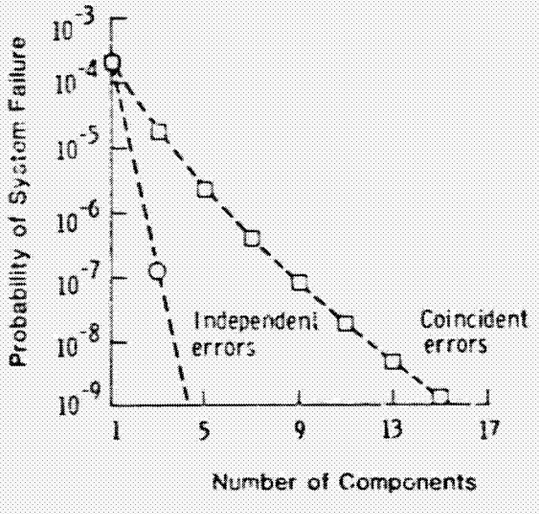

Example of significance of independence assumption on failure probability of multiversion software.

model permits an analytical study of the effects of coincident errors and provides new insight into the reliability gains that can be achieved with software redundancy. For example, it is well known that if failures are assumed to be independent (as with hardware devices), then an average component failure probability of less than 0.5 implies that on average, redundancy improves reliability. However, for the analogous redundant software system, this condition is not sufficient. A stronger condition suggested by the new model (the intensity distribution of coincident errors bounded by 0.5) implies that a multiversion software system is a better strategy than reliance on a single version of software. Even under this condition, however, the model shows that the reliability gains may not approach the gains suggested by models that assume independent component failures.
(Dave E. Eckhardt, Jr., 3681)

Advanced Navigational Interface for Modern Transport Aircraft

As part of the Crew Station Technology research effort to integrate and consolidate information management systems, an advanced concept for managing the navigational tasks of a modern transport aircraft was studied in a flight simulator environment. This concept emphasizes the simplification of the pilot interface.

The advanced navigational interface is composed of a color navigational display (NAV), a multifunction keyboard (MFK), and a video graphics terminal (VGT). The NAV display is created and driven by a rastergraphics programmable display generator. The display is essentially an integrated map that shows the pilot's situation relative to the flight plan. The MFK is a programmable light-emitting diode (LED) keyboard that contains a scratch pad area and 15 tactile feedback keystations. This device, which can be used in place of dedicated switches in the cockpit, thus declutters the console. The VGT consists of a matrix-addressed thin-film electroluminescent (TFEL) flat-panel display with touch overlay. The navigational interface is menu driven through the MFK. The VGT is used mainly for displaying data and entering new flight plans through the touch overlay. Intelligent automation was incorporated into the interface to anticipate the desires and actions of the pilot and thus reduce the number of interactions necessary to accomplish an objective.

Subjective evaluation revealed that the concept of the navigational interface greatly simplified the navigational tasks of the operator. Pilot reaction to the use of touch overlay in controlling the scaling of the NAV display and in modifying the flight plan was highly favorable.
(Denise R. Jones, 3457)

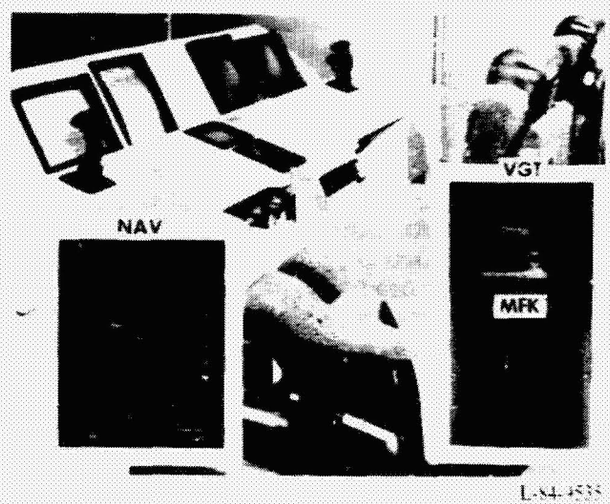

L-84-4535

Advanced navigational interface mounted in part-task transport simulator.

All-Raster Generation of Integrated "Tunnel-in-the-Sky" Display

Recent advancements in raster display technology at Langley have provided new opportunities to aid aircraft pilots. Providing information in more natural, more readily assimilated "real world" formats is one of these opportunities. In a three-dimensional world, it is more natural to present information in a three-dimensional format. An all-raster three-dimensional display capability has been developed in which a "tunnel-in-the-sky" and a perspective runway can be added to a typical primary flight display. This type of flight display may prove useful in steep, strongly curved, and descending landing approaches for obstacle avoidance and noise abatement. The object of this flight display is to provide the pilot with

a "tunnel" emanating from the runway to show the approach path to be followed. The tunnel is formed from a series of targets suspended along a predetermined flight path. These targets are connected to vertical vectors which drop down to a series of ground track vectors. The tunnel provides the pilot with altitude trend and deviation information and horizontal trend and deviation information in an integrated, natural way.

The all-raster display is generated with a programmable display generator (PDG) which has features developed for high-speed flight display performance. The PDG makes use of a hardware matrix multiplier that performs perspective transformations on the tunnel and runway. A software algorithm was developed to perform three-dimensional clipping of the tunnel/runway information. Large areas of solid shading (e.g., sky/ground and runway shading) are performed with symbol-fill hardware. The display has been introduced into a simulator and real-time operation has been validated in conjunction with a dynamic aircraft model.

(Jack J. Hatfield, 2171)

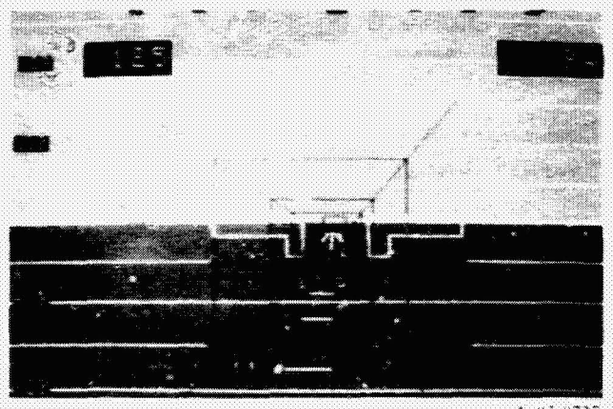

L-85-8737

Integrated primary flight display showing perspective "tunnel-in-the-sky" emanating from runway.

Three-Color LED Display for Multifunction Switches

Tricolor LED (light-emitting diode) displays have been developed for use as programmable legends on the face of multifunction switches. Multifunction switches were created to help declutter aircraft cockpits by a reduction in the number of individual switches in the cockpit. When a multifunction switch is given a new function, it must be given a new legend; LED arrays are presently used to create these legends because they have the brightness, resolution, and ruggedness necessary for use in an airborne environment.

The effectiveness of the legend and the amount of information it can transfer are increased if it uses multiple colors. Optotek Ltd., under a joint USAF/NASA/Canada contract, has developed a red/green/yellow LED display. A green monolithic LED array was superimposed over a red monolithic LED array to create the display. The arrays are addressed separately. The green LED layer is transparent to the red light from the red LED layer underneath. If a red diode and its superimposed green diode are both emitting light, the eye perceives the light as yellow. Thus, with suitable addressing, either a red, a green, or a yellow picture element is available. The displays have a resolution of 64 lines/in., are 0.4 by 1.0 in., and can display both graphics and alphanumerics.

(James B. Robertson, 3716)

Tricolor LED display module showing combined graphic and alphanumeric capability.

Microprocessor-Based Electronic Compass

Magnetic heading is one of the basic parameters that must be measured in order to implement almost any navigational procedure for aircraft or other vehicles. The usual combination of wet compass and directional gyroscope employed in most light aircraft

suffers from a number of errors that affect the compass as well as from the high cost of purchase and maintenance and the limited reliability of the gyroscope. Modern electronic and computer technology has been employed at Langley in the development of a simple low-cost solid-state magnetic compass in which most of the inherent errors of the mechanical wet compass have been avoided or compensated for so that the use of a directional gyroscope is no longer required.

The voltage outputs of a two-axis flux gate magnetometer are processed by a single-chip microcomputer to yield a digital output of the vehicle's magnetic heading in degrees. This output may be used to drive a simple display, or it may be used as an input parameter for a more sophisticated navigation system. Inertial and damping problems inherent in mechanical compasses do not occur because no moving parts are used. Deviation errors due to airframe and engine magnetism can be avoided by remote mounting of the sensing element, and northerly turning error is corrected by a technique previously developed for the Electro-Fluidic Autopilot.

A thorough review and reevaluation of existing flux gate magnetometer technology preceded the development of the magnetic sensing element and the signal processing electronics, and every effort was made to simplify the design and fabrication of these components. An accuracy of 1° is readily attained.

(H. Douglas Garner, 3321)

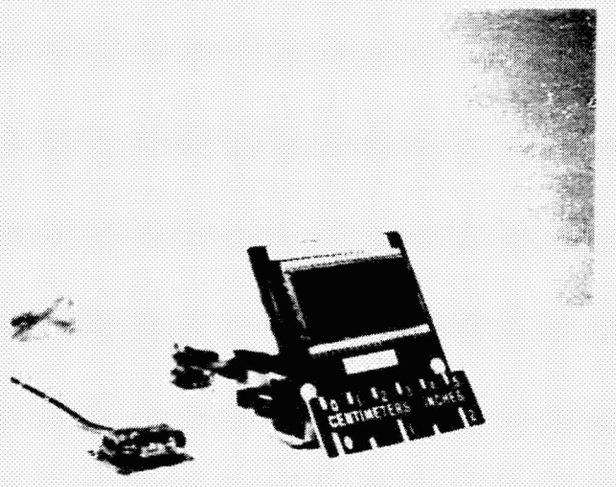

Electronic compass — magnetometer, data processor, and readout.

Windowing Algorithm for Electronic Flight Displays

As increasing use is made of new data links, sensors, and digital systems onboard modern aircraft, electronic flight displays are being utilized to present, consolidate, and integrate flight information. However, this wealth of new information raises the problem of a new form of "cockpit clutter" that may exceed the crew's information assimilation capability. A window manager capability for electronic displays has been developed to help meet this challenge. The advantage of the window manager is that a single electronic display on which numerous display formats can be arrayed makes efficient use of the limited space in the cockpit. Furthermore, the partitioning of the screen can be controlled either dynamically, by direct crew intervention, or automatically in response to conditions.

The window manager algorithm can independently select, scale, and position any flight display. It can also present the formats in any of four 90° orientations so the display screen can be mounted either horizontally or vertically. Because all parameters (scale, position, and orientation) can be changed dynamically, the partitioning of the displays can be reconfigured instantaneously. The window manager and all display formats are programs residing in a programmable display generator, with the window manager being the main program. All display formats are procedures that are called by the window

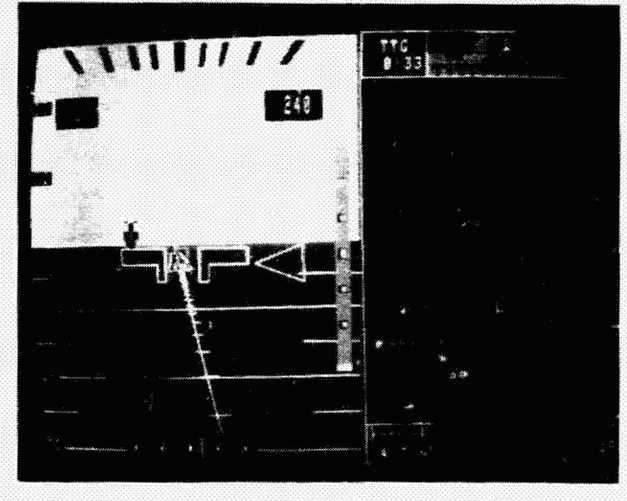

Horizontal orientation of combined primary flight and navigation display created with windowing algorithm.

manager. Each procedure has an identical argument list that contains parameters controlling the scale, position, and orientation. These parameters are controlled by the window manager, which determines how multiwindow displays appear on the screen. The data for the display formats are all scaled to a nominal window size, so the windowing operation is transparent to the programmer of individual displays.
(Jack J. Hatfield, 2171)

Multicolor Flat-Panel Electroluminescent Display

Today's advanced transport aircraft are already using electronic displays to reduce clutter and pilot workload in the cockpit through consolidation and integration of many display functions into one display. The color CRT (cathode ray tube) is currently filling this display role, but flat-panel displays are urgently needed because of space limitations in the cockpit.

Matrix-addressed TFEL (thin-film electroluminescent) displays are prime candidates for the flat-panel displays to replace the bulky CRT. (TFEL displays are already being used aboard the Space Shuttle as the display terminal for a portable computer.) However, these TFEL displays are available only in monochrome form. Full-color or multicolor displays are needed to display the new electronic instrument formats.

Under a joint Army/Navy/NASA contract, a two-primary-color flat-panel TFEL display has been successfully fabricated by Planar Systems, Inc., of Beaverton, Oregon. The display is a 1- by 1-in. laboratory breadboard with a resolution of 16 lines/in. Developed primarily to test phosphor systems and multilayer construction addressing techniques, the device is made by superimposition of a green EL display and a red EL display. This gives a choice of red, green, or yellow (red + green) at each picture element. Yellow-green and rust (amber) can also be produced by electronic variation of the emissions from the red and green primary phosphors. The display produces vivid colors. This accomplishment is an exciting step on the way to full-color flat-panel TFEL displays which can replace the bulky color CRT.
(James B. Robertson, 3716)

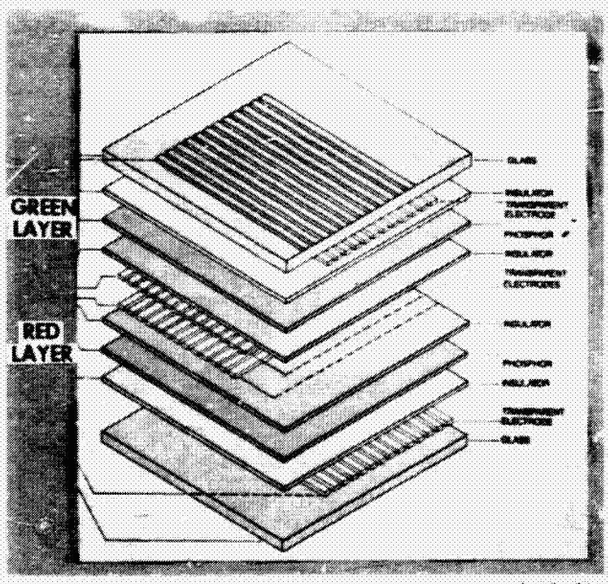

L-85-4290

TFEL display utilizes red and green phosphor layers to achieve multicolor capability.

Modified-Edge Compact Range Measurement System Reflector Uses Large Curved Surface Edge Termination

The compact range is an electromagnetic measurement system used to simulate a plane wave illuminating an antenna or scattering body. The plane wave is necessary to represent the actual use of the antenna or scattering from a target in a real-world situation. Traditionally, a compact range has been designed as an offset-fed parabolic reflector with a knife edge or serrated edge termination. The edge termination of the parabolic surface has limited the extent of the plane wave region or, more significantly, the antenna or scattering body size that can be measured in the compact range. As a result, the compact range has had limited use as well as limited accuracy. The compact range concept has not been applied to larger systems because of the large discrepancy between target and reflector sizes.

The signal reflected by the parabolic reflector is basically a plane wave which exists over the surface. If a simple straight edge is used, the diffracted signal is quite strong about the edge. This diffracted signal

interferes with the plane wave and causes amplitude and phase variations of the field illuminating the test antenna or scattering body. Several schemes to overcome this problem were examined, and it was found that a large curved edge termination was most appropriate. The large curved edge termination reduces the edge scattered field in the target area by 1 order of magnitude. The large curved edge treatment, which involves a radius of curvature equal to or greater than the focal distance, provides this improvement by creating a reflected field which goes smoothly from the parabolic surface to the curved surface termination. A curved edge reflector has been installed in the antenna test laboratory at Langley.
(Melvin C. Gilreath, 3631)

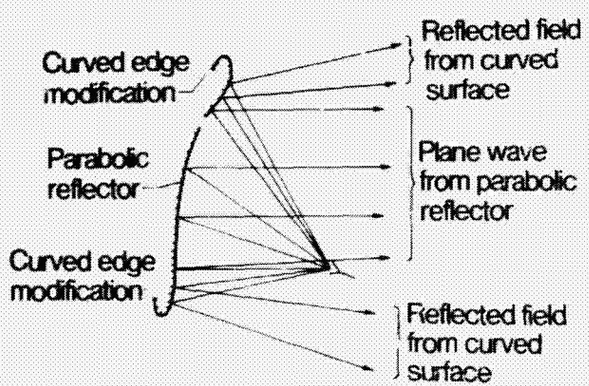

Reflected fields from modified reflector.

Sensitivity Analysis of Idle Thrust Modeling for Optimal Flight Path Computation

Advanced flight management systems are being developed which are capable of calculating optimal four-dimensional flight trajectories with arrival time accuracies on the order of 5 sec. Errors in mathematical models of airplane performance utilized in these systems result in off-optimal flight profiles which penalize performance. A critical parameter for optimal descent determination is the idle thrust produced by the aircraft engines.

A simplified computer simulation of the NASA Boeing 737-100 Transport Systems Research Vehicle (TSRV) aircraft was utilized in conjunction with a flight profile optimization program (OPTIM) to investigate the sensitivity of optimal descent trajectories to errors in idle thrust modeling. The batch aircraft simulation followed reference optimal profiles with and without parametric variations in the nominal idle thrust produced by the aircraft engines. Throttle and/or speedbrakes were utilized to null airspeed and altitude differences created by the idle thrust variations. Fuel and cost penalties associated with the idle thrust errors were the primary measures in this analysis.

Fuel penalty is plotted versus idle thrust error for a minimum fuel profile and a typical minimum cost profile in which a time cost of $600/hour was factored into the optimal trajectory calculations. Both profiles exhibit a greater fuel penalty for positive thrust errors, with the minimum fuel case showing the most penalty. These results illustrate the importance of accurate idle thrust modeling, especially in light of rising fuel prices.
(David H. Williams, 3621)

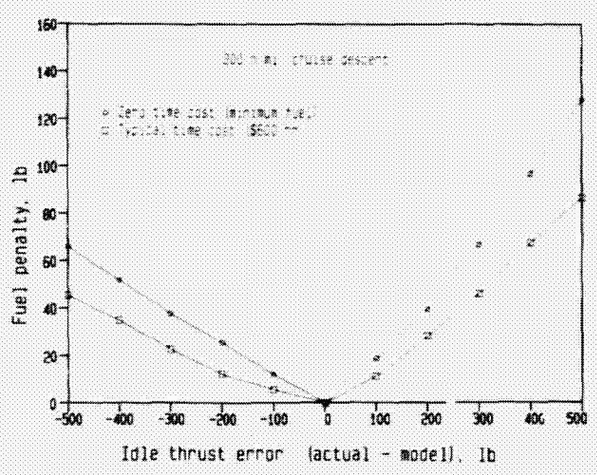

Fuel sensitivity to idle thrust errors.

Impact of Communication Complexity on Design of Parallel Numerical Algorithms

It has become clear that one of the most important characteristics affecting the performance of algorithms on parallel computing systems is the amount and pattern of communication dictated by

the algorithm. Because the spectrum of parallel architectures suitable for scientific computation is so broad, it is difficult to derive one analytical model of computation which characterizes the performance of every machine. Researchers at the Institute for Computer Applications in Science and Engineering (ICASE) have considered three families of machine architectures and have developed analytical models for each to characterize the effect of communication costs on system performance.

The first model is that of a "medium-scale" shared-memory multiprocessor with perhaps 2 to 32 processors, each capable of exploiting substantial local vector parallelism. Examples of such machines include the CRAY X-MP and ETA-10. Several standard but important numerical problems were studied and a number of alternate implementations were analyzed. In particular, it was shown that for machines with two levels of parallelism, the performance of algorithms strongly depends on the way the problem is partitioned to fit on the architecture.

The second model is that of a highly parallel Multiple Instruction Multiple Data (MIMD) system in which processors communicate through a large network and there is no shared memory. Such systems are assumed to have a number of processors ranging from perhaps 32 to a few thousand, but the processors are of less power than those in the shared memory model. The Intel Personal Super Computer, with its hypercube interconnection scheme, is an example of such a system. The analysis and design of algorithms for such systems are significantly different than for the shared memory machines. The appropriate parameters for this analysis were the ratio of message transmission times to arithmetic speed and the relation of the problem being solved to the topology of the communication network. Specific algorithms were looked at to show that many of the derived upper bounds are exact.

The third model is a variant of the second architecture with machines interconnected by packet-switched communications networks. Analysis of algorithms for such machines is similar to analysis of algorithms for other nonshared memory machines, except that communication delays play a central role.
(Susan J. Voigt, 2083)

Toolkit for Developing Computer Language Translators

A research project conducted for Langley at the College of William and Mary to investigate the automated generation of language compilers has been successfully completed. The MYSTRO system exists and has been distributed to more than 30 sites. This translator writing system has been used to develop compilers, assemblers, and interpretive command language translators.

The system consists of a parser generator (PARGEN), a code generator generator (CGG) and language (CGGL), and a number of utilities designed to support the translator development process. The system also uses a number of application-dependent "skeletons" (e.g., compiler or interpreter skeletons). The skeletons are Pascal programs which must be enhanced with code suitable for the type of translator being developed.

A formal grammar description of the subject language is input to the PARGEN process to create a parser. To construct a full language compiler, an additional major step is the construction of the target machine code generator. This is based on a specification for the target machine posed in CGGL and the intermediate code from the compiler parse phase. This process is shown in the figure.

The MYSTRO system has demonstrated the feasibility of automated support for the construction of large and complex software components such as compilers.
(Edmond Senn, 2558)

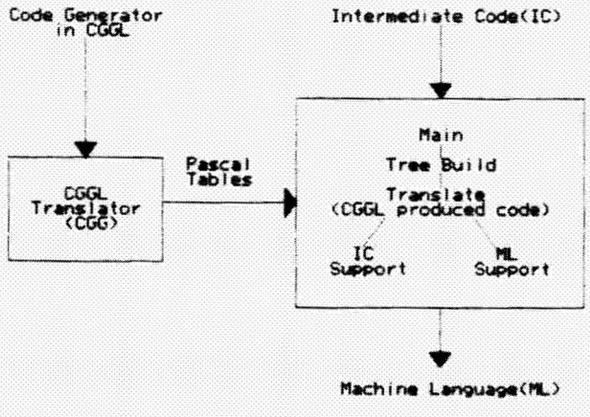

Code generation with CGGL.

Dual-Camera OH Visualization System

A special dual-view UV-sensitive imaging instrument system has been developed to study fuel ignition and flame holding techniques in the Langley hypersonic propulsion research program. This unique system provides real-time test visualization and simultaneous recording of OH density distribution data for post-test analysis. The two cameras utilize UV-sensitive vidicons and optical filters specific to OH emission in the 310-nm spectral range. This UV sensitivity allows direct viewing of the normally invisible OH emission combustion byproduct. The instrument control panel is remotely located from the propulsion test cell and provides remote operator control of shutter, interference filters (two each), and attenuation. The recorded data are automatically marked with time, test number, and view information for post-test data correlation.

An early important application of this instrument involved the exploration of a continuous-operation plasma torch as an ignitor and flame holder for a scramjet combustor. The figure shows the complete system and a typical single-channel view of recorded data in an early experiment. The OH visualization system utilizes a naturally occurring feature of the combustion process to provide the experimenter with a full-view picture. Data obtained from the OH visualization system allowed rapid evaluation of experimental parameter variations.

(Ray W. Gregory, 2791)

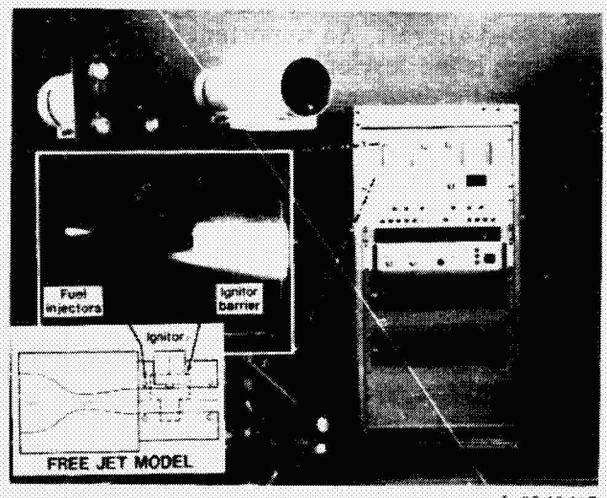

L-85-10,167

UV-sensitive imaging system.

Interpretation and Statistical Characterization of Direct-Strike Lightning Data

The planned use in advanced aircraft of composite structures and flight-critical digital electronic systems that are potentially susceptible to upset by electrical transients motivates the need to quantify the lightning environment affecting such aircraft. A typical transport aircraft is struck by lightning about once a year. The new composite structure will not provide the electrical shielding of onboard electronic systems against lightning-induced transients which is provided automatically by current metal aircraft. A statistically quantified characterization of the lightning environment is required to establish lightning threat criteria and devise efficient lightning protection measures for critical electronic systems onboard the advanced aircraft.

Direct-strike lightning data on about 650 strikes at altitudes ranging from 15,000 to 40,000 ft have been acquired by the NASA F-106. Emphasis in the research has been on determining the rates of change of the lightning interaction with the aircraft, since induced voltages and currents are proportional to the rates of change of the lightning process. The direct-strike research has acquired a multitude of time domain waveforms which are being used by EMA, Inc., of Denver to develop lightning/aircraft interaction models as part of the interpretation and analysis of the F-106 data. The models will ultimately be used to characterize the lightning threat to generic aircraft of different geometry and structure.

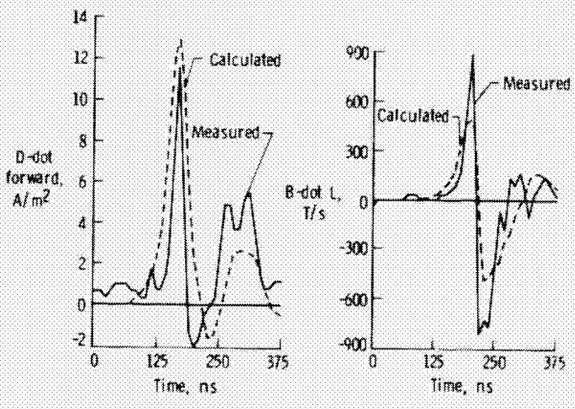

Nonlinear computer model and flight results.

The figure shows EMA computer model data and measured data obtained for the rate of change of electric flux density (D-dot) and magnetic flux density (B-dot) at two locations on the aircraft. Statistical techniques have been developed at Langley for examination of the distribution of the peak, or largest, values of the electromagnetic variables measured during the strikes. These statistical data are being used by the Air Force and the Federal Aviation Administration in developing new lightning criteria for new aircraft.
(Felix L. Pitts, 3681)

Basic Display/Guidance Requirements for Flying Near-Optimal Trajectories

The advent of the flight management computer in airplanes has provided the potential to compute cost-optimal flight profiles and has fostered the development of several profile optimization algorithms. Assuming these algorithms can be implemented into flight management computers, the basic guidance requirements to fly these optimized trajectories must be determined. The trajectories generated by these algorithms differ characteristically from conventional handbook profiles in that they are constantly varying in both flight path angle and airspeed. The result is approximately a 2 percent improvement in cost efficiency. Considering the dynamic nature of the pilot's control task, various guidance concepts require testing to assure pilot acceptability with low workload levels. In an effort to address this issue, simulation tests were conducted which investigated the basic display/guidance requirements for flying the near-optimal trajectories.

Three display configurations and four control modes were tested in the experiment to investigate their relative merits in flying the climb and descent trajectories. The path tracking accuracy and the pilot's control activity were the quantitative measures used to evaluate the various display/guidance options. A subjective evaluation of the associated workload and situation guidance was provided through a pilot questionnaire. Although the study was preliminary in nature, the trends in the data and the pilot comments yielded some interesting results. The study indicated that both current state-of-the-art flight director type display/guidance and the two more advanced display/guidance configurations tested were acceptable for flying these profiles.
(Dan D. Vicroy, 3621)

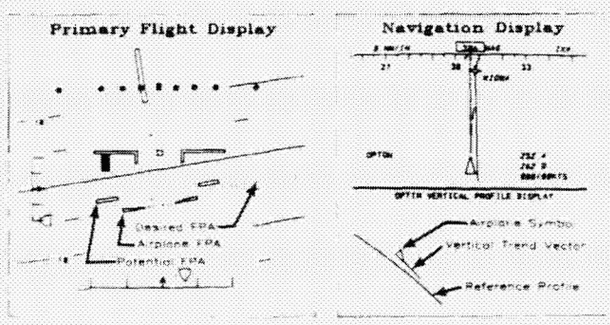

Advanced display/guidance configuration for flying cost-optimized profiles.

Evolutionary Time-Based Terminal Flow Control Investigation

An extended terminal area time-based flow control concept has been developed and incorporated into the Terminal Area Air Traffic Model (TAATM) with Denver routes. The process provides ground-aided profile descent instructions to aircraft without four-dimensional (4-D) capability but provides only metering fix and runway time objectives to 4-D equipped aircraft. An important element of this research is the development of simple models that represent the dynamics of several classes of commercial aircraft performing flight-idle profile descents. The process integrates en route flow control, terminal area sequencing and spacing, and fuel-saving flight-idle profile descent procedures. The algorithm is designed for integration with today's manual voice-linked air traffic control system in an evolutionary manner and also accommodates National Airspace System (NAS) upgrade features such as data link and further ground automation. With this concept, inter-arrival time separations can be flexible as well as fixed. This capability allows the investigation of variable reduced spacing, which may be possible depending on the success of research and development efforts in the areas of vortex advisory systems, aerodynamic vortex reduction, runway guidance, and high-speed turnoffs.

A fast-time parametric sensitivity evaluation of the basic extended terminal area flow control concept was completed. This was accomplished by the TAATM simulation in a four corner-post Denver runway 26L configuration with instrument flight rules (IFR) commercial arrival traffic. The effects and interrelationships of such variables as metering fix delivery error, aircraft separation requirements, traffic density, delay discounting, and horizon of control were explored. Simulation results plotted in the figure show the impact of metering fix (MF) delivery error on the runway arrival rate under two separate sets of separation requirements. The 3/4/5 n. mi. separation corresponds to today's IFR rules, and the 2.5/3.5/4.5 separation approximates visual separations.
(Leonard Credeur, 3917)

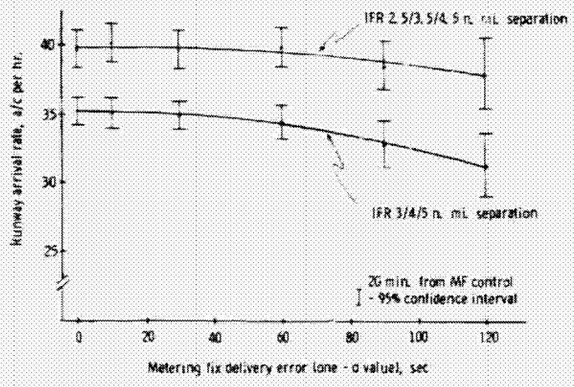

Effect of metering fix delivery error on capacity.

Takeoff Performance Monitoring System

An algorithm developed to monitor aircraft takeoff performance is aimed at improving safety in that flight phase. The algorithm consists of a pretakeoff segment and a real-time segment. Inputs of ambient temperature, pressure, runway wind, airplane gross weight, and selected flap and stabilizer setting are used by the pretakeoff segment in generating a set of standard acceleration performance data prior to the takeoff roll.

The real-time segment requires knowledge of the runway length available for rotation and stopping as well as an estimated rolling friction coefficient. It also uses measured throttle position, engine pressure ratios (EPRs), calibrated airspeed, along-track acceleration, and ground speed during takeoff roll. Engine parameters and airplane acceleration are computed along with the amount of runway used, remaining, necessary to achieve rotation speed, and needed to stop the airplane. A comparison of measured and predicted values is used to detect performance deficiencies. These comparisons and the runway length computations lead to Go/Abort signals or commands to the airplane systems.

The algorithm has been evaluated with a six-degree-of-freedom nonlinear airplane simulation for several design point cases and two types of engine malfunctions. The algorithm did not cause any false alarms and the error in the predicted runway required to achieve rotation speed was within 5 percent of the runway actually used. The algorithm is not capable of detecting engine failures that do not affect the EPRs; however even for this type of failure the runway predictions were within 5 percent of that used. Engine malfunctions affecting the EPRs are identified early in the takeoff run.

Plans include generation of display formats, pilot-in-the-loop real-time simulation testing, and ground roll testing on the Transport Systems Research Vehicle (TSRV) Boeing 737.
(R. Srivatsan, 3608)

Total Energy Rate Feedback for Automatic Glide Slope Tracking During Wind Shear Penetration

Research was conducted at Langley to evaluate the application of a total energy rate sensor in the design of an automatic longitudinal control system for the landing of the Transport Systems Research Vehicle (TSRV) Boeing 737 airplane in severe wind shear and gusts. The control system was designed with modern optimal control theory techniques, implemented with and without total energy rate feedback, and evaluated with a nonlinear simulation of the TSRV 737 airplane and a severe wind shear and gust data package developed by SRI International. The ILS (Instrument Landing System) autoland system onboard the TSRV 737 airplane was also evaluated in this environment as a baseline for comparison.

Results indicated that the system design with and without the energy rate sensor was much more effective in penetrating this environment than the autoland system. Also, only minor differences were evident between the design with and without the sensor. The figure shows time history plots of the aircraft altitude error with respect to the desired glide slope for the autoland system and the control system design with and without energy rate sensing. The results indicate that the control system design was effective in maintaining stability and control regulation in a severe wind shear and gust environment, but the energy rate sensor did not add significant additional information to the measurement set already available on this airplane. Therefore, the sensor may be better applied to the control of commuter or general aviation aircraft, where fewer measurements are available. Flight tests are planned to verify these results.
(Christine M. Belcastro, 3934)

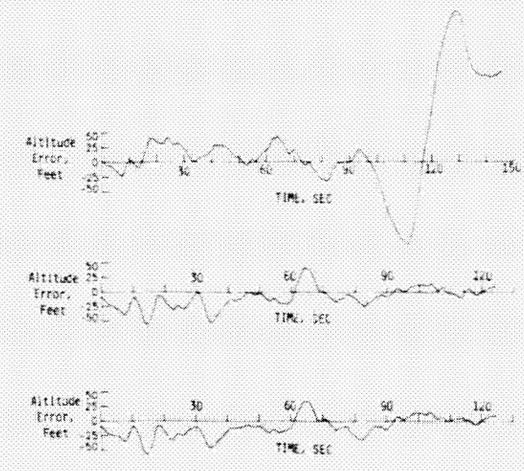

Computer-simulated altitude error with respect to desired 3° glide slope for ILS autoland system (top), control system design with energy rate feedback (middle), and control system design without energy rate feedback (bottom).

Line-Narrowed Tunable Ti:Al_2O_3 Solid-State Laser Demonstrated

Langley has built and demonstrated a line-narrowed tunable titanium-doped sapphire (Ti:Al_2O_3) laser. Ti:Al_2O_3 belongs to a class of "vibronic" laser materials which have strongly coupled vibrational and electronic laser transitions. As a result of this coupling, these materials exhibit broadband laser emission. Ti:Al_2O_3 has an emission gain cross section of up to 10 times that found in presently available solid-state tunable lasers, and it has a broad lasing range from 660 to 1100 nm.

The 25-mJ frequency-doubled output (532nm) of a 10-Hz Nd:YAG laser was used to longitudinally pump a 5- by 30-mm Ti:Al_2O_3 crystal. The laser cavity end mirror is highly reflective and the output coupler is 30 percent transmissive at 750 nm. Typical energy output is 2 mJ per pulse; the pulsewidth is 50 nsec but increases with larger pump energy. To achieve tuning and line narrowing, a three-plate birefringent filter tuning element was constructed. Further line narrowing was accomplished with the insertion of an air gap etalon. The 0.25-nm linewidth laser was tunable from 780 to 840 nm with the available mirrors. The tuning range of this laser can be extended to cover the entire lasing range of Ti:Al_2O_3 with the use of additional sets of coated mirrors. Narrower linewidths are achievable with the insertion of additional etalon(s).

The Ti:Al_2O_3 output encompasses wavelengths that are applicable to NASA lidar and DIAL measurements which include aerosols, H_2O vapor, and temperature and pressure (O_3).
(James C. Barnes, 3761)

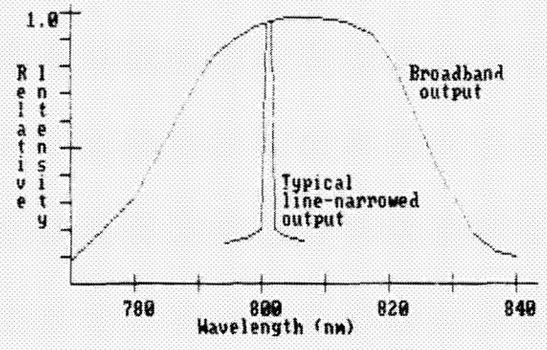

Titanium-doped sapphire laser outputs.

Machine Vision Based Control of Manipulator

Langley is investigating manipulator control based on integrated sensor systems. The research testbed is structured such that varying combinations of sensor systems and control configurations can be incorporated in the manipulator system. In the past year a sensor-based control system has been developed and demonstrated. The demonstration consists of close-tolerance insertion of a peg in a cylinder. Machine vision techniques were used to update the cylinder's location in the manipulator's axis system and force/torque feedback was used to maintain peg alignment during insertion. The peg-in-the-hole task provides experimental continuity with previous studies that used human sensing and control. The orientation and location of the target (cylinder) in the manipulator's axis system is determined according to methods based on perspective transform.

The figure shows the hardware involved in the demonstration. The vision sensor system includes a solid-state camera mounted at the manipulator's wrist, a commercial image processor, and a PDP-11/73 computer. The target is a cylindrical hole located in a taskboard that contains other plausible targets such as pushbutton and toggle switches. The sensor detects four LEDs (light-emitting diodes) mounted on a pad located at the upper right corner of the taskboard and transmits their image to the image processor. The processor in turn transmits the target location and orientation, derived from the image data, to the manipulator controller. The controller processes all sensor data and derives manipulator joint angle commands necessary to move the peg to the hole. The peg is subsequently inserted according to information from the force/torque sensor.
(Plesent W. Goode IV, 3871)

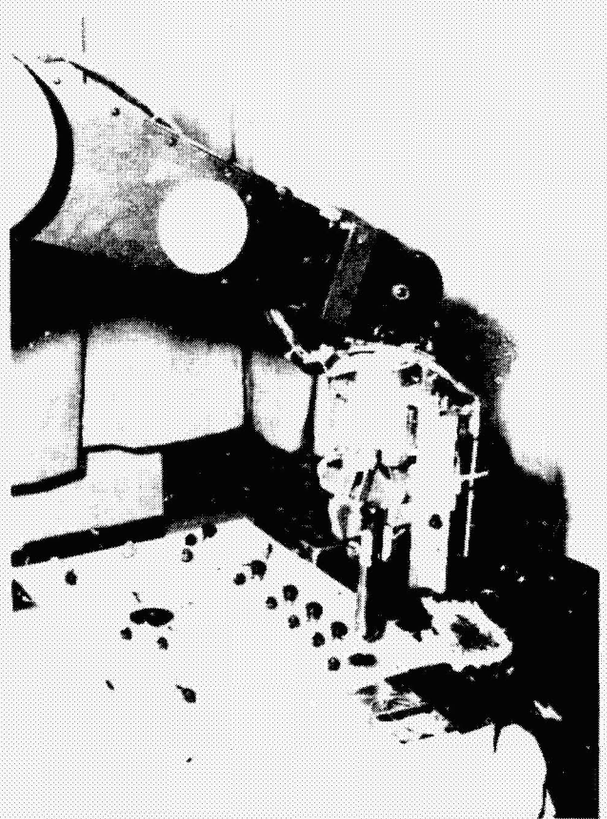

L-85-1717

Computer vision guides manipulator arm to target.

Force/Torque Display and Control for Telerobotic System

Force/torque feedback from a robotic end effector is being used to control and monitor the movements of a manipulator arm in a telerobotics system. Signals from strain gauges in the fingers of the end effector are fed back to the manipulator controller through a hierarchy of computers to give a sense of touch to the automated system as it inserts a peg into a close-tolerance hole. The peg-in-hole task

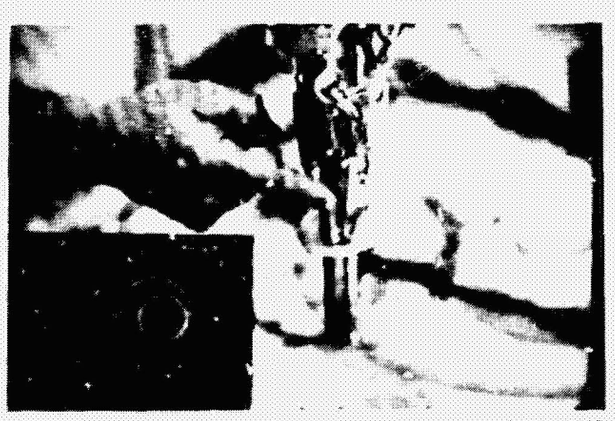

L-84-11,545

Strain gauges provide telerobotic system with sense of touch.

is representative of a large class of tasks that require precise alignment of an object with a receptacle: e.g., a bolt in a hole or a module in a mounting rack. A computer-generated graphic display of the force/torque information is provided to the operator to enable him to monitor the automated system or perform the task manually if desired. The display appears as two concentric circles representing the ends of a cylindrical object such as a peg. Signals from the fingers cause the circles to move concentrically in response to forces and differentially in response to torques to give the operator an easily interpreted visual representation of nonvisual information. The figure shows pressure applied to a finger of the end effector with the concentric circle display inserted into the operator's TV monitor.
(Marion A. Wise, 3871)

Failure Detection and Accommodation in Structural Dynamic Systems

A failure accommodation system that uses analytic redundancy between noncolocated sensors on a structural dynamic system has been demonstrated in a laboratory experiment. The experiment makes use of inertial grade sensors and microcomputer technology to implement an identification system that might reasonably be expected to fly on an operational flexible space structure. The problem of failure accommodation on these spacecraft arises from the expected heavy dependence on active control methods to suppress flexible motion of the structures.

The failure accommodation technique uses sequential probabilistic testing of the error signal from a Kalman filter to determine the validity of four rate gyro signals distributed on a flexible grid test structure. After the particular failure is detected and identified, the Kalman filter gains are reconfigured to produce an optimal estimate of the structural motion based on the remaining sensor set. The tests are accomplished in real time at a sample rate of 10 Hz for the tenth-order Kalman filter operating on four rate gyros. The failures can be detected within one cycle of the lowest frequency mode, and reconfiguration of the gains is achieved within one sample period after the failure is identified.
(Jeffrey P. Williams, 4591)

L-84-10,319

Grid apparatus used to test analytic redundancy technique.

Self-Structured Current Accessed Device

An investigation by the Sperry Corporation has demonstrated the feasibility of a self-structured current accessed bubble memory device. This novel device could provide a four-fold increase in storage density and an order-of-magnitude increase in data rate over conventional bubble devices and hence offers significant potential enhancement in spacecraft onboard memory systems. The device concept appears to be feasible with either double bubble techniques, which require two bubble film layers, or a wall coding method which requires only a single bubble film.

Experimental device components were designed and fabricated in single layer form. The component set included all generic components required for a functional device: input/output propagation tracks, transfer gates, merge gates, swap gates, generators, detectors, and annihilators. Although device optimization was not attempted at this stage, functional components of all types were demonstrated. The figure illustrates the operating margin of only one component type, a propagation track based on mesa barrier containment of the bubbles. The operating bias margin is approximately 17 percent of the normal

bias field, compared to a minimum goal of 10 percent. The propagation structure was also shown to be tolerant to photolithographic defects due to the bubble/bubble interaction characteristics of the self-structuring bubble pattern. Based on selection of the most promising of each type of component, a prototype 10-megabit chip was designed and analyzed for power dissipation. Calculated power values of 1 W in the data recorder mode and 4 W in the worst-case access mode indicate that the device concept is compatible with current packaging technology.
(Paul J. Hayes, 3777)

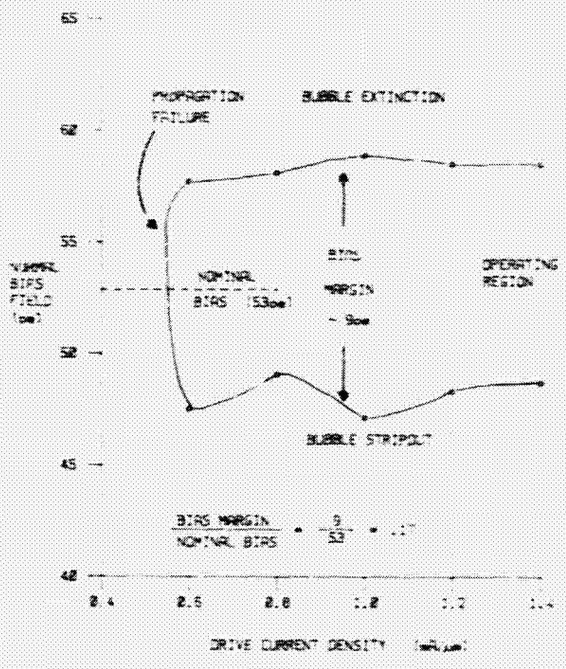

Propagation margin for mesa barrier track.

Bubble Memory System Design

A functional memory system design based on bubble memory devices has been developed at Langley. This all-solid-state memory with no moving parts was developed for onboard aerospace applications that require improved reliability and functional performance. Functional improvements provided by the design include first-in/first-out data access, simultaneous read/write, asynchronous data rates, command reconfigurable memory setup, and expandable capacity. The modular design provides potential onboard system capacities in the 100- to 1000-megabit range with the use of 1-megabit and 4-megabit chips now commercially available. A space-qualified 4-megabit bubble chip that is compatible with this system design is under development by the Air Force.

The system architecture provides a number of features needed in an onboard system. Up to eight bubble devices are simultaneously operated in parallel to attain high data rates. Banks of bubble devices are accessed by a given bubble controller to minimize controller parts. Power strobing techniques are used to minimize the average power dissipation. A fast initialization method uses electrically erasable programmable read-only memory (EEPROM) devices to enable fast access. Flight memory systems that incorporate the concepts and techniques of this research could now be developed for application.
(Paul J. Hayes, 3777)

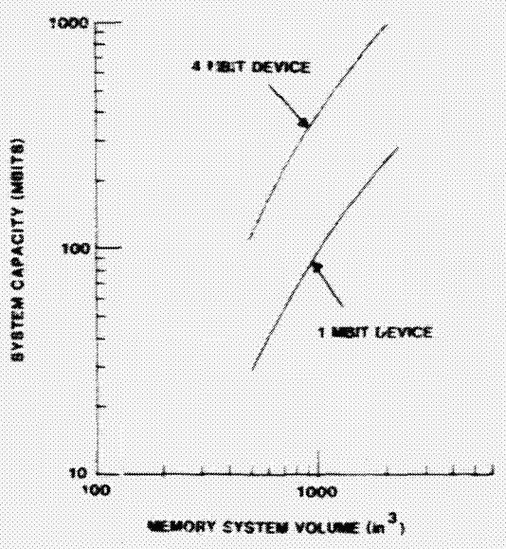

Potential spacecraft bubble memory systems.

AlGaAs Semiconductor Lasers for Data Systems

Semiconductor lasers provide a unique source with many wavelengths for wavelength division mul-

tiplexing (WDM), a high-speed modulation capability and a high-power budget for applications in a variety of fiber optics networks for applications such as Space Station. In particular, semiconductor lasers have been demonstrated with 6-nm spacing between lasers in a 12-channel WDM data system operating in the 820-nm region.

These devices were packaged in a DIP (dual in-line package) laser package (which also contained the photodiode feedback controller, thermoelectric cooler, and controller) with an 850-MHz bandwidth response which was capable of emitting 2 mW of power. In addition, a new channeled substrate planar AlGaAs laser design has been demonstrated with a maximum power output in single mode of 100 mW. An individually addressable array of 10 lasers has also been demonstrated.

(H.D. Hendricks, 3777)

Electromagnetic Analysis Method for Mesh Deployable Antennas

A phase perturbation electromagnetic analysis method for mesh-deployable reflector antennas has been developed and verified by Langley and Martin Marietta on the 15-m hoop column antenna. The radio frequency performance of the 15-m mesh-deployable antenna was predicted before the antenna was tested in the Martin Marietta Near Field Facility, and significant results were observed. The analysis and tests were extended over four frequencies ranging from 2 to 12 GHz. The analysis method verified has the capability to include pillowed surface distortions that generate grating sidelobes in the far-field radiation pattern from the antenna. A typical example of computed and measured radiation patterns at 7.73 GHz for the 15-m antenna is shown.

(Marion C. Bailey, 3631)

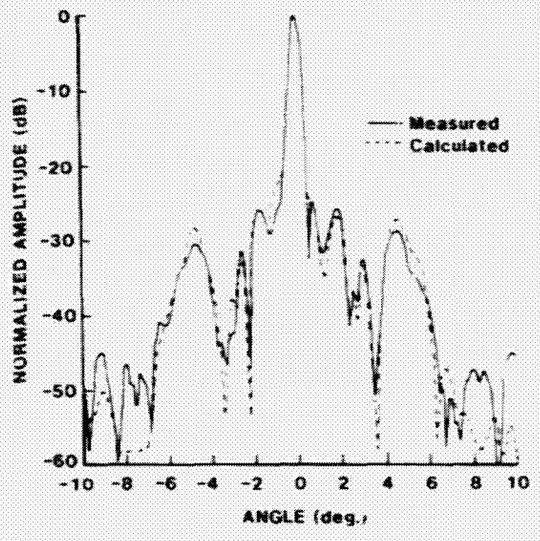

H-plane radiation pattern at 7.73 GHz.

Characterization of Antenna System Technology Mesh Materials

A gain degradation problem was observed on several flight-deployable antennas for the Tracking and Data Relay Satellite (TDRSS). This problem was eventually determined to be corrosive contacts on the mesh material. This TDRSS problem emphasized the need to develop a quantitative method for characterizing the electromagnetic properties of mesh materials. The gain degradation problem is severe for a communication mission, but emissivity values must be extremely low and nearly constant for radiometer missions. In that regard, a mesh characterization program has been initiated at Langley.

Two experimental test configurations have been developed, an enclosed system that uses liquid nitrogen cold load and an open-bucket reflector system that reflects the sky brightness temperature into the mesh target and radiometer system. The transmissivity, reflectivity, and emissivity values are determined through interactive procedures that use mesh, absorber materials, and precision calibration splash

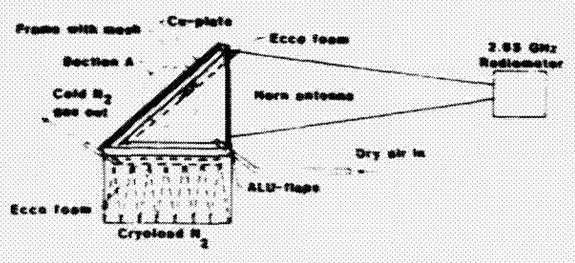

Radiometer system for electromagnetic measurements of surfaces.

plates and target conditions. Advanced proprietary mesh materials have been measured and found to be in the range of acceptability for radiometer missions that use large space antennas. The Naval Research Laboratory has requested that the mesh measurement laboratory be used to evaluate candidate materials for the Navy Remote Sensing System (NROSS) satellite. The mesh material for the 15-m antenna and samples from General Dynamics Convair have been tested

(Richard F. Harrington, 3631)

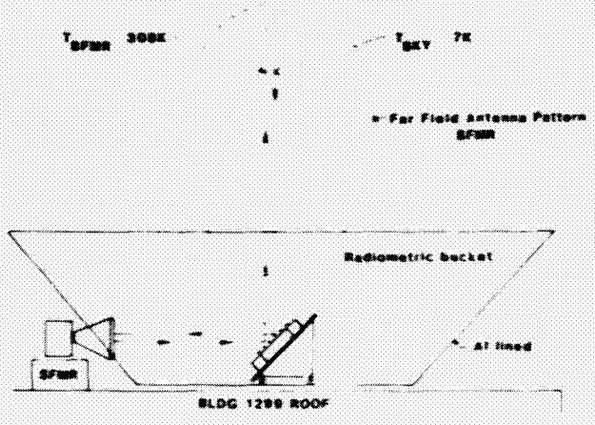

Open-bucket reflector system.

test of a 15-m hoop column deployable structure and antenna system.

Final structural and electromagnetic performance measurements have been completed on a 15-m engineering model. The test results include deployment kinematics, modal characteristics, reflector surface accuracy characterization during simulated zero gravity conditions, and near-field electromagnetic testing. The far-field electromagnetic tests of the 15-m antenna were conducted with the largest near-field antenna facility capable of measuring a structure of this size. The experiment and analytical results obtained through the 15-m antenna program will provide new opportunities for technology development flight experiments in structure, dynamics and control, and electroscience activities.

(Thomas G. Campbell, 3631)

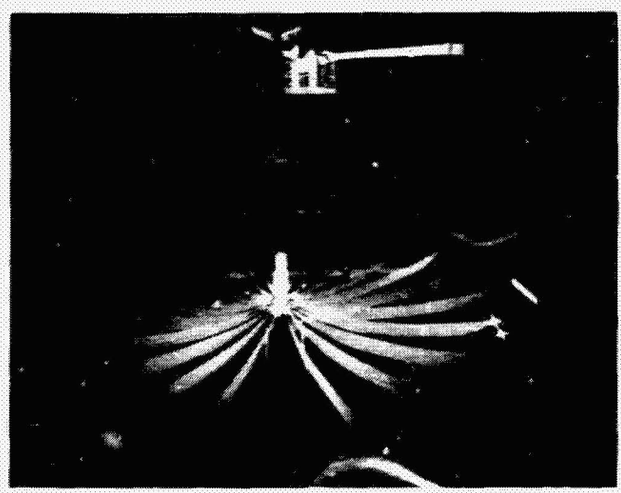

Deployment of 15-m antenna in Near-Field Facility.

Development of 15-Meter Hoop Column Deployable Antenna System With Final Structural and Electromagnetic Performance Results

Recent advances have been made in the technology development of large space antenna systems. These technological advances now provide new opportunities for the application of large space-based antennas in a variety of science and application experiments in the areas of remote sensing, multiple-beam communications, and radio astronomy. During the past 6 years, Langley and the Harris Corporation have been developing the technology of cable-stiffened deployable antenna structures. This effort has now culminated in the development, assembly, and

Measurement of Solid-Liquid Interface in Crystal Growth

A technique developed at Langley makes visible the position and shape of the solid-liquid interface in opaque crystals. This technique uses either x- or y-radiation to penetrate both the furnace and the crystal growth ampoule to record density differences

between the solid and liquid materials. The choice of radiation type is determined by the atomic density of the materials. Computer-aided image enhancement techniques are being developed to further extend the contrast and density delineation such that in situ compositional measurements can be made in the liquid phase. The development of this technique is part of the ground-based science for the NASA Microgravity Science Program.
(Archibald L. Fripp, 3777)

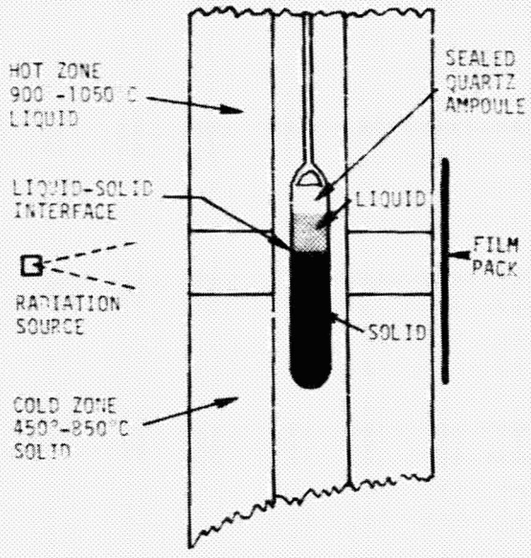

Schematic of irradiation experiment showing liquid-solid interface.

Space Directorate

The Space Directorate conducts research in atmospheric and Earth sciences, identifies and develops technology for advanced transportation systems, conducts research in energy conversion techniques for space applications, and provides the focal point for development activities for both large antenna systems technology and Space Station activities.

The Atmospheric Sciences Division is a leader in the area of atmospheric sciences. Its researchers are involved in seeking a more detailed understanding of the origins, distributions, chemistry, and transport mechanisms that govern the regional and global distributions of tropospheric and stratospheric gases and aerosols, and in the study of the Earth radiation budget and its effect on climate processes. The research seeks to better understand both natural and anthropogenic processes and covers a wide spectrum of activities, including the development of theoretical and empirical models; collection of experimental data from in situ and remote sensing instruments designed, developed, and fabricated at Langley; organization of extended field experiments; and development of data management systems for the efficient processing and interpretation of data derived from airborne and satellite instruments.

The Space Systems Division conducts research and systems analysis of advanced transportation systems, large antenna systems, and space station concepts as well as basic research into energy conversion techniques for potential space application. The division is a leader in the development of highly interactive and user-friendly computer-aided design (CAD) tools that enable the rapid evaluation of system concepts and the identification of technology necessary for the development of space transportation systems, large antenna systems, and the orbiting Space Station. The evaluation of advanced space transportation systems covers a wide range of capability, including Earth-to-orbit vehicles, Shuttle II, orbit-on-demand launches, service vehicles, and orbital transfer vehicles.

Involvement in Space Shuttle flight data and trajectory analysis is an ongoing activity that seeks to increase the efficiency and cost effectiveness of the Space Shuttle. Development of orbiter experiments that utilize the Shuttle as a reentry research vehicle to study radiative heat transfer and flow field chemical kinetics and to determine the aerothermodynamic and aerodynamic characteristics of the Shuttle has been a key activity and one which will lead to the development of advanced vehicle systems.

The Space Station Office is the focal point for Langley involvement in the Agency-wide Space Station Program and is responsible for the implementation and/or coordination of Langley's direct support of this program. The Space Station Office is the NASA lead for the identification, definition, and evaluation of the Evolutionary Space Station capabilities and for the identification of technology and advanced development required for long-term evolutionary development. The office represents the engineering community as technology users of the Space Station. It also advocates flight experiments on future Space Shuttle flights which contribute to Space Station technology use as well as flight experiments from technology programs which can contribute to both the initial operational capability and the evolutionary station. The office provides Langley support to the NASA-wide in-house Space Station systems engineering and integration in areas consistent with demonstrated Langley capabilities and expertise.

Analysis of Atmospheric Emission Spectra in Submillimeter Region

An analysis method that uses the nonlinear least-squares fit technique has been developed for emission spectra obtained with a Fourier transform spectrometer. This method is then applied to the analyses of atmospheric emission spectra obtained with a balloon-borne Fourier transform spectrometer operating in the submillimeter region. With this method,

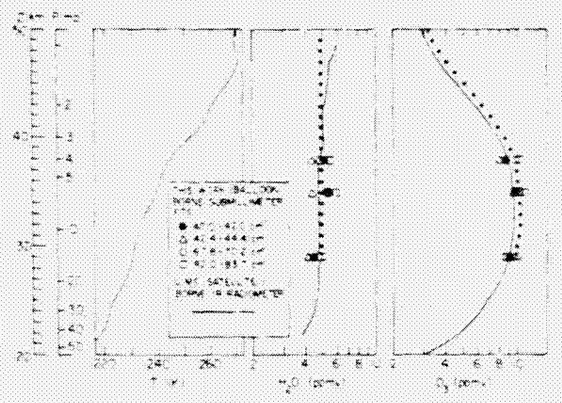

Retrieval mixing ratio profiles of H_2O and O_3 compared with those of LIMS (solid line).

the instrument line shape, the instrument response functions, and the emitting gas concentrations have been retrieved simultaneously. The atmospheric gases that can be retrieved from these data are H_2O, HDO, O_3 and isotopes, HCl, HF, HCN, OH, HNO_3, $O(^3p)$, O_2, and several others. Shown in the figure are the retrieved mixing ratio profiles of H_2O and O_3 from four spectral intervals with errors of about 20 percent. These profiles are in good agreement with data obtained from the LIMS satellite experiment.
(Jae H. Park, 2576)

Tentative Spectroscopic Identification of Stratospheric Chlorine Nitrate

The destruction of stratospheric ozone caused by the continued release of chlorine from chlorocarbon compounds is recognized as a key factor in the prediction of changes in stratospheric composition and climate. Observations of chlorine nitrate ($ClONO_2$), a major temporary reservoir of stratospheric chlorine, can place important constraints on the chemistry.

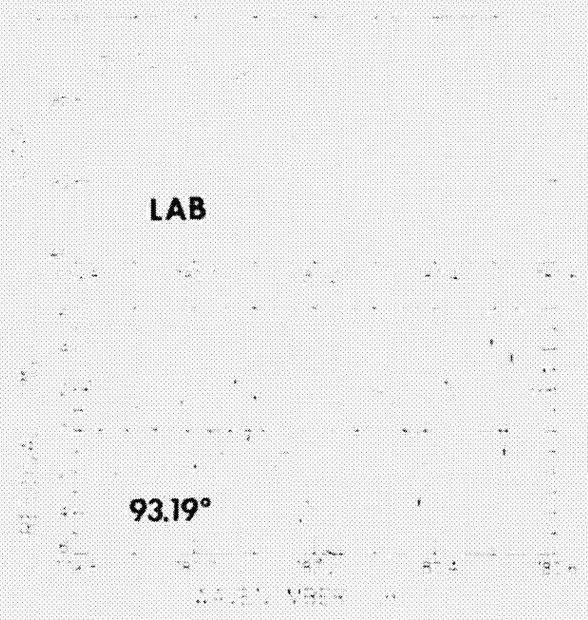

Laboratory spectrum of $ClONO_2$ (top) and residuals of least-squares best fit to stratospheric solar absorption spectrum (bottom).

High-resolution infrared stratospheric solar absorption spectra have been analyzed for the possible presence of absorption by $ClONO_2$. A nonlinear least-squares spectral curve-fitting analysis that uses new spectroscopic line parameters deduced from high-resolution laboratory spectra of $ClONO_2$ and O_3 shows the presence of a broad absorption feature near 780.227 cm^{-1}. As shown in the figure, this feature agrees closely in position and shape with the $ClONO_2$ ν_4 band Q branch, and the absorption is too strong and broad to be explained solely by the presence of known overlapping weak lines of CO_2 and O_3. Assuming that the additional absorption is due to $ClONO_2$, a stratospheric $ClONO_2$ altitude profile with a peak mixing ratio of about 1.1 parts per billion by volume near 28 km has been determined from the infrared solar spectra. Within the estimated experimental uncertainties, the results of this analysis are in agreement with the predictions of current photochemical models.
(Curtis P. Rinsland, 2576)

Ozone Emissions From Fires

Forest, grass, and cropland fires (biomass burning) in the tropics have been identified as a primary source of several trace gases released into the atmosphere. Some of the gases emitted during burning, such as carbon dioxide, are radiatively active at infrared wavelengths and contribute directly to the warming of the atmosphere through the "greenhouse" effect.

In industrialized areas, nonmethane hydrocarbons such as nitric oxide and carbon monoxide often react photochemically to produce high levels of ozone in the summer when insolation is sufficient to initiate the reactions. In the tropics, heavy burning can produce high ozone concentrations in the same manner. The photograph illustrates the magnitude of burning that takes place in Brazil. The smoke near the center of the left-hand photograph, from fires started on August 7, 1980, covered more than 1 million km^2 by August 8. Satellite data are being used at Langley to study regions where significant forest or savannah fires are occurring and to examine the relationship of these fires to anomalies in ozone concentrations.

Total ozone concentrations have been measured globally on a daily basis since 1979 by the Total Ozone Mapping Spectrometer (TOMS) aboard the Nimbus

7 polar-orbiting satellite. The TOMS instrument was developed as a tool to define the global distribution of ozone and provide some insight into the behavior of stratospheric ozone. Localized "hot spots" with a spatial domain on the order of 100 to 500 km have been found to appear quite often, with total ozone enhancements that are well above the 2-percent accuracy of the TOMS data. The existence of these features suggests that pollution (in particular, ozone) from widespread tropical burning may be identifiable from the TOMS data.
(Jack Fishman, 2294)

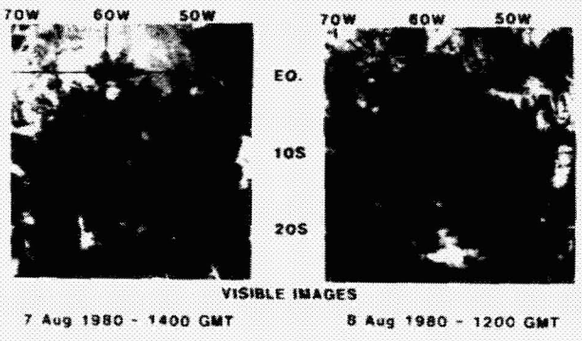

Biomass burning in the Amazon basin.

Methane, Carbon Monoxide, and Hydroxyl in the Troposphere

A major discovery in atmospheric chemistry was the finding that levels of two environmentally significant gases appear to have been increasing with time since at least 1977. Continuous ground-based measurements obtained since the end of 1977 indicate that increases in methane (CH_4) may be 1 to 2 percent per year and increases in carbon monoxide (CO) may be about 2 to 6 percent per year. These discoveries raise two important questions: Have atmospheric levels of CH_4 and CO been increasing prior to 1977, and what are the impacts of these increases on the photochemistry and chemistry of the atmosphere?

To shed light on the first question, ground-based solar infrared absorption spectra data obtained in 1950 and 1951 are being analyzed. Preliminary analyses indicate that both CH_4 and CO have been increasing since 1950. To answer the second question, a photochemical model is being used to study the impact of increasing CH_4 and CO levels of the chemistry of the atmosphere. These calculations indicate that increasing levels of CH_4 and CO since 1950 may have caused a 25-percent decrease in tropospheric levels of the hydroxyl radical OH. Although it is only a trace species, carbon monoxide is the overwhelming chemically active species in the troposphere and readily and rapidly transforms one atmospheric species to another. OH chemically cleanses the atmosphere of many man-made species and is involved in the photochemistry of ozone and acid precipitation.
(Joel S. Levine, 2187)

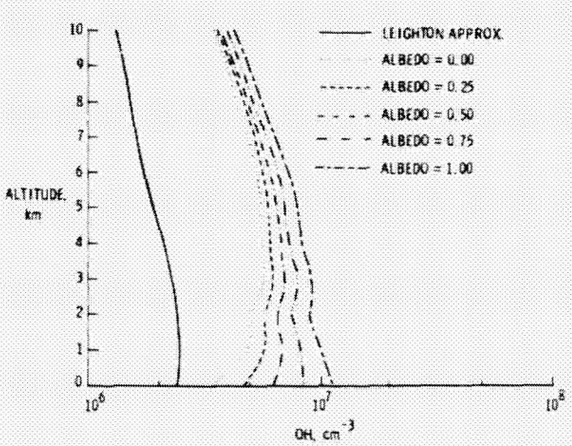

Vertical distribution of OH in the troposphere based on photochemical calculations showing absorption of incoming solar radiation (no scattering), called the "Leighton approximation," and scattering for five different values of surface albedo.

Airborne Lidar Studies of the Tropical Atlantic Troposphere

The NASA Ultraviolet Differential Absorption Lidar (UV-DIAL) system was flown during June 1984 as part of the NASA Global Tropospheric Experiment (GTE) Atlantic Boundary Layer Experiment (ABLE-1). Investigations of aerosol and ozone distributions were conducted primarily in the tropical Atlantic troposphere east of Barbados. Aerosol backscattering was observed simultaneously at wavelengths of 300, 600, and 1064 nm with 15-m vertical

and 20-m horizontal resolution. Ozone profiles were obtained with a 100-m vertical and 2-km horizontal resolution. In situ measurements of aerosol mass distribution, aerosol scattering, aerosol number density, and ozone were also obtained.

The lidar aerosol distributions provided detailed pictures of atmospheric structure and dynamics in the tropics. For example, lidar-derived spatial distributions of Saharan dust layers observed during undisturbed atmospheric conditions provided unique information on long-range aerosol transport and horizontal extent of these layers. Shown in the photograph is a horizontal cross section of aerosol backscattering as observed by the UV-DIAL system during about 10 minutes of a flight on June 21, 1984. The Saharan dust layer, which has been transported over the Atlantic, is seen clearly between about 1.8 and 4.2 km altitude with a central core around 3 km. Aerosol scattering at multiple wavelengths has been used to estimate the wavelength dependence of scattering for continental, marine, Saharan dust, and tropical rain forest aerosols. UV-DIAL measurements of ozone profiles combined with in situ data provide a comprehensive description of ozone variations in the tropical Atlantic boundary layer and free troposphere.

(Edward V. Browell, 2576)

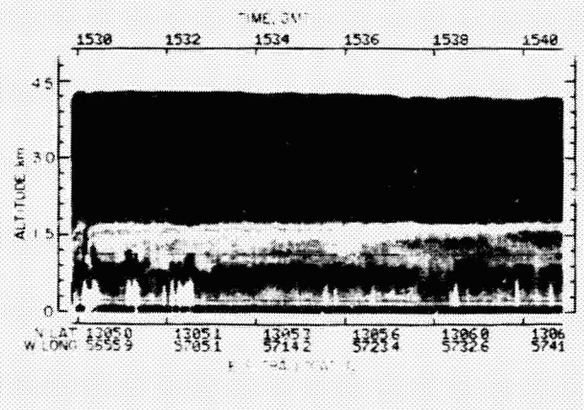

Airborne DIAL aerosol measurement of Saharan dust layer over the western Atlantic.

Orbiter Flight Data Extraction

A unique methodology has been developed at Langley to analyze Shuttle entry flight data. This methodology utilizes an interpretation of the traditional flight vs prediction correlation plot combined with a multilinear regression for parameter identification.

This technique has been utilized to analyze the hypersonic trim anomaly encountered during orbiter entry. The analysis indicates that the sources of prediction deficiencies in the preflight Aerodynamic Design Data Book (NASA CR-160903, 1980) were caused by a deficiency in the prediction of real-gas effects on the basic vehicle's pitching-moment characteristics, underprediction of the positive body flap effectiveness (δ_{BF}) below Mach 15, and an overprediction of negative elevon effectiveness (δ_e). The results of this analysis, when applied to the first 14 flights of the orbiter, significantly improve the correlation and reduce flight-to-flight variation.

A combination of this analytical tool and other flight data (i.e., aerothermodynamic, pressures, and maneuver extraction results) will allow a quantification of the sources of the hypersonic trim prediction deficiency to an accuracy required to improve prediction methodology.

(James C. Young, 4952)

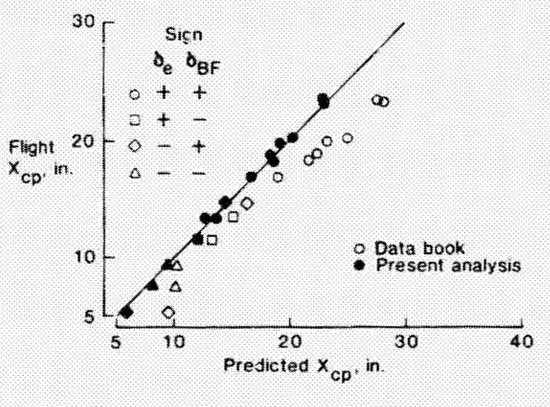

Impact of analysis on X_{cp} correlation at Mach 9.

Measured and Predicted Hypersonic Aerodynamic Coefficients for Orbiter-Like Configuration

Aerodynamic coefficients for an orbiter-like configuration were measured in several Langley hy-

personic wind tunnels at angles of attack between 15° and 45°. These facilities provided a range of Reynolds number at Mach 6 and Mach 10 in air and simulated the low-gamma aspect of a real (dissociated) gas. To achieve this simulation, tests were conducted at Mach 6 in tetrafluoromethane (CF_4), a gas with a lower value of gamma than air. The primary purpose of the study was to compare these measurements with the aerodynamic coefficients predicted with HALIS (high-alpha inviscid solution), a three-dimensional inviscid flow field code developed at Langley. The model tested, which is identical to the geometry used in HALIS, represents an accurate scaling of the forward 93 percent of the orbiter windward surface. The leeward surface was replaced by a series of elliptical cross sections.

The effect of Mach number, Reynolds number, and gamma on the normal force coefficient was quite small (less than 5 percent), and this coefficient was predicted accurately by HALIS. The expected increase in axial force coefficient with decreasing Reynolds number was observed, but there was no appreciable effect of Mach number or gamma on this coefficient. As expected, the inviscid HALIS code underpredicted the measured axial force coefficient. Particularly noteworthy was the effect of gamma on the pitching-moment coefficient. Although the pitching-moment coefficient was independent of Mach number and Reynolds number, a lower gamma caused more pitch up, especially at the higher angles of attack. This phenomenon was also predicted by HALIS and implies a significant real-gas effect on pitching-moment characteristics for this orbiter-like configuration.

(John R. Micol, 3031)

Computation of Shuttle Lower-Surface Flow Field

Three-dimensional flow field solutions on the windward side of the Space Shuttle orbiter during reentry were obtained by solution of the full set of viscous shock layer equations. These simplified equations are derived from the Navier-Stokes equations and govern the three-dimensional attached flow bounded by the body and bow shock. The computer

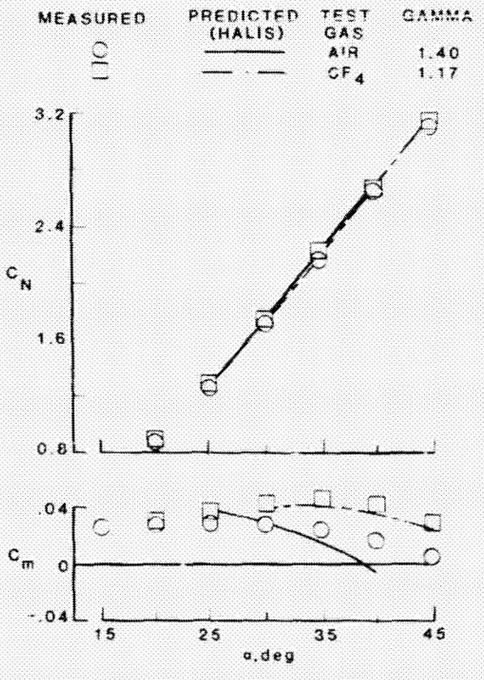

Effect of gamma on normal-force (C_N) and pitching-moment (C_m) coefficients at Mach 5.9.

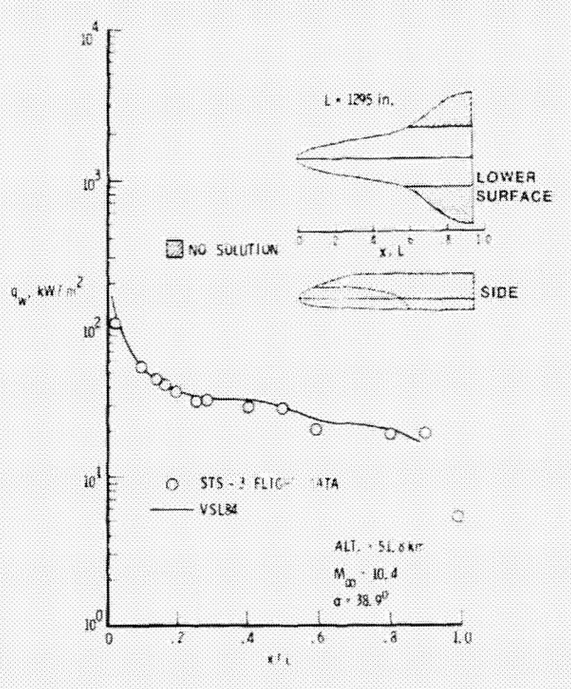

Heating rates along lower surface symmetry plane of Shuttle orbiter.

code used for this work (VSL84) was a Langley modified version of a program (FSL81) developed by Szema and Lewis at Virginia Polytechnic Institute under grant from Langley. The modified code reported here is significantly more accurate and more usable for general applications.

The ability of the method has been demonstrated by computation of most of the windward flow field over a model that closely simulates the lower surface of the Shuttle orbiter. Calculations have been done for free-stream conditions taken from actual points along STS reentry trajectories and include cases in which the flow was laminar or turbulent and in which the chemistry in the shock layer was that of a perfect gas or reacting air in chemical equilibrium. Results of these computations have been compared with flight measurements and other numerical solutions. The figure shows the typically good agreement obtained between prediction and flight for surface heating rates (q_w) along the windward symmetry plane of the orbiter. It was concluded in this study that the method can provide accurate surface pressure and heating predictions and should be useful for the aerothermodynamic analysis of hypersonic vehicles.

(Richard A. Thompson, 4328)

Three-Dimensional Hypersonic Flow in Chemical Nonequilibrium

A new computer code, Langley Aerothermodynamic Upwind Relaxation Algorithm (LAURA), has been developed to solve the three-dimensional hypersonic flow over blunt-nose vehicles. Both sonic-corner (i.e., wide-angle bodies) and nonsonic-corner bodies can be treated by the code. Tests of computational stability and convergence are substantially complete, and comparisons with experimental pressure and heat transfer data are being performed for code validation. The code is constructed around a single-level-storage upwind-differenced finite-volume scheme with a solution-adaptive grid capability. High-order accuracy is achieved with a total variation diminishing (TVD) derived flux limiter. The solution at each computational cell (or plane of cells in vectorized mode) is relaxed in pseudo time through the simple inversion of a 5×5 matrix. The relaxation time step is essentially unlimited in the first-order scheme, and rapid convergence is routinely achieved with local iterations and alternating directional sweeps through the computational domain.

Program LAURA uses a unique chemistry package which permits calculation of flows in chemical equilibrium, near-equilibrium, or nonequilibrium. The routine independently solves the species continuity equations for air (11 species, 26 reactions) with an upwind-differenced finite-volume scheme. The convective and diffusive contributions to the species continuity equations are turned off to achieve equilibrium calculations. The figure illustrates a typical equilibrium/nonequilibrium comparison for hypersonic inviscid flow over a 2-m radius sphere at 71 km. The results are indicative of a thicker, higher temperature shock layer for the nonequilibrium case.

(Peter A. Gnoffo, 2921)

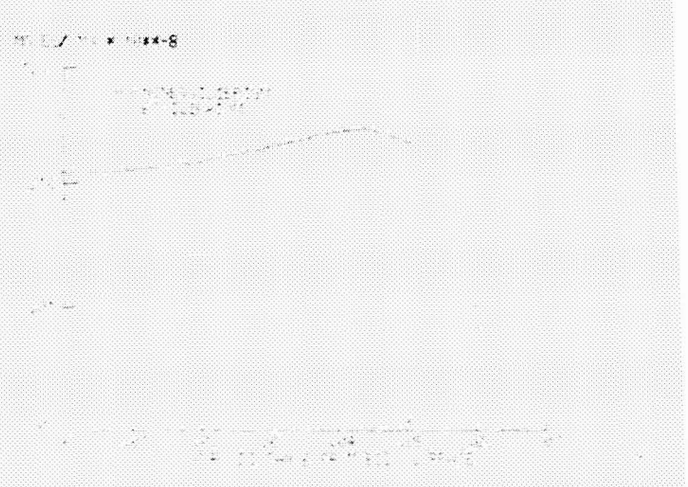

Electron number densities across shock layer of sphere from coarse grid (16 cells) shock captured inviscid calculation.

Aeroassist Vehicle Flow Field Computation

The HALIS (high-alpha inviscid solution) code was developed at Langley to compute the inviscid flow field about vehicles at high angles of attack in supersonic/hypersonic stream with large regions of embedded subsonic flow. The HALIS code has been shown to generate windward surface pressures on the Shuttle vehicle which are in very good agreement with

both wind tunnel and flight data. When an axisymmetric analog for the three-dimensional boundary layers is added, the predicted windward surface heating rates are in good agreement with flight data.

This technology is being used to generate flow fields and surface properties on proposed aeroassist vehicles. In general, this family of vehicles is characterized by short, very blunt shapes which may or may not be axisymmetric. Due to their bluntness, either all or a large portion of the flow about these bodies is subsonic, as illustrated in the Mach number contour plot. The shaded area between the bow shock and the body represents the subsonic portion of the flow. In the second figure, the symmetry plane pressure distribution (C_p) as a function of nondimensional surface length (s/s_b) is compared with wind tunnel data for the same shape. Heating rates have also been computed for this and similar shapes.

(K. James Weilmuenster, 3272)

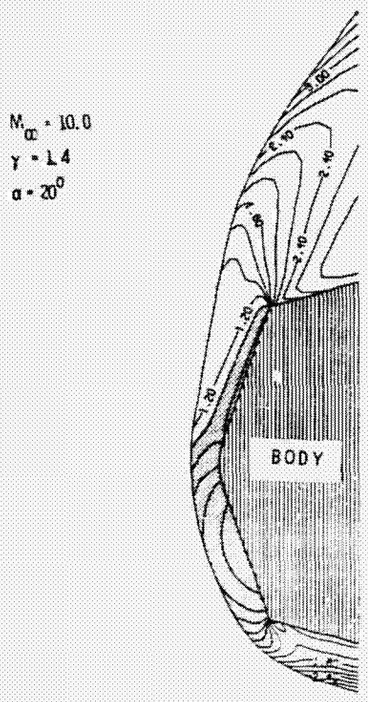

Flow field Mach number contour plot in the symmetry plane of 70° sphere cone with conical afterbody at 20° angle of attack.

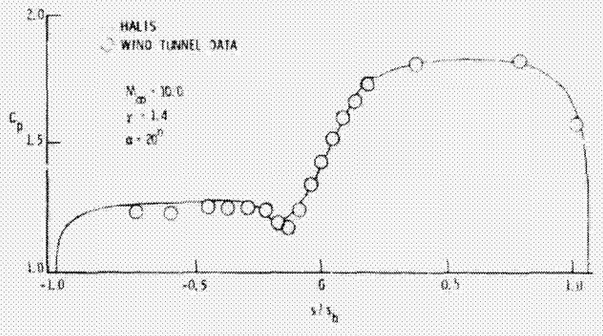

Symmetry plane pressure coefficient distributions.

Flight Experiment To Measure Shuttle Orbiter Lift-to-Drag Ratio in Rarefied Flow Regime

The aerodynamic forces on vehicles in rarefied flow have become a research area of increased importance, partly because of the need to develop aeroassisted orbital transfer vehicles. These future vehicles will make use of aerodynamic forces in an atmospheric pass in order to accomplish an economical orbit change. A key parameter in assessing such vehicles is the lift-to-drag (L/D) ratio. Very limited data are available because flow field predictions and ground facility simulations are difficult at rarefied flow conditions. Therefore, flight data are very valuable, particularly in the transition regime between free-molecular and continuum flow. The Shuttle orbiter offers the first opportunity to make repeated L/D flight measurements at high angle of attack on winged entry vehicles.

Such measurements are presently being obtained and analyzed at Langley, beginning with the STS-6 mission. These measurements are a part of the High Resolution Accelerometer Package (HiRAP) experiment. The HiRAP instrument consists of a triad of sensitive linear accelerometers, and measurements are obtained during entry from the first perception of atmospheric deceleration until the sensors reach saturation at the 90-km altitude. The figure shows an example of the processed results, including IMU (inertial measurement unit) data, from two early flights of the equipment on STS-6 and STS-7.

These data have also provided the basis for a significant correction to the current empirical bridging formula used to predict the aerodynamic behavior in the transition regime. This important prediction technology advancement could impact the future

design of NASA reentry missions, and preliminary inputs have been provided for assessments. It is fully expected that as future data flights are folded into the ongoing analysis, an unprecedented data base on rarefied-flow aerodynamics will emerge.
(Robert C. Blanchard, 4950)

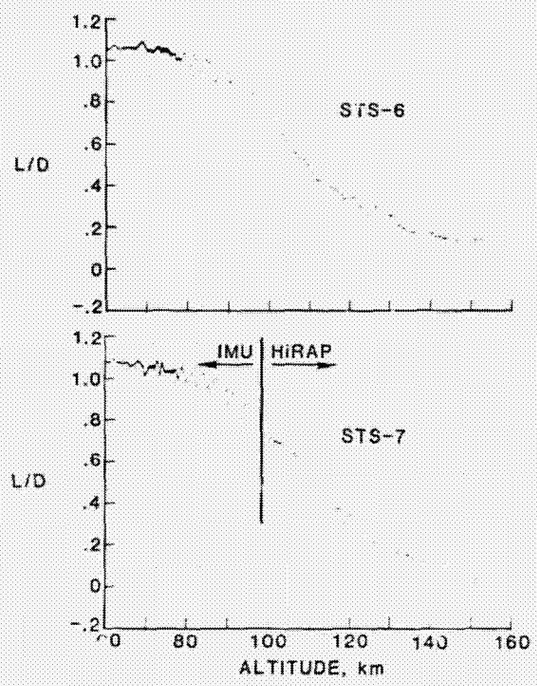

L/D *measurements in rarefied flow regime.*

Direct Simulations in Support of Shuttle Experiments

The Direct Simulation Monte Carlo (DSMC) method has been used to calculate both the external flow about the nose region of the Shuttle orbiter and the internal flow in an inlet tube that provides the initial path between the shock-processed gases and a mass spectrometer mounted inside the orbiter. The objective of the Shuttle Upper Atmospheric Mass Spectrometer (SUMS) experiment is to determine the free-stream density based on the mass spectrometer measurements for an altitude range of 160 to 90 km (essentially the transitional flow region). The link between the inlet pressure and free-stream conditions is being accomplished by numerical simulation studies. A three-dimensional version of the DSMC method was recently developed along with the procedures for interfacing the external and internal flows. The calculations that have been performed were for a gas mixture that consisted of five chemical species and simulated the effects of translational, rotational, vibrational, and chemical nonequilibrium.

The flow in the entry region of the inlet tube is three-dimensional and undergoes significant changes within the first few diameters (D = 2.35 mm). This is clearly evident in the results shown for the 140-km-altitude case. Even so, the flow becomes axisymmetric within three tube diameters or less. The pressure correction for the entry region is significant for the transitional flow regime in that the pressure within the tube is substantially less than the pressure at the external surface (p_s).
(James N. Moss, 3770)

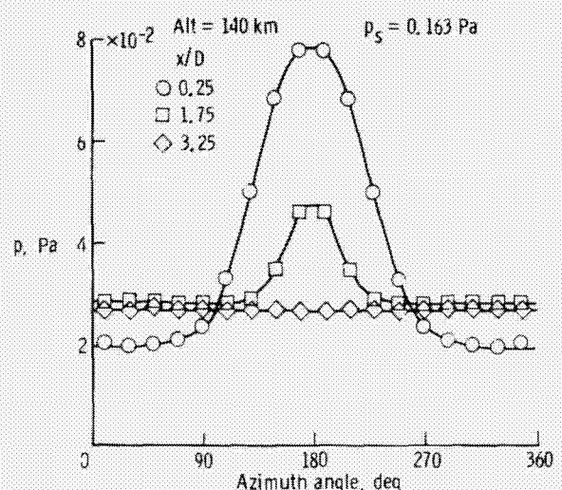

Azimuthal sidewall pressure distribution in entry region of inlet tube.

Box Truss Antenna Design

A design program for large box truss antennas for communications and/or radiometry has been completed under contract with Martin Marietta. Deployment and dynamics tests of 5- and 15-ft models have validated the basic structural design. A direct tieback system for mounting the r.f. reflecting mesh

on the structure and for shaping the reflector has been designed. The figure shows a box truss structure for the reflecting dish and boom support for the antenna feed as well as the mesh tie system for the surface of one of the boxes for the large reflecting dish.

In addition to designing the complete antenna, the program also uses manufacturing conditions and operational environments with a finite-element model of the mesh tie system to evaluate the reflecting surface topography and to estimate the r.f. performance patterns, gain, and beam efficiency. The integrated system design and analysis program is now part of the IDEAS (interactive design and evaluation of advanced spacecraft) capability at Langley. Current work involves experimental checking of the shape and smoothness of a parabolic reflector on a 15-ft box truss composite structure and comparison of performance results with those obtained by other large lattice structure mesh-tie designs.

(Lloyd Keafer, 4974)

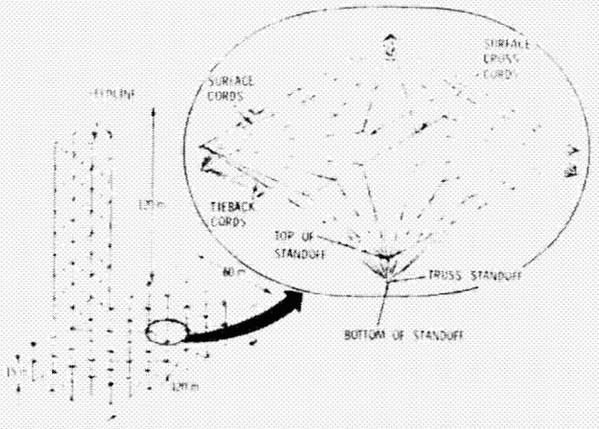

Large box truss antenna structure with direct tieback mesh support.

Continuous-Wave Solar-Pumped Laser

Orbiting power stations that generate power from sunlight and transmit the power to user satellites by means of a laser beam are being considered where very high power requirements exist in space. Orbital transfer vehicles could use the laser beam to heat hydrogen propellant and thus eliminate the need to transport great quantities of oxygen to space. Users could also be factories in low Earth orbit which require megawatts of power but cannot tolerate the drag exerted on solar photovoltaic panels large enough to provide that power.

An iodine laser being investigated at Langley for space power applications uses a curved reflector to concentrate light from a solar simulator onto a glass tube through which an iodide gas is flowing. Flow is maintained by an evaporation-condensation cycle in which liquid perfluoroalkyliodide lasant at −10°C evaporates, flows through the laser tube, condenses in a chamber cooled to −50°C, then flows back to the original chamber to be recycled. While flowing through the laser tube, the gas is dissociated and its iodine component is excited by the light. The excited iodine atoms lase at a wavelength of 1.3 μm.

Gas circulation is needed to keep a fresh supply of lasant in the laser tube. Lasing will endure for only about 50 msec if the gas is not flowing; used gas slowly undergoes recombination to [illegible]e itself while being recycled. Pulsed [illegible]eration can be achieved when the gas flows slowly [illegible]. For continuous-wave operation, the flow must be fast enough to flush the laser tube in less than 50 msec. Recently, a perfluoroalkyliodide laser with a high-speed flow system was operated, and CW lasing was obtained in a series of tests, the longest duration being 10 sec. Heat management problems, not fundamental problems with the laser, limited the lifetime of the laser. Another organic iodide laser, which had adequate thermal protection, lased continuously for 1 hour. This laser did not have a return line from the condensation chamber to the evaporation chamber, so lasing was limited by the amount of lasant placed in the evaporation chamber.

(D. Humes, 3781)

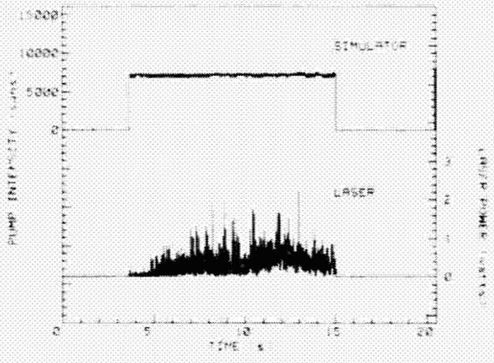

CW operation of solar-pumped laser.

Orbit-on-Demand Vehicle Study

Future vehicles for Earth-to-orbit transportation may need to respond within a few hours of a mission launch requirement, support a high level of mission activity, and do so at reasonable cost. In the Langley Orbit-on-Demand Vehicle Study, 11 vehicle concepts were designed with these capabilities to determine technologies in need of development as well as the most suitable vehicle configurations. Several key performance and operations technologies were identified, including metal matrix composite tanks, foam insulation for tank walls at near liquid-hydrogen temperatures, hydrocarbon-fueled rocket engines, and on-board testing to monitor health status and servicing requirements.

The 11 concepts studied included vertical and horizontal takeoff, airbreathing and rocket propulsion, single and multiple stages, and reusable and expendable components. From this broad range of concepts, two were chosen as having the greatest potential. One of these, a fully reusable concept with two stages, vertical takeoff, horizontal landing, and rocket propulsion, would be economical, small, suitable for a wide range of missions, and relatively low in risk. The other concept uses an airbreathing booster similar to current airliners with a rocket-powered second stage. The second-stage launch point would be offset by several hundred miles to provide a capability for rapid rendezvous missions. Further mission analyses are required to assess the relative value of these two concepts.

(James A. Martin, 4953)

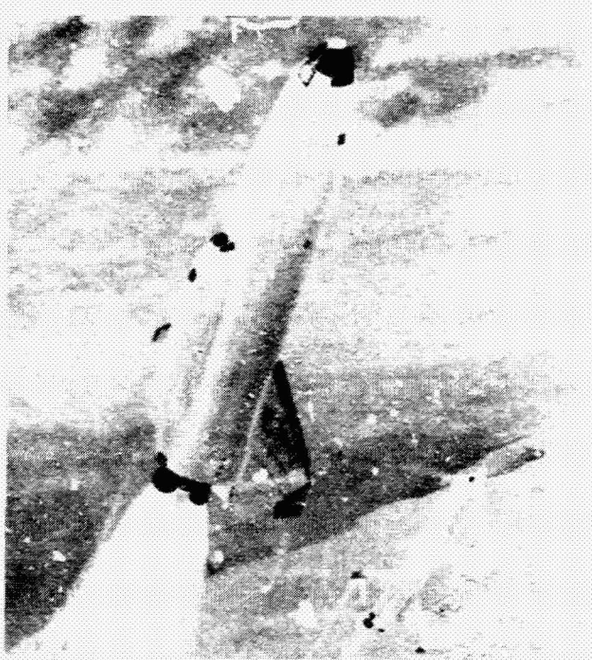

L-84-11,555

Two-stage orbit-on-demand vehicle concept.

Space Station Trace Contaminant Analysis

Trace contaminant levels in the spacecraft cabin atmosphere were not analyzed in situ on past manned space missions because of the short mission durations and limited cabin space available to carry out experimental and commercial operations. In contrast, the Space Station will be a permanently manned multipurpose facility in which trace contaminants could build up and present a hazard to the crew. In order to assess the magnitude of this hazard, a trace contaminant model was developed under grant with the College of William and Mary to predict the contaminants that may be produced within the Space Station by subsystem interactions, commercial operations, and crew activities. This model provides the capability to analyze the effects of chemical reactions and physical processes on concentrations of trace contaminants inside the Space Station as a function of time. Physical and chemical production and loss parameters for 190 contaminant species and 36 chemically important species have been included in the model. Interactive

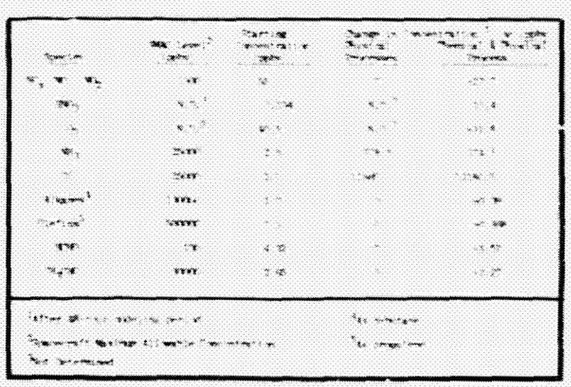

Effects of chemical and physical processes on concentrations inside Space Station.

changes in input parameters such as crew size, lighting systems, leakage, and pressure changes are easily implemented.

To determine whether chemical reactions produce significant changes in trace contaminant concentrations, two sets of calculations were performed. One set included only physical production and loss parameters, and the other included physical processes as well as chemical reactions. A comparison of results of the calculations for a 48-hour modeling period is shown. Significant changes in species concentrations were produced when chemical reactions were included, and these changes will become large as the lengths of the missions increase. Results of this analytical tool will be useful in designing air quality monitoring and air revitalization equipment and in assessing the potential toxicological hazards of proposed experiments.
(Dana A. Brewer, 2487)

Space Station Data Management System Concepts Assessment Model

The Space Station Data Management System (SSDMS) controls the station and all onboard functions, including communications to the outside world. This full-time management role necessitates rigid reliability requirements over at least a 20-year lifetime expectancy. The selection of appropriate system architecture, hardware, and software to meet this need yet also permit station growth and upgrade over the years is a complex engineering design problem. It is essential that NASA be able to verify the system performance and predict cost, size, weight, and power requirements for the candidate architectural concepts.

Langley and Computer Sciences Corporation have developed the methodology to construct a computer model that can assess candidate architectural configurations for data management systems. The model methodology permits system performance requirements, design options, and technology options to be evaluated or assessed for a candidate architectural concept. Within the model's methodology, assessment algorithms are divided into three categories: advanced distributed architecture model analysis (ADAM); advanced reliability, availability, maintainability model analysis (ARAM); and advanced trade assessment model analysis (ATAM). The ADAM algorithm predicts the candidate architecture's performance parameter (e.g., transaction rate, response time, capacity). ARAM assesses the redundancy scheme and system reliability and also predicts mean time to repair and system availability. ATAM is used to assess the amount of hardware required to implement the candidate system, assess technology risks, and compute cost, weight, volume, and power consumption. Assessment data for a given architectural concept are then compared with results from other candidate concepts to select the most promising design for the data management system.
(William R. Jones, 4978)

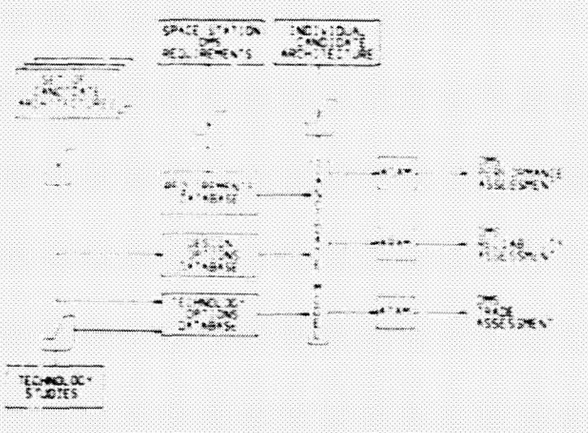

SSDMS assessment model configuration.

Space Station Environmental Control and Life Support Systems Integration Analysis

The evaluation of integration options to provide a functional Environmental Control and Life Support System (ECLSS) has become a concern for the Space Station designer. The ECLSS equipment must be distributed within the Space Station modules to provide an environment in which the crew can live and work safely. Integration options must accommodate the initial Space Station mission requirements and also allow for Space Station growth as these requirements dictate the need for additional crew and working area. Advances have been made at Langley in developing and refining a methodology for selection of the most promising options for various inte-

gration concepts. The analysis methodology consists of a data base and algorithms which provide the basis for the evaluations as functions of Space Station mission requirements.

The analysis methodology was applied to the NASA Space Station reference configuration and three integration options that included equipment distribution within the Space Station modules according to both central distributed and common module approaches. Variations in crew size were evaluated for both three- and six-person units. The reference configuration included regenerative technologies for water and metabolic oxygen recovery which utilized a Bosch process for CO_2 reduction. These three-person size units were centrally distributed in the two habitability modules of the Space Station reference configuration. Option 1 was identical to the reference configuration except that a Sabatier process was substituted for the Bosch process. Option 2, including the Sabatier, was similar to Option 1 except that the technologies were sized for six-person crews. Option 3, including the Sabatier, was a common module approach that included three-person size units distributed in the two habitability modules and the two laboratory modules of the reference configuration. Significant crew growth potential can be realized if Option 2 is implemented in the initial space station. It is estimated that this benefit can be realized with a modest increase in the ECLSS cost compared to that of the Space Station reference configuration. **(John B. Hall, Jr., 4971)**

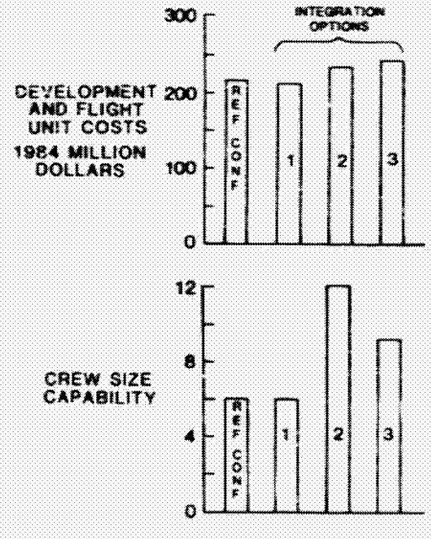

Cost and crew size capability for Space Station reference configuration and integration options.

Study of CO Enriched Air Mass Observed Over Eastern Mediterranean

Isentropic (constant-temperature) trajectories for the 310 K surface were computed for a carbon monoxide enriched tropospheric air mass observed over the eastern Mediterranean by the Shuttle-borne Measurement of Air Pollution from Satellites (MAPS) experiment on November 14, 1981. The three-dimensional flow of these carbon monoxide enriched air parcels was analyzed from the source regions of Europe to the measurement locations. The resulting trajectories were calculated over a 36-hour time period and a distance on the order of 1800 km.

Large-scale storms over northwestern and southeastern Europe were linked to convective processes by which surface air was transported vertically to detection altitudes near 500 mb. Both Meteosat imagery, which is provided by the European Space Agency, and the United States National Meteorological Center vertical velocity analyses indicated widespread ascending airflow over Europe preceding the measurements of the MAPS experiment. The convective storms associated with frontal activity lifted the surface air from northwestern and southeastern Europe, the source regions of the CO enriched air mass, to the altitude of the measurement, where it was entrained by the planetary scale general circulation. These results, when combined with the isentropic analyses, enhance our understanding of the interdependency of meteorological and chemical processes in the free troposphere. **(Vickie S. Connors, 2576)**

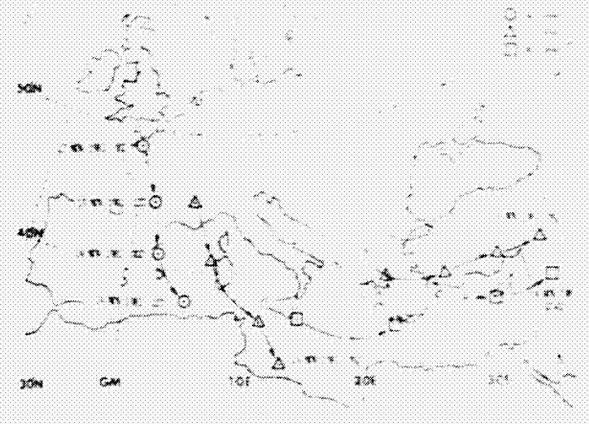

Isentropic back trajectories over 36 hours at 310 K for four air parcels within CO enriched air mass.

Results of First Flight of MAPS Experiment

The MAPS (Measurement of Air Pollution from Satellites) experiment, which flew as part of the OSTA-1 payload aboard the Space Shuttle on November 12-14, 1981, has demonstrated the ability of a spaceborne remote sensor to measure the volume mixing ratios of carbon monoxide at the few tens of parts per billion by volume (ppbv) level in the middle and upper troposphere. The mixing ratio has been determined with a repeatability of about 10 percent and a measurement accuracy of about 20 percent.

The figure shows the MAPS carbon monoxide data set with volume mixing ratios averaged over 5° latitude by 5° longitude areas. As expected, lower mixing ratios were found in the Southern Hemisphere, with the lowest readings (about 40 ppbv) found south of 20°S over the eastern Pacific Ocean and South America. The highest values (greater than 100 ppbv) were found in a band between 15°N and 5°S which extended from just west of South America eastward at least to central Africa, but not as far east (at least at these latitudes) as the Indian Ocean south of India. The second highest group of readings was found over southeastern China and the adjacent ocean areas. These high values appeared to spread eastward as far as the central Pacific Ocean. Somewhat enhanced mixing ratios were found in the vicinity of the eastern Mediterranean Sea and over the eastern North Atlantic Ocean.

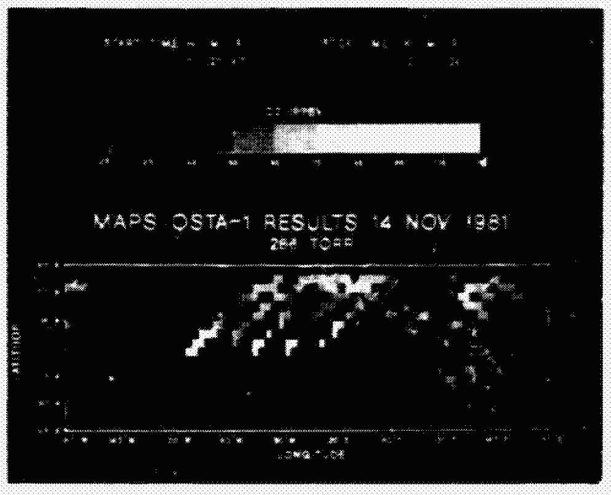

Volume mixing ratio of midtropospheric carbon monoxide as measured by high-pressure channel of MAPS experiment.

Because the experiment is not very sensitive to gas in the mixing layer, there must be some mechanism (e.g., thunderstorms) that rapidly transports the CO to the middle and upper troposphere from its surface (combustion) or mixing layer (photochemical) source. The MAPS data show that the carbon monoxide mixing ratio in the middle and upper troposphere is a function not only of latitude but also of longitude.

(Henry G. Reichle, Jr., 2576)

First Data From Earth Radiation Budget Experiment

On October 5, 1984, the first of three satellites of the Earth Radiation Budget Experiment (ERBE) was launched by Space Shuttle *Challenger*. The second satellite carrying ERBE instruments, NOAA-F (now NOAA 9), was launched on December 12, 1984, and the third, NOAA-G, is expected to be launched late in 1985 or in 1986. Earth-viewing data collection commenced in early November 1984, and since that time data, including numerous solar calibrations, have been obtained on a continuous basis. Initial examination of the data strongly suggests that the ERBE is providing the best calibrated broadband measurements of radiation from the Earth yet obtained.

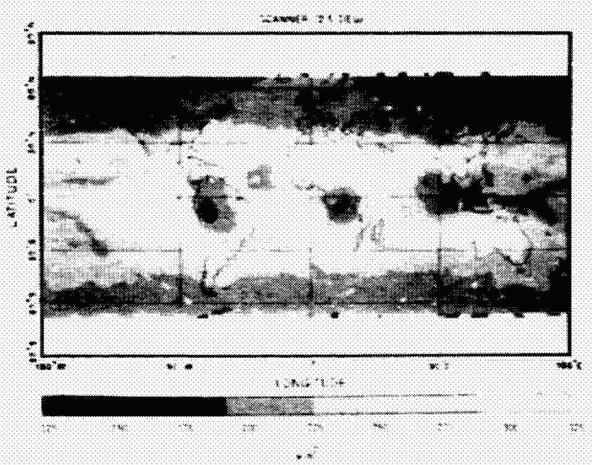

Average outgoing longwave radiation for November 1984 from ERBE scanner.

The average outgoing longwave radiation (OLWR) at the top of the atmosphere is shown for November 1984 as determined by measurements from the ERBE scanner. The figure shows a generally zonal structure in the midlatitudes and a complex longitudinal structure in the tropical regions between 30°N and 30°S. In the tropics, the darkest regions (very low OLWR values) are areas of deep convective cloudiness, whereas the lightest regions (high OLWR values) are cloud-free areas of subsiding air. The low OLWR values near Indonesia and a companion region of high values in the eastern equatorial Pacific Ocean are associated with the El Nino-Southern Oscillation, whose strength has significant climatic impact. Comparison with earlier OLWR measurements shows that the November 1984 pattern is similar to the one that developed during November 1977. In the months ahead, the subsequent evolution of these patterns as revealed by the ERBE data will provide new insight concerning the atmospheric and oceanic flow processes, which vary from year to year and affect weather and climate globally.
(B.R. Barkstrom, 2977)

The ERBE solar constant monitoring effort will be supplemented with the launch of a third spacecraft, the NOAA-G, in late 1985. It is expected that the three spacecraft will permit the continuous monitoring of the solar constant through 1990. Such extended measurements will permit the identification of long-term changes greater than 0.1 percent.
(R.B. Lee III, 2977)

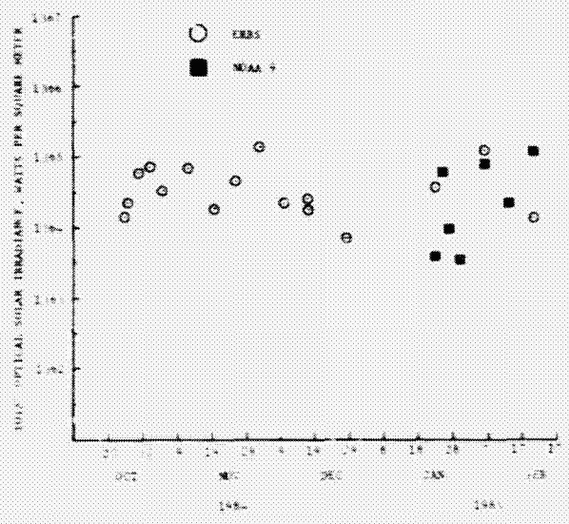

ERBE derived solar constant as a function of time.

ERBE Solar Constant Measurements

The solar constant is the amount of solar power per unit area which is incident upon the Earth at the mean distance between the Earth and Sun. It is the primary source of light, heat, and energy required to sustain life on the Earth and is one of the parameters that governs the Earth's weather and climate. It is being monitored to determine if it is decreasing or increasing with time and to provide measurements that may be used to understand the impact of changes in its magnitude upon long-term weather and climate forecasts. Data obtained from the Earth Radiation Budget Experiment (ERBE) spacecraft have been used to compute the magnitude of the solar constant.

The averaged computed solar constant values are shown in the figure as a function of time. The circles represent the Earth Radiation Budget Satellite (ERBS) measurements and the squares represent the NOAA 9 spacecraft measurements. For the period from October 1984 through February 1985, the measurements from both spacecraft indicate that variations in the solar constant were less than 0.1 percent. The measurements from both spacecraft were consistent to within 0.1 percent.

Bidirectional Desert Models

Broadband shortwave and longwave radiance measurements obtained from the Nimbus 7 Earth Radiation Budget (ERB) scanner were used to develop reflectance and emittance models for the Sahara, Gibson, and Saudi Deserts. These deserts will serve as long-term inflight calibration targets for three Earth Radiation Budget Experiments (ERBE) being flown on one NASA and two NOAA satellites. Deserts were chosen because they offer long-term stability, minimal cloudiness and precipitation, high albedos, and uniformity over the required spatial scale.

The ERB scanner viewed the deserts at zenith angles ranging from 6° to 87°, but because of the noon Sun-synchronous orbit of the Nimbus 7 spacecraft, measurements were obtained at solar zenith angles only from 0° to 53° during the 19 months of scanner

operation (November 1978 to May 1980). Because ERBE scanner measurements will be taken over the full range of solar angles, shortwave bidirectional models are needed to provide radiance estimates for the deserts at the higher solar angles. Semiempirical models were developed based on approximate solutions to the radiative transfer equation. The models exhibited zenith angle reciprocity; that is, the viewing and solar zenith angles could be exchanged without the reflectance being altered. This feature of the desert models permitted the larger range of viewing angle data obtained from the ERB scanner to be substituted for its lower range of solar angles. Albedo calculations for the Saudi, Sahara, and Gibson Deserts can now be extended beyond the solar zenith angle range of the Nimbus 7 ERB data with a degree of confidence.

(W. Frank Staylor, 2977)

Initial SAGE II Observations

The Stratospheric Aerosol and Gas Experiment II (SAGE II) was launched from the Space Shuttle aboard the Earth Radiation Budget Satellite (ERBS) on October 5, 1984. SAGE II, a seven-channel sunphotometer, is designed to monitor the vertical distribution of stratospheric aerosols, ozone, nitrogen dioxide, and water vapor from 80°N to 80°S latitude by measuring the extinction of solar radiation through the Earth's atmosphere during the ERBS observatory sunrise and sunset. Routine data collection was initiated October 21, 1984, and since that time three comprehensive correlative measurement campaigns have been conducted at Laramie, Wyoming; Natal, Brazil; and Fairbanks, Alaska, to assist in the validation of the SAGE II data set. These correlative observations included multiwavelength aerosol backscatter profiles with the Langley airborne lidar system, aerosol concentration profiles with University of Wyoming balloon soundings, water vapor concentration profiles with NOAA frost point hygrometer balloon soundings, and ozone concentration profiles with both balloon and rocket soundings.

Preliminary comparisons of the SAGE II data with the correlative observations and other global data sets showed excellent agreement. The SAGE II data also indicated that the stratospheric aerosol loading from the El Chichon volcanic eruption has spread globally and begun to decay, but is still well above background levels. The figure shows the zonal mean cross section of aerosol extinction ratio (ratio of aerosol extinction and Rayleigh extinction to Rayleigh extinction) at 1.0 μm wavelength and illustrates the current distribution of stratospheric aerosol loading.

(M. Patrick McCormick, 2065)

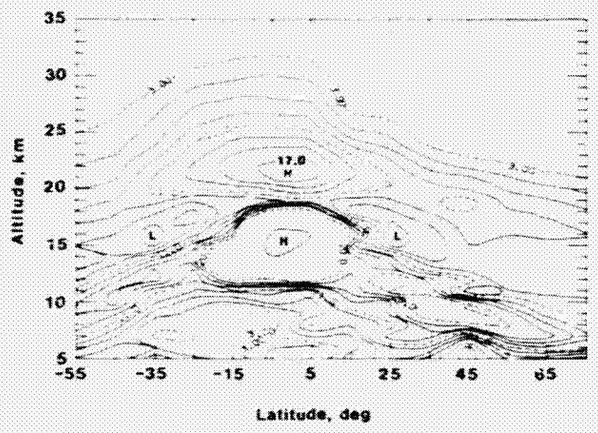

SAGE II zonal mean aerosol extinction ratio for April 1985.

Arctic Polar Stratospheric Cloud Characteristics Measured by Airborne Lidar

Polar stratospheric clouds (PSCs) have been observed at times during Arctic and Antarctic winters since 1979 by the SAM II (Stratospheric Aerosol Measurement) satellite instrument. They are believed to form when diluted sulfuric acid (H_2SO_4) aerosol droplets freeze as the local stratospheric temperature falls below a certain threshold value (−88°C to −78°C, depending on atmospheric pressure and water vapor content). PSCs were probed for the first time by airborne lidar during a January 1984 mission flown on the NASA Wallops Electra aircraft.

Clouds were encountered on three separate flights north of Thule, Greenland (76.5°N, 68.7°W), in locations that correlated strongly with areas of low stratospheric temperature. The extent of their geographical coverage was greater than had been previously reckoned from satellite measurements; on one

flight, coverage extended continuously from about 80°N to the pole. The PSCs occurred in layers, with sharp vertical gradients in backscattering and a horizontal structure that at times changed over a few tens of kilometers. The observed structure was not apparently related to any pre-existing structure in the background stratospheric aerosol and can likely be attributed to small-scale perturbations in the temperature field. At times, backscattering was enhanced by a factor greater than 100 relative to that of the background aerosol. This occurred at an altitude of about 20 km, close to that of minimum temperature. Companion measurements of polarization diversity in backscattered signals indicated the likely presence of frozen particles in the clouds. Calculations made with a theoretical model based on the freezing H_2SO_4 droplet mechanism for cloud formation agreed well with experimental measurements at pressure levels for which consistent temperature data were available. Continuing studies will be aimed at gaining further insight into the physical and optical characteristics of PSCs as well as their influence on the polar climate. **(Lamont R. Poole, 2065)**

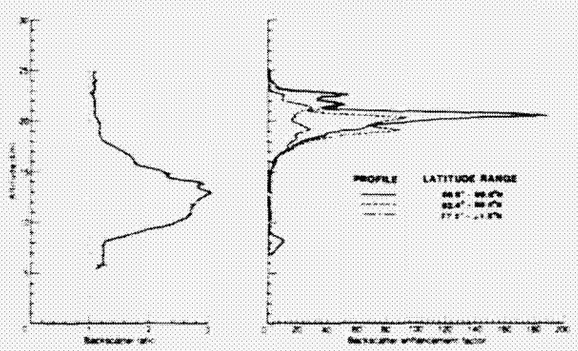

Profiles of background aerosol backscatter ratio (left) and backscatter enhancement factor (right) for three flight segments on January 24, 1984.

Sizes of Stratospheric Aerosols Associated With Polar Vortex Inferred From SAGE Data

The SAGE satellite experiment provides profiles of aerosol extinction coefficient at wavelengths of 0.45 and 1.0 μm. The ratio of the aerosol extinction coefficient at these two wavelengths is a measure of the aerosol size distribution. A smaller ratio corresponds to a larger average size of aerosol particles, and vice versa. Analyses of the temporal and spatial variation of the extinction ratio have provided valuable information on the formation, growth, and dynamics of aerosol particles in the stratosphere. One example is the study of aerosols associated with the cyclones and anticyclones in the winter Arctic region in late February 1979.

In this study, an analysis was performed at four specific pressure levels below 25 km (namely 30, 50, 70, and 100 mb). Data of aerosol extinction ratios in each level were divided into three groups: cyclones, anticyclones, and transition, according to whether their locations were close to the low-pressure center, close to the high-pressure center, or in between. The average aerosol extinction ratios at two wavelengths for aerosols inside cyclones were in general larger than those inside anticyclones. Since the average temperature inside a cyclone is about 14°C lower than that inside an anticyclone, and since aerosols will grow through a heterogeneous condensation process in a cold environment, the average sizes of aerosols inside cyclones were much smaller than those of aerosols in anticyclones. The dynamic effect associated with the sinking air motion during the development of the circumpolar cyclonic vortex may have played an important role in generating the size difference of aerosol particles observed by the SAGE experiment. **(Glenn K. Yue, 2065)**

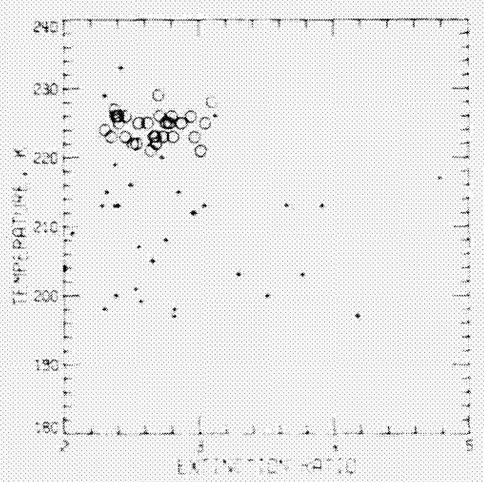

SAGE observation of aerosol extinction ratio at two wavelengths and corresponding ambient temperature in cyclonic (+) and anticyclonic (o) polar vortex at pressure height of 30 mb.

Zonal and Geographical Distributions of Cirrus Clouds Determined From SAGE Data

The Stratospheric Aerosol and Gas Experiment (SAGE) program was developed to begin global monitoring of stratospheric aerosols. SAGE provided vertical profile measurements of extinction due to scattering from aerosols as well as scattering and absorption by ozone and nitrogen dioxide. It was initially anticipated and later shown that these profile measurements would extend well into the troposphere and thus provide the means for useful studies of cirrus clouds. It has been well established that cirrus clouds are a major factor in the Earth's radiation balance and may influence the long-period variations of global temperature.

An analysis of SAGE data for the period February 1979 to November 1981 was performed to determine the spatial extent and frequency of occurrence of cirrus clouds over a large portion of the Earth's surface. The zonal results of the analysis showed that optically thick cirrus clouds form most often in the midlatitudes and over the tropics with distinct minima near latitude bands of 20° to 30° north and south. The percentage of tropospheric observational opportunities down to 7 km was as high as 60 percent in the upper latitudes.

The figure shows the cirrus cloud frequency results summarized for the entire 34-month period. In general, cirrus clouds are produced in regions of rising moist air that are associated with low-level convergence zones. An example is the Micronesia area in the tropical Pacific, usually referred to as the monsoon region. Similarly, there are more cirrus over tropical rain forests, the coastal region of the American state of Washington, and the northwest part of the Pacific Ocean. Features in the figure and also found in previous studies by others include a high-frequency cloud level in the monsoon region bounded by longitudes 60°E to 170°W and by latitudes 20°S to 20°N. Relatively cirrus-free areas exist over the oceans off the western coasts of the continents of the Southern Hemisphere and the central Pacific near the Hawaiian Islands. These areas correspond to persistent high-pressure regions. Also, as expected, the desert areas of northern Africa, the Saudi Arabian peninsula, central Australia, and South Africa are free of high clouds for most of the year.
(Gerard E. Woodbury, 2065)

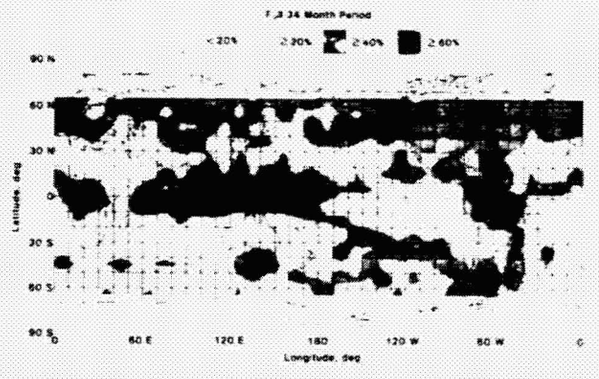

Geographical presentation of frequency of occurrence of cirrus clouds from February 1979 to November 1981.

Behavior of Zonal Mean Aerosol Extinction Ratio and Temperature During Stratospheric Warming

SAM II and auxiliary meteorological measurements during the January-February 1979 stratospheric sudden warming have been used to study the variation of zonal mean aerosol extinction ratio and

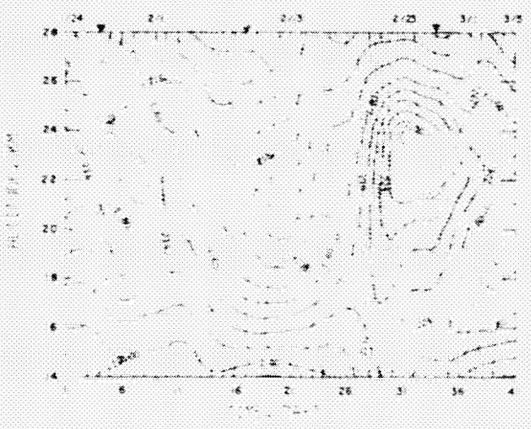

Zonally averaged aerosol extinction ratio (solid line) and zonal mean temperature (K, dashed line) near 75°N during stratospheric warming event of January-February 1979. Inverted triangles denote approximate day of each warming peak. Contour interval is 0.1 for zonal mean aerosol extinction ratio and 2 K for mean temperature.

its relationship with mean temperature near 75°N from altitudes of 17 to 28 km. Results of this analysis indicated distinct changes in the distribution of the mean aerosol extinction ratio during this warming. Relatively low mean aerosol extinction ratios were formed during the second warming pulse in regions above altitudes of about 20 km. On the other hand, the variations of mean aerosol extinction ratio correlated positively with mean temperature variations during most of the third warming pulse. It was also found that below about 20 km these variations were correlated positively throughout almost the entire warming event.

In addition, the concurrent rapid increase of mean aerosol extinction ratio and mean temperature from February 17 to February 23 is of particular interest. An examination of the meridional horizontal transport of aerosol extinction ratio due to planetary waves in the same set of SAM II and meteorological data found that the eddy transport may have played a significant role in the distribution of zonal mean aerosol extinction ratio in the polar region during this winter 1978-1979 stratospheric warming.
(M.P. McCormick, 2065)

Interannual Variation of Infrared Radiation

The Earth Radiation Budget (ERB) instrument on Nimbus 6 and Nimbus 7 has been providing continuous measurements of the Earth's radiation budget beginning with Nimbus 6 in July of 1975. Thus, the ERB's wide-field-of-view (WFOV) sensor has established a continuous 10-year data set of shortwave and longwave radiation measurements for scientific studies.

In a recent study, annual and interannual variations of 5 years of longwave measurements for the months of July and January have been analyzed. The figure shows a contour map of the 5-year interannual variance for January. High and low values of variance are designated by H and L. Large variances over a 5-year period occur in the equatorial and tropical regions. The largest interannual variance is concentrated near the equator off the western coast of South America. Another region of high interannual variance is the region of Indonesia. For July, the largest variances occur over the African continent and Indonesia. The ocean regions of the Southern Hemisphere show very little interannual variance for either July or January. The remaining data set of Nimbus 7 through 1984 is currently being analyzed. This will provide a 10-year time series of longwave measurements and should be invaluable for comparison with the Earth Radiation Budget Experiment (ERBE) results.
(T.D. Bess, 2977)

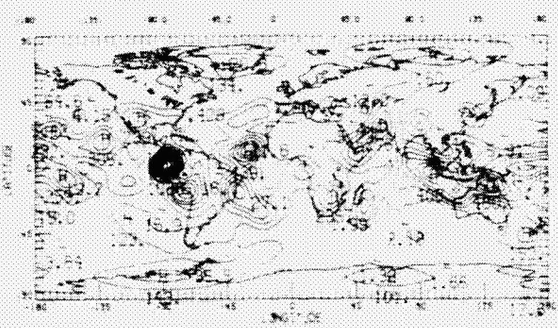

Interannual variance of longwave radiation (W^2/m^4).

Atmospheric Radiation Studies

Radiation balance at the Earth's surface greatly affects atmospheric and oceanic circulations and thus almost all aspects of our weather and climate. Downward atmospheric radiation is one of the important components in the surface radiation balance equation, and weather and climate scientists have attempted to find techniques for local to global scale estimations of this component for many years. Many empirical methods have been developed from climatological data gathered mostly from land areas where measurement sites existed. Polar-orbiting satellites have offered the best Earth coverage, but the interference of the atmosphere on the radiation signal has prevented satellite techniques from being successful. An estimation technique which allows a satellite approach to be used has now been developed and proven at Langley. Satellite-derived meteorological data are used to describe the local atmospheric condition. This allows accurate estimates of the resultant downward atmospheric radiation to be computed. The figure shows monthly averages of the estimated downward atmospheric radiation flux computed by this technique for five sites in the U.S. (identified by

state). These data are for the 1-year period from July 1981 through June 1982.

Future work will involve global mapping of the downward atmospheric radiation component and development of satellite techniques for the estimation of all other components of the surface radiation budget. Complete development of these radiation models will allow detailed study of the effects of clouds, water vapor, other atmospheric gases, and aerosols on the Earth's surface radiation balance.

(Wayne L. Darnell, 2977)

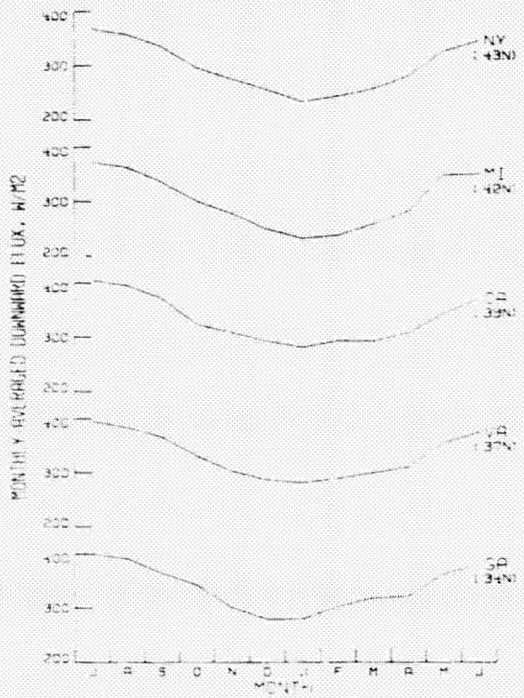

Monthly averages of satellite-derived downward atmospheric radiation at five U.S. sites. Latitudes given in parentheses.

Structures Directorate

The Structures Directorate conducts basic research and develops technology in the areas of advanced aerospace materials and composites, structural loading and aeroelasticity, noise generation by aircraft propulsion systems and structures, and methodologies for interdisciplinary design and optimization. This technology development is directed toward reduction in both weight and cost of aircraft and space structures along with an increase in their reliability and service life. The technology developed also provides improved design capability through more accurate prediction of aerostructural loads, vibration, and noise.

The Materials Division conducts research on advanced materials and their application to aircraft and space structures. The division also develops novel polymeric, metallic, and carbon-carbon materials for these applications. The materials processing and fabrication sciences are developed, and the application of materials to specific flight and space structures is demonstrated. The division conducts research on thermal protection materials and hot structure systems for application to supersonic and transatmospheric vehicles. The fatigue and fracture behavior of materials is studied in specialized laboratories to provide practical methods for insuring structural integrity. Specialized facilities are also used to study the behavior of materials under extreme conditions of high and low temperature, pressure or vacuum, and electron radiation.

The Structures and Dynamics Division conducts research on structures for advanced aircraft, space vehicles, and the space station. Analytical methods are developed for the prediction of static and dynamic stresses and strains in complex structures. Research is conducted on transient response of structures to aircraft control systems and landing dynamics. Specialized facilities are used to study the dynamics and deformations of aircraft crashes. The division develops new structural systems for aircraft and space structures and is also active in research and development of advanced computational methods for structural analysis and design.

The Loads and Aeroelasticity Division conducts research in aeroelasticity, aerothermal loads, high-temperature structures, unsteady aerodynamic loads, and aeroservoelasticity. Analytical methods are developed for calculating aeroelastic deformations and instabilities, for dynamic, vibratory, and thermal response of structures, and for the active control of aeroelastic and dynamic behavior of aircraft. Unique facilities are employed in experimental studies of unsteady aerodynamics, aeroelastic behavior, and aerothermodynamic flows.

The Acoustics Division conducts research on the generation and propagation of aircraft noise and seeks to understand the relationships between unsteady aerodynamics, structural dynamics, and noise generation by the interaction of fluids with solid surfaces. This research is directed toward predicting and reducing the noise from helicopter rotors, conventional and advanced aircraft propellers, and turbofan engines. Research is conducted on the propagation of noise from its source through the atmosphere and through aircraft structures.

The Interdisciplinary Research Office develops methodologies for aircraft and spacecraft design which will provide a means of understanding and quantifying interactions among multiple engineering disciplines. The goal is to control and exploit these interactions for improved vehicle performance and increased efficiency of the design process. This research has focused on the development of algorithms and techniques for integrating strength and stiffness designs of large-aspect-ratio wing transport aircraft. The methodology has been developed for the optimization of space antenna dish shapes subjected to thermal loadings. Controls, structures, and structural dynamics have been integrated for use in the design of space station type structures.

Analysis and Design for Space Station

Methods are needed which allow quick development and evaluation of possible space station configurations. As part of this effort, an integrated multidisciplinary analysis tool (IMAT) has been developed which links structural analysis codes and controls analysis codes by input and output data transfer through a common database system. A finite-element model of a current space station concept was originally developed at NASA Johnson Space Center and was transferred to Langley. The capabilities of IMAT were used to convert this model to Langley analysis codes. Vibration modes and frequencies were calculated and stored in the IMAT database. A controls program was used to calculate the control moment gyro (CMG) response due to an orbiter docking impulse. The loads data from the

controls analysis were transferred back to the structural analysis program through IMAT. A transient response analysis was then made to give deflections and stresses of the structure. A typical response showing displacement of a particular point is presented in the first figure.

An additional aid to the conceptual design of space station was the fabrication of a 1/72-scale model of the 75-kW IOC power tower. The three-dimensional model allows visualization of the relationship between various components. This is a great aid in arriving at their most effective placement to satisfy mission requirements and constraints.
(Paul A. Cooper, 3787)

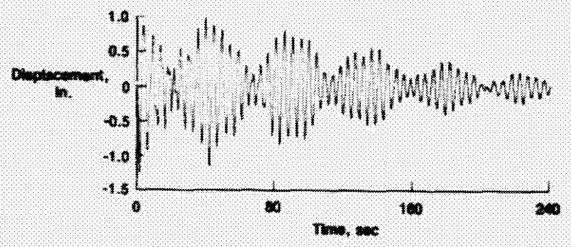

Docking transient response at point A.

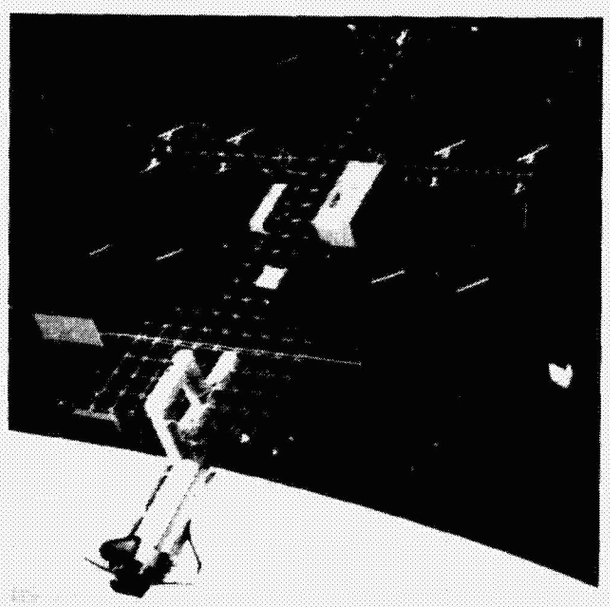

L-85-6735

Scale model of Space Station concept.

Acoustic Loading From Twin Supersonic Jets

The similarity in spacing between the exhaust nozzles of the B-1 and F-15 aircraft suggests that the cause of the damage to the nozzle exterior found on both aircraft could be due to the intense acoustic loading produced by an interaction of the jet exhausts. A scaled model of their exhaust configuration was constructed from ⅝-in. pipe mounted in a wooden housing. A microphone was mounted on the interfairing of the nozzles to enable comparison of the acoustic near field generated by the twin jet configuration with that of a single jet (attained by blocking off the flow in one of the pipes). From this it could be

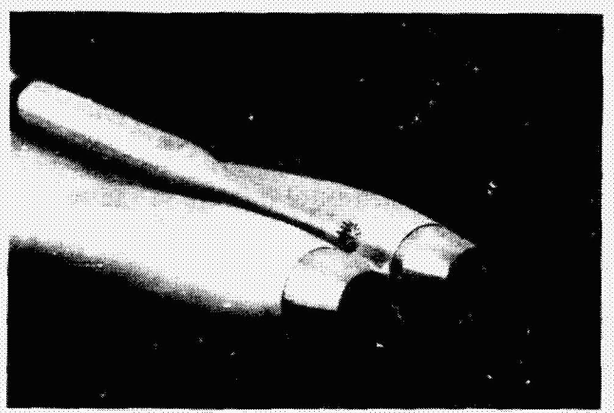

L-85-8765

B-1 dual-nozzle configuration with microphone.

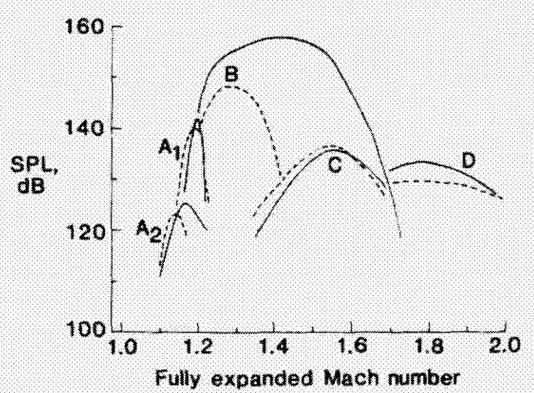

Screech tone amplitudes (SPL) for twin jet (solid line) and single jet (dashed line).

determined if closely spaced dual nozzles generate significantly higher acoustic loading than a single nozzle.

The noise radiated upstream from imperfectly expanded supersonic jets is generally dominated by a series of high-amplitude tones. These are generated in the screech process, which consists of a feedback cycle between the nozzle exit and shocks within the jet plume. Different stages of screech exist; the five most commonly found are labeled stages A_1, A_2, B, C, and D. Stage changes consist of discrete jumps in both the wavelength of the radiated tone and the spacing of the downstream shocks within the jet.

The amplitudes of the screech tones were measured for both the single and twin jets over a wide range of jet fully expanded Mach number. The amplitudes were similar for both nozzle configurations for all but the B stage. The presence of the second jet greatly enhanced both the B stage amplitude and the Mach number range over which it dominated. The enhanced resonance of the closely spaced twin jets could increase the pressure impinging on empennage by more than 20 dB. Its amplitude exceeded 155 dB over a range of jet Mach numbers, a level that could certainly cause structural damage in the twin-jet configuration.

(T.D. Norum, 2645)

Acoustic Properties of Nonaxisymmetric Supersonic Nozzle

Future propulsion system concepts for high-performance aerospace vehicles may have to consider potential sonic fatigue criteria to achieve overall mission goals. As an illustration of this point, consideration was recently given to the associated noise field of a 2-D C-D (two-dimensional convergent-divergent) supersonic exhaust nozzle with partial sidewalls. Performance studies showed that partial sidewalls enhanced vectoring capability, lowered cooling requirements, and reduced nozzle gross weight with negligible performance losses. Acoustic studies performed in the Anechoic Noise Facility, however, indicated that relative to the same 2-D C-D nozzle with full sidewalls there was a drastic increase in acoustic energy emitted. This increase was composed of high-amplitude tones, as shown in the power spectral density (PSD) plot. The tone level was as much as 50 dB (300 fold) higher than the broadband component.

The high energy tones obtained in this study, when scaled to a full-size engine and fuselage location, would require additional structural weight to safeguard against sonic fatigue damage. This increase in structural weight could dramatically compromise overall mission goals for the vehicle. Further tests are currently being conducted to determine the aerodynamic origin of the increased acoustic energy with a view to developing efficient methods for suppression.

(John M. Seiner, 3094)

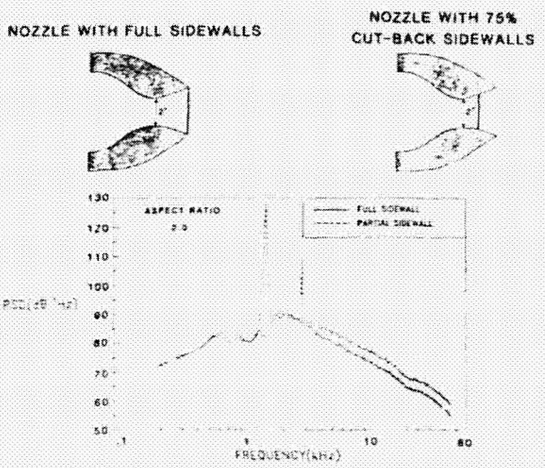

Effect of partial sidewalls on acoustic emissions from low-aspect-ratio 2-D C-D nozzles.

New Aluminum Alloys Offer Enhanced Superplasticity

Superplastic forming (SPF) is a revolutionary new process for forming advanced aluminum aerospace components. When heated to 970 °F and subjected to low stresses (250 psi), fine-grained 7475 aluminum can be stretched to 6 to 10 times its original length, provided a proper strain rate is maintained. The process offers cost savings of approximately 50 percent and weight savings of approximately 30 percent compared with similar components fabricated by conventional means. Cost savings result from reduced labor cost and weight savings from improved structural efficiency. The increased formability makes it possible to fabricate geometric configurations to

exacting tolerances that are not possible with conventional metal-forming methods.

Prior studies have verified the significant cost and weight savings potential of superplastic forming. In the present studies, the chemistry of the 7000-series aluminum alloys is being modified to increase both the permissible forming strains and forming rates. Initial results obtained are illustrated in the figure, which shows total elongation versus true strain rate for both 7475 aluminum alloy and an alloy of similar composition with a reduced amount of iron and silicon. The data show that the modified alloy is capable of being formed at approximately three times the strain rate of conventional 7475 aluminum over the range of strain rates evaluated. These results point to the potential of additional cost savings through reduced forming times.

(Thomas T. Bales, 3405)

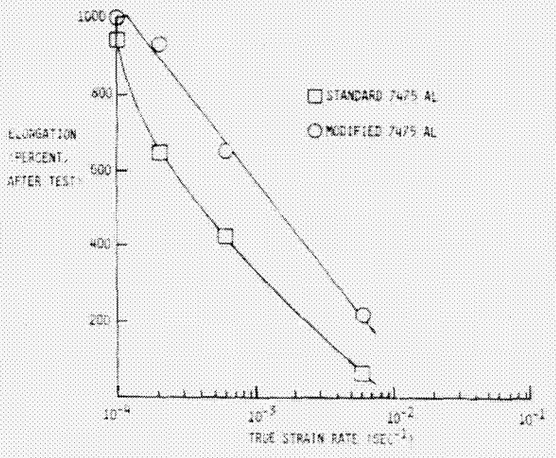

SPF elongation versus strain rate for standard and modified 7475 aluminum alloys.

Study Explains Growth of Small Fatigue Cracks

Numerous investigators have observed that the growth characteristics of small fatigue cracks (less than about 1 mm long) differ from those of large cracks. Small cracks have been found to grow much faster than should be predicted from large crack data and to grow at stress levels well below the threshold for large cracks. Because crack growth from small pre-existing flaws in many engineering structures occurs during a major portion of the component's fatigue life, the growth behavior of small fatigue cracks is important to the understanding of the total fatigue process.

In a joint study by Langley and Kentron International, Inc., the growth of small cracks (5 to 500 μm) from semicircular edge notches in 2024-T3 aluminum alloy specimens was monitored with the use of a replica technique. Replicas of the notch surface were made periodically during the fatigue test and were examined in the scanning electron microscope. Crack lengths were traced backwards in time from easily located large cracks to the small crack sizes. Microstructural features, such as grain boundaries and inclusion particle clusters, were used to locate cracks down to sizes of less than 10 μm. Crack initiation at inclusion particle clusters was commonly observed. The micrographs show two replicas of a fatigue crack after 3000 and 9000 cycles.

The experimental results exhibited the small-crack effect; that is, the small cracks grew faster than the large cracks at the same stress levels, and small cracks grew below threshold stress levels for large-crack growth. An existing analytical model, called the crack closure model, considers detailed stress distributions at the crack tip. This model was used to analyze the growth of small cracks from small defects (inclusions) at the notch surface. Reasonable agreement was found between measured and predicted crack growth rate. This indicated that with closure included, fracture mechanics may be able to accurately predict crack growth in this regime.

(Mary H. Swain, 3011)

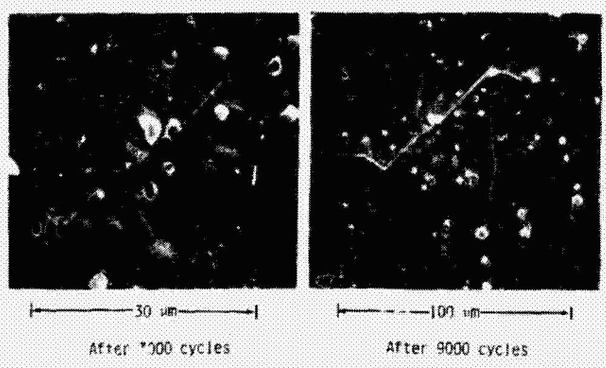

Micrographs of small fatigue cracks.

Improved Aluminum Matriv Composites

Potential applications for aluminum matrix composites include aircraft structures, propulsion systems, and space structures, particularly in areas that may require a good blend of strength, stiffness, thermal stability, and formability. However, the use of these materials has not been widespread because of their historically low strain to failure and poor fracture toughness. Lockheed California, under contract to Langley, has made significant progress toward the resolution of these problems through primary processing controls, innovative secondary processing, and alloy chemistry modifications.

The figure shows strength-ductility combinations for 2124 powder aluminum alloy reinforced with silicon carbide whiskers (SiC_w). The large increase in both strength and ductility of the extruded product is primarily due to improved quality control on the reinforcing whiskers. This resulted in increased whisker length and minimization of intermetallic inclusions and contaminants. Chemistry changes, such as the addition of small amounts of zirconium to the base alloy for microstructural stabilization and homogenization, have further increased the elongation of the extruded product by as much as 5 percent with a modest reduction in strength. Selected secondary processing such as stretching or rolling has added another significant increment to the elongation of the composite (up to 7 percent) with no loss in other properties. The combinations of properties achieved exceed the target goals, which were based on an equivalent weight of titanium, and could lead to high payoffs in terms of structural efficiency and cost.
(William D. Brewer, 4193)

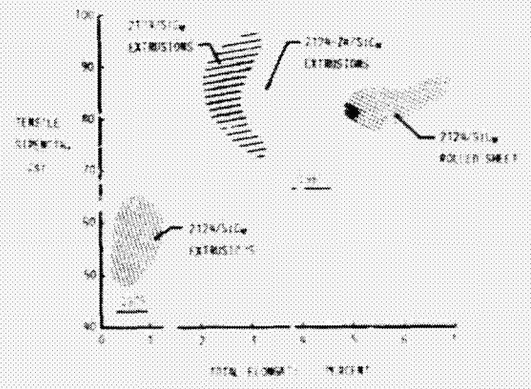

Evolution of strength and elongation combinations for SiC_w reinforced aluminum matrix composite.

Analysis estimates of Matrix Crystallinity in Composites

Crystallinity, a measure of the degree of molecular order within a polymer, is related to toughness and solvent resistance and is generally determined by wide-angle x-ray diffraction scattering (WAXS) procedures. A composite of carbonaceous fiber with a poly(etheretherketone) or PEEK matrix is currently under study and shows promise as an aerospace material. This study attempts to correlate mechanical properties with the polymer matrix crystallinity; however, the usual methods of crystallinity determination from WAXS data are made very difficult (or impossible) by the obscuring effect of scatter from the fiber.

A computer program has been written to resolve the combined WAXS data into crystalline scatter from the polymer matrix, crystalline scatter from the fiber, and a noncrystalline contribution. In this program the crystalline peaks are represented as a linear combination of theoretically expected Cauchy and Gaussian expressions, and the noncrystalline contribution is expressed as a cubic polynomial. The resolution of the WAXS data is displayed in the figure, the top curve of points being the measured data. On this figure the crystalline contribution, as represented by the reflections from crystalline planes defined by the indices 110, 113, 200, and 213, is 25 percent of the total scatter from the polymer. The resolution, which was performed in the least-squares sense with numerical algorithms, permits an estimation of crystallinity.
(Noel T. Wakelyn, 3041)

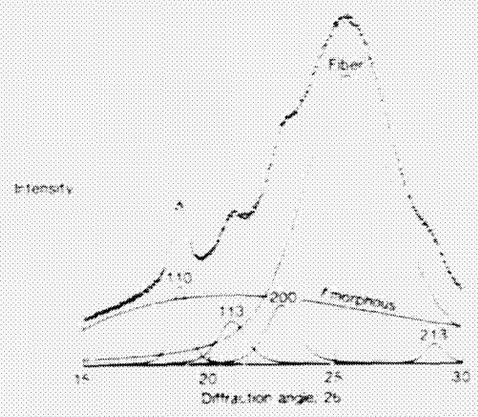

Resolution of wide-angle x-ray scattering from PEEK composite material.

Semi-Interpenetrating Polymer Networks Improve High-Temperature Polymers

Extensive research in polymer chemistry in the last several decades has seemingly exhausted the discovery of any new classes of polymers. An area of increasing importance, therefore, is finding new ways of modifying the existing polymer systems to obtain improved properties. One such method involves the combination of a thermoplastic and a thermoset polymer such that the thermoset reacts within a matrix of the thermoplastic to form a semi-interpenetrating polymer network (semi-ipn). Thus, when two polymers become physically entangled they can produce synergistic properties.

In a joint research project with Kentron International, Inc., Langley developed novel semi-ipn by the combination of two nearly identical high-temperature polymers, polyimidesulfone and acetylene-terminated polyimidesulfone, in various ratios. This eliminated the phase separation problems seen in most semi-ipns.

Characterization of these semi-ipns indicated that several of them had improved thermooxidative stability. The semi-ipns retained adhesive strengths well above the target value of 2000 psi. Fiber-reinforced composites prepared from the semi-ipns gave near-target mechanical strengths without optimization work. Most significantly, the semi-ipns produced a great improvement in processability. These results indicate that similar avenues of investigation may be open to many polymer systems previously thought to have been fully developed.

(Annemarie H. Egli, 4197)

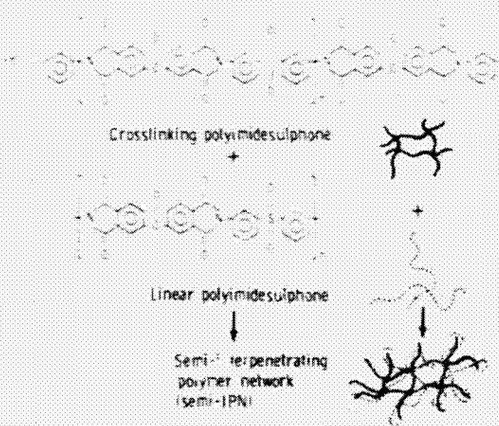

Preparation of semi-ipns.

Polyimide Cure Studies Clarify Processing Requirements

Several new polyimide resins synthesized from somewhat exotic starting materials are soluble at all stages of cure in a number of common nondegrading solvents. This behavior allows solution property measurements to be made as a function of cure temperature to yield information not generally available on more conventional but insoluble polyimides. Thus, new insights into polymer cure can be obtained through characterization of these soluble materials.

Viscosity measures how easily a material flows, and lower values mean easier flow. Room temperature inherent viscosity measurements (η_{inh}) were made on a polyimide (starting from poly(amic acid) dissolved in dimethylacetamide (DMAC)) at 25°C intervals as the polymer was cured. The figure shows that the viscosity goes through a minimum (maximum flow) between 125°C and 175°C and increases dramatically during final stages of cure. The inflection in the curve around 225°C corresponds with the glass transition or softening temperature (T_g) of the polymer. Average molecular weight measurements made by membrane osmometry and corroborated by gel permeation chromatographic analysis indicated that molecular weight increased from 21,200 at 175°C to almost 42,000 at 300°C.

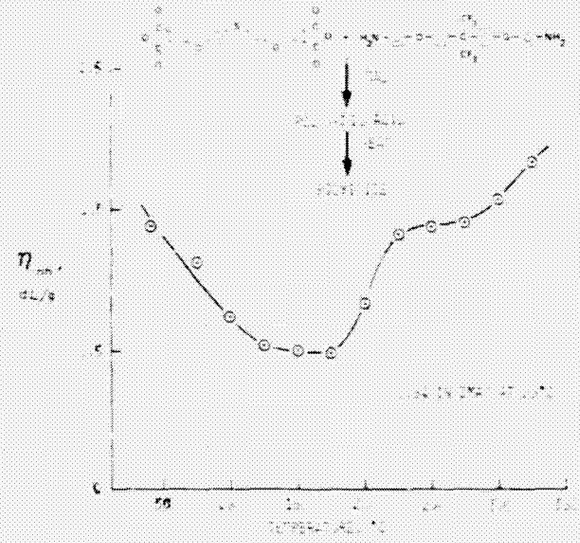

Inherent viscosity of thermally staged polyimide film.

These unique results have been correlated with the behavior of conventional polyimides of more immediate interest through an extensive infrared spectroscopic study. The new information increases our fundamental understanding of how polyimides are formed. It also provides insight into how they might be more easily processed into useful articles. For example, to achieve maximum resin flow during processing of fiber reinforced composites, pressure should probably be applied below T_g rather than above. This conclusion has been partially verified in processing studies.
(Philip R. Young, 3041)

New Formulation of Airplane Dynamic Loads Equations

The two most common methods of calculating airplane dynamic loads are the mode displacement method (MDM) and the summation of forces method (SFM). Both methods give theoretically identical answers for a sufficient number of modes. However, it has been shown that the SFM converges more quickly (that is, with fewer modes) than does the MDM. A major difference between the MDM and the SFM is that the dynamic loads equations obtained with the SFM contain frequency-dependent aerodynamic coefficients, whereas the dynamic load equations obtained with the MDM do not. Until now, the dynamic load equations obtained with the SFM have been formulated only in the frequency domain. A new formulation has been developed which uses s-plane approximation methods (previously applied only to the equations of motion) to transform the dynamic loads equations from a second-order frequency domain formulation with frequency-dependent coefficients into a linear-time-invariant state space formulation. This allows the use of the superior (in terms of modal convergence) SFM for multivariable control system analysis and synthesis tasks. The results of several numerical examples have demonstrated the usefulness of the new technique and the high quality of the results.

The s-plane approximation and corresponding tabular values for an element of one of the aerodynamic matrices are illustrated at the left of the figure for one of the examples. A comparison of dynamic load frequency response functions (FRF) is presented at the right of the figure. They both represent wing root bending moment due to oscillation of the outboard control surface on the wing, and both contain inertia, motion-aerodynamic, and disturbance-aerodynamic components. One frequency response function was computed with the frequency domain formulation of the dynamic load equations, the other with the time domain reformulation. There is excellent agreement in the magnitude comparison and very good agreement in the phase angle comparison.
(Boyd Perry III, 3323)

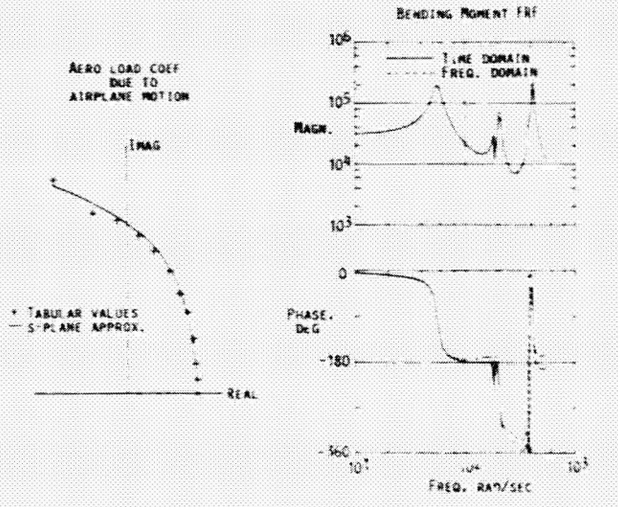

Transformation of dynamic loads equations.

Transonic Vortex Flows Past Highly Swept Wings Calculated by Integral Equation Method

The ability to accurately calculate the complicated transonic vortical flows around highly swept wings at high angles of attack is a key problem in the future development of highly maneuverable fighter aircraft. These flows involve shock waves as well as large velocity variations and produce pressures on wing surfaces that differ drastically from those predicted by classical small-perturbation methods. With the efforts of Dr. Osama Kandil of Old Dominion University, this problem has been formulated by use

of the full-potential equation. This equation was converted to integral equation form, in which the velocity at any point in the flow field is expressed in terms of a surface integral of vorticity on the wing and on the free vortex sheets in the flow and a volume integral of source-like terms within a volume around the wing and its vortex sheets. Solution is obtained by iterations in which the boundary conditions on wing and free vortex sheets are satisfied and the volume distribution of sources is successively updated.

The figures show a crude proof-of-concept application to a thin aspect-ratio-1.5 delta wing at 15° angle of attack and Mach 0.7. Spanwise variation of pressure on the upper surface is shown at a location 80 percent of the root chord downstream from the wing apex. Calculated pressures are compared with experimental data, with a much more expansive finite-volume computation by Euler equation, and with a computation for incompressible flow. Improved agreement between experiment and the present computations should be obtained when the leading-edge vortex sheet is allowed to roll up an additional half turn before being transferred to the vortex core. That calculation is under way. The figure also shows the calculated Mach number contours, the shape of the leading-edge vortex sheet, the captured shock, and the cross flow velocity field and deforming free vortex sheets from leading and trailing edges at a location 27 percent of the root chord downstream from the trailing edge. The present method, which does not suffer from the numerical diffusion of existing Euler solvers, is being further refined and generalized.

(E. Carson Yates, Jr., 4346)

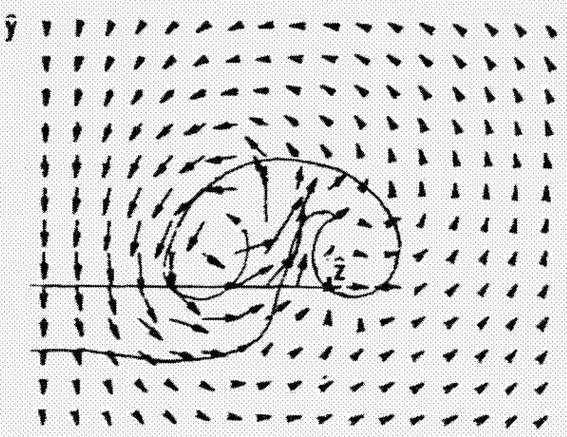

Velocity field and vortex sheets behind trailing edge.

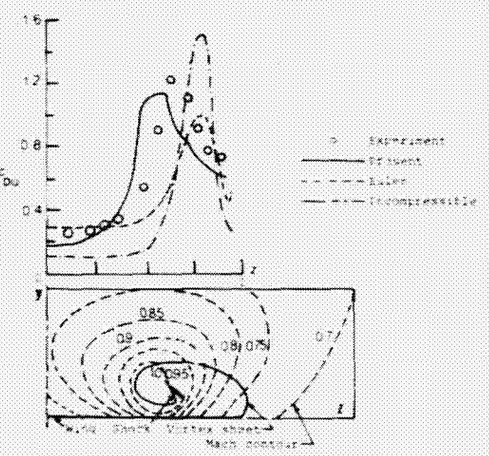

Pressure variation (c_{pu}) and details of flow in cross flow plane.

Eigenvalue Gradient Information Used To Stabilize Linear Systems

Most optimal control law synthesis techniques require an initial control law that results in a stable closed-loop system. The methods presently used to determine such a control law are largely trial and error and can therefore be time consuming, especially for open-loop unstable systems. The objective of this research was to develop a method that was mathematically based and overcame the difficulties associated with the trial and error approaches.

A stable system is one in which all real parts of the system eigenvalues (λ) are less than zero. The problem was therefore to determine the control law parameters P (e.g., gains, poles, and zeros) which make all the real parts of the eigenvalues negative. The method developed to solve this problem employs a gradient-based optimization algorithm to determine a search direction for the control law parameters that will move all eigenvalues into the left half of the complex plane. An important element in employing the optimization algorithm is the calculation of the gradients. The present research included the development of analytical expressions for the gradients of the eigenvalues with respect to control law design variables. An indirect constrained optimiza-

tion method (a penalty function approach) was adopted in which the objective function was a penalty function of all the real parts of the eigenvalues. A flow chart of the overall method is illustrated.
(Carol D. Wieseman, 4232)

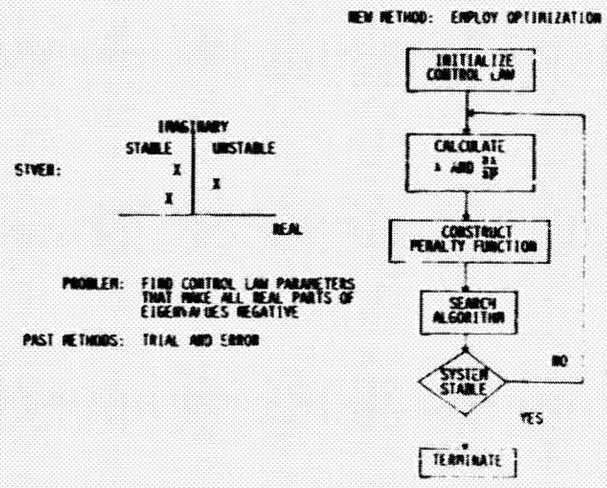

Flow chart of method developed to determine a control law that stabilizes unstable systems.

Flight Tests Demonstrate Effectiveness of Decoupler Pylon Flutter Suppression System

Flutter of wings with external stores is an important aeroelastic problem that can penalize airplane performance because it is often necessary to placard the operational envelope to ensure safe flight. The decoupler pylon (DCP) is a novel device that dynamically isolates the wing from external store pitch inertia effects by means of soft-spring and damper components that increase the flutter speed. An alignment system is incorporated to minimize static pitch deflections of the store due to maneuvers and aerodynamic loads. Because analyses and wind tunnel tests of YF-17 and F-16 flutter models with stores have shown increases in flutter dynamic pressure in excess of 100 percent over the same stores mounted on standard pylons, a flight demonstration program was undertaken to further investigate the effectiveness of the DCP. The flight test program demonstrated flutter suppression on the F-16 with the same store configuration tested in the wind tunnel with a goal to demonstrate a 70-percent increase in flutter dynamic pressure over a production pylon. The flight tests brought into focus the effects of turbulence, flight maneuvers, store ejection, and flight control system interactions. These are factors that could not be simulated in previously conducted wind tunnel tests.

The flight test stores configurations included the following: AIM-9J wingtip missiles, GBU-8 bombs near midspan, and half-full 370-gallon fuel tanks. The flights were first made with 2250-lb GBU-8 bombs mounted on the F-16 production pylon. The continual strong pounding oscillations which characterize the flutter with the midwing store mounted on its standard pylon are shown at the right in the figure. The flights were then repeated with GBU-8 mounted on decoupler pylons. As can be seen in the figure, the decoupler pylon successfully suppressed the wing/store flutter. No evidence of flutter was detected throughout the flight envelope of this stores configuration. An 84-percent increase in dynamic pressure over the production pylon was demonstrated by the decoupler pylon. Maneuvers up to 4 *g*'s were performed throughout the flight envelope. Only small pitch deflections of the store were recorded, so the alignment system was seldom needed although it performed well and realigned the store when activated. At the conclusion of the flight test program, the GBU-8 was ejected to demonstrate that weapon separation is normal from the decoupler pylon.
(Frank W. Cazier, Jr., 2661)

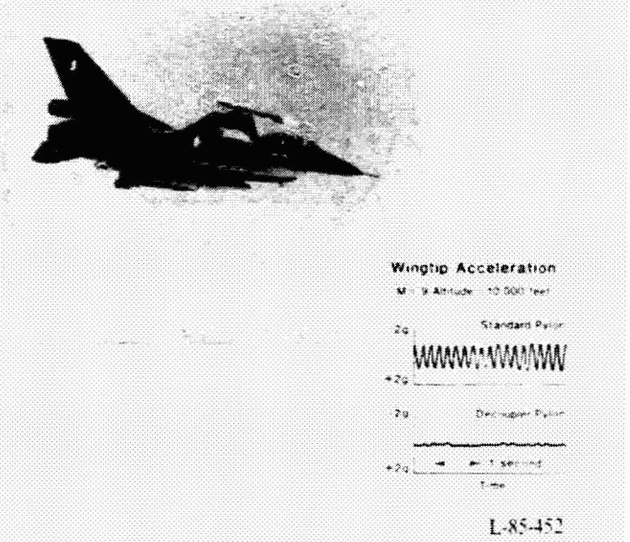

Decoupler pylon suppresses flutter.

Transonic Code Extended to Multiple Lifting-Surface Configuration

The three-dimensional finite-difference computer code XTRAN3S, which provides a time-marching solution to the nonlinear small-disturbance potential equation for transonic flow, has been extended at Langley to apply to combinations of lifting surfaces such as canard-wing and wing-tail configurations. The figure shows results of an application of the extended code to a closely coupled canard-wing geometry. Both lifting surfaces have NACA 0010 airfoil sections. The free-stream Mach number is 0.9 and the mean angle of attack is 2.0° for both canard and wing. The canard was forced to oscillate harmonically in pitch at a reduced frequency of 0.3 and the wing was held fixed. Spanwise distributions of sectional lift coefficients are plotted for the canard ($C_{l,C}$) and wing ($C_{l,W}$) as functions of fractional canard semispan $\bar{\eta}_c$ and fractional wing semispan $\bar{\eta}_w$, respectively, where S is the separation distance measured in units of wing root chord. The canard sectional lift shows only very small differences between the isolated lifting surface and canard-wing cases. The spanwise loading on the wing induced by the canard pitching motion is of sizeable magnitude in comparison with the canard loading and is dependent on the distance separating the two lifting surfaces.

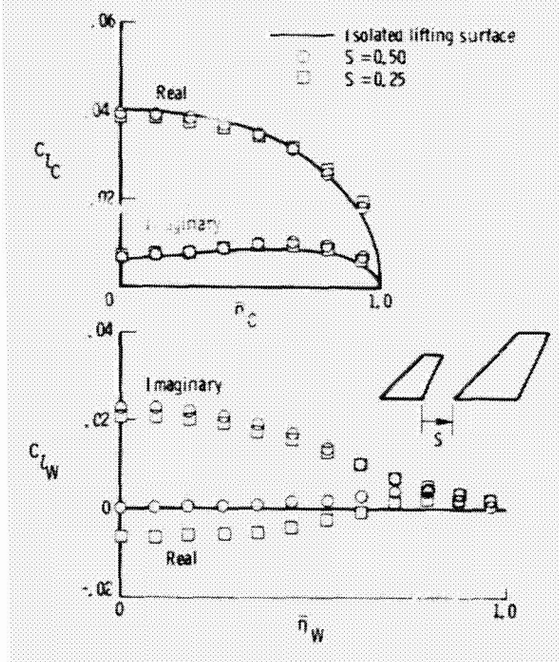

Sectional lift coefficients on canard-wing configuration caused by canard pitching.

The study has assessed the effects of aerodynamic interference on transonic steady pressure distributions and unsteady airloads for simple canard-wing and wing-tail configurations. The calculations were performed for several mean angles of attack and for different separation distances.
(John T. Batina, 4236)

Transonic Steady and Unsteady Aerodynamic Calculations for Wings

A transonic aeroelastic analysis code for wings called XTRAN3S was developed by Boeing under contract with the Air Force. It has been implemented and further developed at Langley on the VPS32 computer. The code is based on the unsteady three-dimensional small disturbance equation and can calculate unsteady aerodynamics, static aeroelastic effects, and flutter. Extensive calculations have been made for steady and unsteady pressures on the AGARD Structural and Materials Panel tailplane configuration, which has a highly swept and tapered planform and a conventional NACA 64A010 airfoil section. The model was tested by the British RAE at Bedford and was oscillated in pitch at several frequencies and Mach numbers. An early release of the data was obtained by NASA through a cooperative agreement with the RAE. The figure shows the first harmonic of the unsteady pressure coefficients per unit of pitch angle, C_p, versus local chord x/c for several nondimensional span locations $\bar{\eta}$. There is generally good agreement of the calculated results except near the leading edge and tip regions. The case presented is for a Mach number of 0.86 with a mild shock wave on the wing and a reduced frequency of oscillation of 0.22. Similar agreement was obtained for subsonic cases, but the agreement deteriorated as Mach number was increased to 0.95. Thus XTRAN3S should give satisfactory flutter results for a configuration such as this when the transonic shock waves are weak.

Extensive calculations, including the effects of static deformation, have also been made for the DAST ARW-2 wing tested in the Langley Transonic Dynamics Tunnel. The static aeroelastic deformation

effects were found to be large and significant, but for this high-aspect-ratio supercritical wing there was poor agreement with measured transonic static data. Efforts to further evaluate and improve XTRAN3S are continuing.
(Robert M. Bennett, 2236)

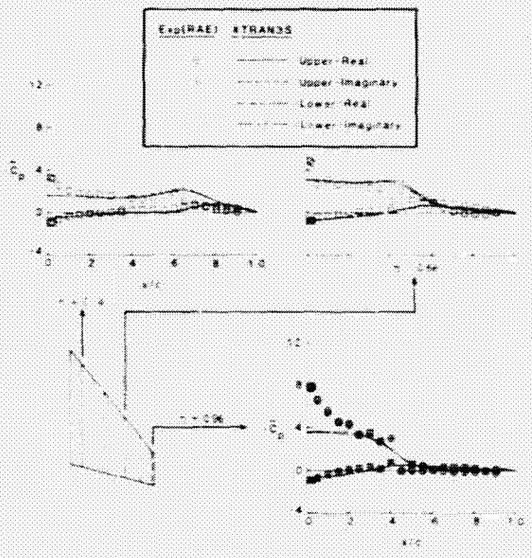

Measured and calculated unsteady pressures.

Active Noise Control

The high noise levels expected in the interior of the new-generation advanced turboprop-powered aircraft have focused efforts to control the low-frequency noise environment of these aircraft. One promising method involves the use of synthesized noise to help attenuate the propulsion noise inside these aircraft. Current research efforts have demonstrated the viability of this technique for controlling random progressive wave fields. These techniques promise to be most effective at low frequencies where conventional passive absorbers have little effect.

The figure shows the configuration used in an initial evaluation for controlling random noise in a one-dimensional waveguide. Estimates of the incoming acoustic field are provided by a microphone upstream of the control speaker location. This signal is processed through a digital filter and combined with the incoming wave field through a control speaker. The object is to minimize the noise transmitted beyond this location. A measure of this noise is provided by a properly located error microphone, which supplies information by which the effectiveness of the controller may be determined. Adaptive filter techniques allow the digital filter characteristics to be altered based on the available information to decrease the noise sensed at the error microphone. This allows the system to adapt to slowly varying conditions while maintaining continual control over the noisy environment. Also shown is the measured sound power level at the error microphone with the control off and with the controller at various iteration levels. Control was restricted to a frequency range from 50 to 400 Hz. Suppressions range from 15 to 30 dB over the frequency range of interest. The adaptive algorithm converges rapidly to a minimum level and maintains the suppression through several iterations.

Work is continuing to extend these control techniques to multidimensional spaces. Modeling of the acoustic spaces provides insight into the necessary number and location of control sources. Multivariate control systems must also be defined to implement these concepts in practical environments.
(Richard J. Silcox, 3561)

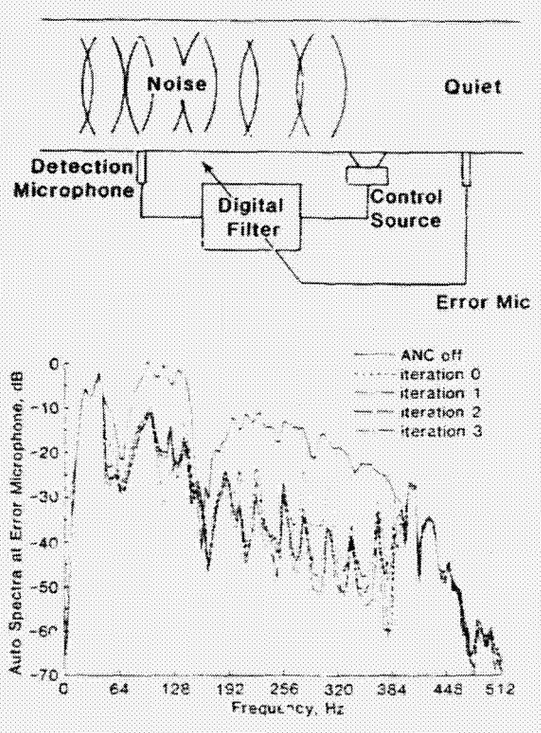

Active control concept and system performance.

Laboratory Study of Sidewall Acoustic Treatment

In recent years much attention has been given to reducing the interior noise of propeller-driven aircraft. Most of the recent experimental work has been performed on flat panels in the laboratory. The measurement of the transmission loss of flat panels, however, does not take into account the interior acoustic space nor the vibrational modes of the aircraft as a whole. Some data from in-flight testing are also available. However, such testing can be expensive and time consuming, and the repeatability of the exterior sound field is questionable. For these reasons, a study was performed on an actual aircraft fuselage in the laboratory.

A small airplane fuselage was placed in a large chamber and surrounded by fiberglass baffles. Broadband noise was emitted from an exponential horn attached to a pneumatic air driver. Interior sound pressure levels were measured and recorded at the approximate head positions of the six passengers. Data were acquired for four fuselage treatments: the baseline treatment (bare walls covered with damping material), the trim-panel treatment (baseline treatment plus the manufacturer's production line trim), the 1.5-in. fiberglass treatment (1.5-in. fiberglass on the baseline treatment), and the 3-in. fiberglass treatment (3-in. fiberglass on the baseline treatment).

The effects of the treatments were evaluated from the standpoint of insertion loss, which is the change in interior sound pressure level due to a specific treatment relative to a second treatment, in this case the baseline. A comparison of the space-averaged one-third-octave-band insertion losses (of the trim-panel and fiberglass treatments) from 100 to 1000 Hz is shown. The insertion loss for the trim panel treatment (circular symbols), which weighed 35 percent more than the 3-in. fiberglass treatment, was less than that for the 3-in. fiberglass treatment (upper band of shaded area), except at 125 and 160 Hz. In the 125- and 160-Hz bands, the insertion loss of the two treatments was nearly the same. In addition, the insertion loss for the trim panel treatment was nearly the same as that for the 1.5-in. fiberglass treatment (lower band of shaded area) from 200 to 500 Hz. Thus the fiberglass treatments seemed to attenuate the sound as well as the trim panel treatment, but with less weight.

(Karen E. Heitman, 3561)

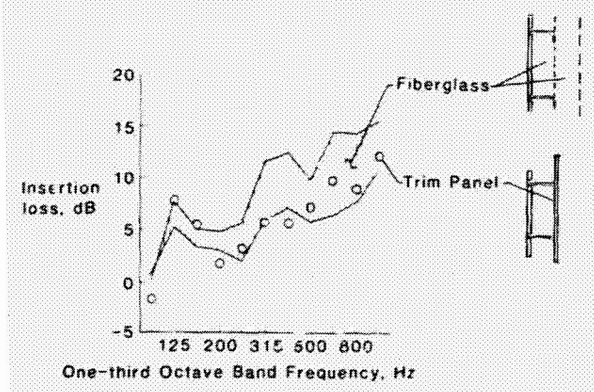

Insertion loss of fiberglass vs trim panel.

Prediction of Propeller Aircraft Interior Noise

Passenger acceptance of propeller aircraft, especially new aircraft such as the planned fuel-efficient high-speed turboprop aircraft, is highly dependent on the control of interior noise levels. It is desirable and efficient to predict the levels and to optimize noise reduction treatments early in the aircraft design stage. In a recently concluded Langley program, an interior noise prediction method was developed to predict the dominant cabin noise levels due to the blade passage harmonics of the propeller.

The analytical prediction model (formulated by Bolt Beranek and Newman under NASA contract) is based on the concept of acoustic power flow into a cylindrical enclosure. The analysis requires a precise description of the propeller noise (pressure amplitude and phase) defined over a grid that lies on the fuselage skin. These data are calculated from the propeller noise prediction module of the Langley Propeller Aircraft Noise Prediction Program. This complex pressure loading is coupled to the dynamic modal response of the shell structure, which includes ring frames, stringers, a stiffened floor, and sidewall trim. The structural modes are coupled to the interior acoustic modes to determine the sound energy radiated into the cabin space, taking into account the geometry of the cabin space and the absorption characteristics of the sidewall trim.

The analysis was initially validated by measurements on a simplified propeller/fuselage model and progressed to models with more realistic structural

and interior trim details. Typical comparisons of the model predictions to full-scale flight test data are shown. The flight measurements are for an executive version of a twin-engine commuter airplane. The predictions for four of the first five harmonics of the fundamental blade passage frequency are only a few decibels greater than the respective experimental data. The deviation from this trend at the fourth blade passage harmonic may be a peculiarity of this particular airplane. Further refinement of the model is being conducted through parametric studies and additional laboratory and flight validations. It is felt that the good agreement between the predicted and experimental data provides flight validation of the model, which had previously been validated only in the laboratory. The Propeller Aircraft Interior Noise (PAIN) computer program is being made available to the U.S. aircraft industry and research organizations.
(Todd B. Beyer, 3561)

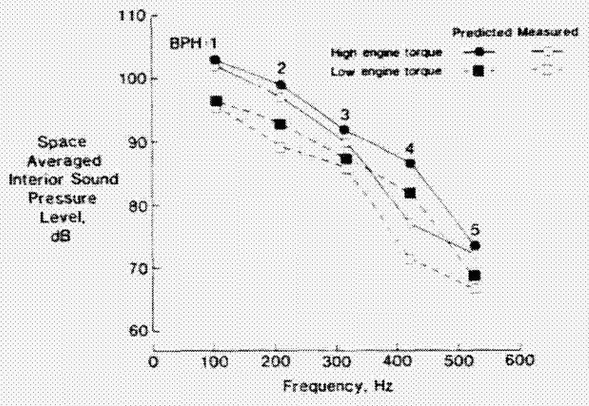

Predicted and measured interior noise levels of twin-engine propeller airplane.

Mir.'mum-Length Mixer for High-Velocity Gases

The mixing of fluid' to achieve a homogeneous mixture usuaiiy req,uires long contact time and lo.g mixing lengths. However, some applications, such as fuel injectors and r' iction chambers, require mixin; of high-velocity fluids in very short leng:hs. Usually the designs ar less than satisfactory and result in incomplete reactions and loss of efficiency. The prototype device shown in the figure sol.e ;iese problems and provides uniform high-temperature flow in the test section of the Langley 8-Foot High-Temperature Tunnel. Hot gas at 4000°R, sonic at the first throat and expanding up to Mach 3, is required to mix with air in varying proportions such that the mixture is at 1600°R or 2200°R and homogeneous before entering the second nozzle. Furthermore, the first throat is less than ½ in. in diameter, the length to the second throat is less than 14 in., the highest velocity is over 3500 ft/sec, and the lowest velocity is over 400 ft/sec.

The figure shows two tangential and two normal injection stations for cold air. The normal injectors start the diffusion/mixing process and the tangential injectors keep the flow attached to the wall. When the flow reaches the step, most of the air is injected, and the flow is quickly decelerated to subsonic, with part of it proceeding backward in a tumbling vortex fashion. A series of flow reversals around the injectors and larger vortices extend to the center of the chamber. The flow has two modes: the vortices and separation are small when the second throat is large and very large when the second throat is smaller. Both modes work well. The air also cools the mixer walls and dampens oscillations from the hot gas.

Tests proved that although the finger injectors were not needed, injection at the step was necessary. The full-scale unit will scale upward by a factor of 13. The mixer will be used to modify the 8-ft HTT so that it can provide flow at Mach numbers 4, 5, and 7 at low simulated altitudes to enable the testing of air-breathing engines that can propel vehicles from Mach 4 to Mach 12. The mixer enables economical modification of the facility. This type of mixer could also be used for other processes such as carburetors and reaction chambers.
(Richard L. Puster, 3115)

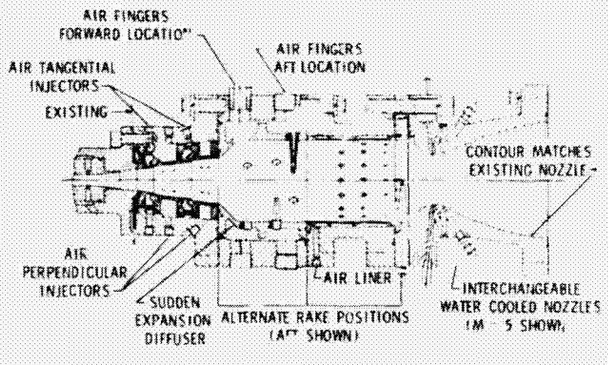

Desig for 8-ft HTT to provide uniform temperature.

Total Rotor Isolation System Very Effective in Reducing Helicopter Vibrations

The development of methods for reducing helicopter vibrations has been an important research area for many years because vibrations can have a significant adverse effect on helicopter performance. A number of methods, both passive and active, have been developed and utilized in flight with varying degrees of success. A promising new system that employs liquid inertia vibration eliminator (LIVE) units, developed by Bell Helicopter Textron, has been employed to isolate the fuselage from vibratory rotor force in all six degrees of freedom. Each LIVE unit is a two-cylinder two-reservoir tuning port arrangement with liquid mercury used as a "hydraulic fluid". This system has been named the total rotor isolation system, or TRIS.

To determine the effectiveness of TRIS in reducing helicopter vibrations, a flight verification study was conducted at Bell Helicopter's Flight Research Center in Arlington, Texas. The objective was to demonstrate 90-percent (or greater) isolation of the helicopter fuselage from forces and moments input at the rotor hub at the blade passage frequency (in this instance, four per revolution). The flight test, performed under a NASA contract with funding by the Army Aerostructures Directorate, used a TRIS configured Bell 206LM helicopter as the testbed aircraft. Flight test data indicated that program objectives were surpassed. The four-per-revolution vibration levels at the pilot's seat were suppressed below the 0.05*g* level throughout the flight envelope, including the traditionally high vibration level transition from hover to forward flight condition. The flight test results generally indicated at least a 95-percent reduction in vibration levels from the rotor hub to the pilot's seat. In addition, the TRIS installation was designed with a decoupled control system and has shown a significant improvement in flying qualities. The improvement was such that it permitted the trimmed aircraft to be flown "hands-off" for a significant period of time. In conclusion, the TRIS program has demonstrated a system that greatly reduces vibration levels of a current generation helicopter, the Bell 206LM, while improving the flying qualities to a point where stability augmentation is no longer required.

(John H. Cline, 2661)

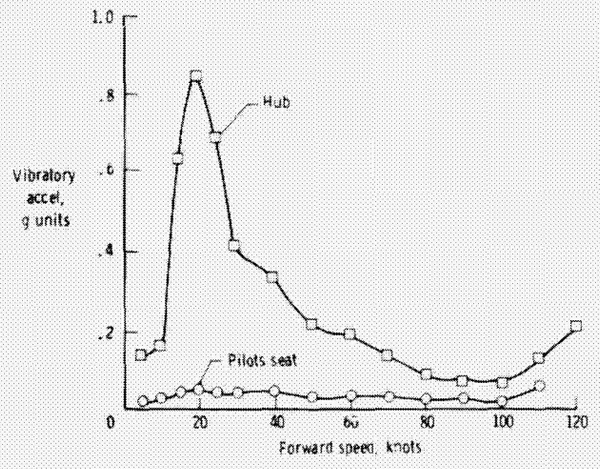

Effect of TRIS on vibration levels.

Improved Failure Characteristics Demonstrated With Composite Fabrics

Conventional graphite-epoxy composite materials consist of an epoxy resin reinforced with a unidirectional tape made of graphite or carbon fibers. To achieve strength in all directions, different layers of the unidirectional tape can be oriented in different directions. Research is being conducted on two-dimensional woven composite fabrics to establish the potential of these materials to provide improved delamination resistance and higher failure strains in graphite-epoxy composite materials.

Double-cantilever-beam and compression-after-impact tests were performed on a family of epoxy-matrix materials reinforced with two-dimensional woven graphite fabrics to determine the interlaminar fracture toughness and delamination growth resistance of these advanced composite concepts. Specimens were used to measure the interlaminar fracture toughness (G_{IC}) of conventional graphite-epoxy composites and a composite reinforced with eight-harness satin weave graphite cloth. In this case, the conventional composite was reinforced with a unidirectional tape oriented along the length of the specimen. Typical data shown indicate an approximate four-fold increase in G_{IC} for the fabric-reinforced composite compared with the G_{IC} of conventional composite. The compression specimens were impacted with a 0.5-in.-diameter aluminum sphere at a velocity of about 450 ft/sec, which corresponds to an impact energy of approximately 20 ft-lb.

Two conventional specimens and three fabric-reinforced specimens were impacted and subsequently tested to failure in compression.

The results show the average compressive failure strains after impact. These data indicate an increase of approximately 30 percent in the strain to failure for the reinforced composite fabric compared to the conventional composite. Ultrasonic analysis of the specimens showed that delamination size was also reduced by the fabric reinforcement. The improved interlaminar fracture toughness of these two-dimensional woven fabric composites decreases the impact delamination size and increases the delamination growth resistance and strain to failure compared with current graphite-epoxy tape-layup composites.
(Jerry W. Deaton, 2848)

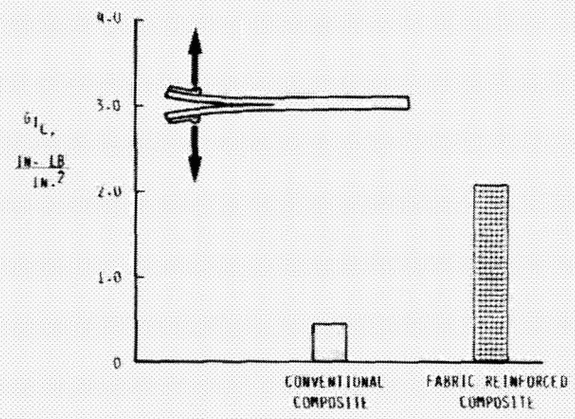

Effect of fiber configuration on interlaminar fracture toughness of composites.

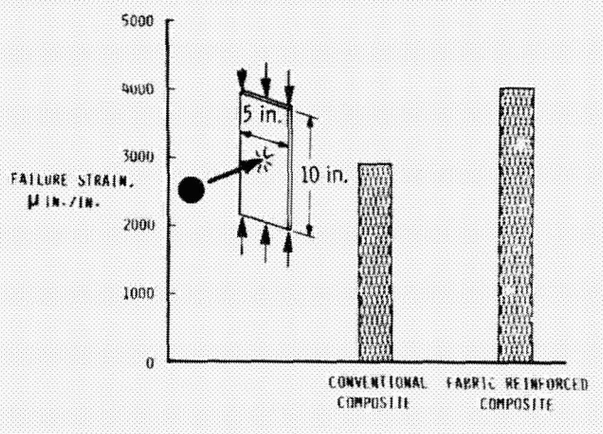

Effect of fiber configuration on compression-after-impact failure strains of composites.

Characterization of Two-Dimensional Blade-Vortex Interaction

Blade-vortex interaction (BVI) is the source mechanism of an intense, impulsive helicopter noise dominant during powered descent and landing. Two-dimensional BVI was examined with flow visualization techniques to understand the fundamental nature of this unsteady aerodynamic interaction.

In order to produce two-dimensional BVI, a vortex generator was placed upstream of a rotor blade section model. The vortex generator, an oscillating airfoil, created a wake of alternating transverse vortices that impinged the blade model parallel to the blade span. The vortex structure, rendered visible by smoke, was optically recorded. Vortex trajectories and details of vortex changes during the interaction process were extracted from the data.

Data analysis resulted in a qualitative characterization of a close-encounter region depicted schematically in the figure. Representative data illustrating BVI in each encounter zone are shown at the right of the figure. A region within a half-blade chord length, $c/2$, above and below the blade defines a close-encounter region, outside of which the blade has little or no apparent effect on the trajectory or structure of the vortex core. Inside this region is a deflection zone, in which the blade deflects the vortex trajectory but causes no change in the vortex core (diameter d_c). A distortion zone, in which distortion of the vortex core is dominant, lies inside the deflection zone. Finally, in

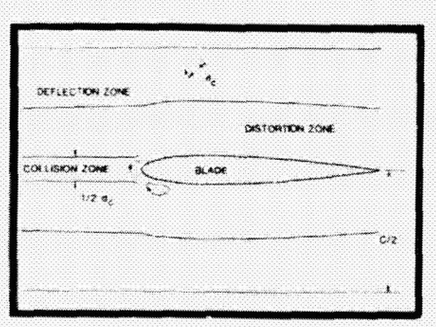

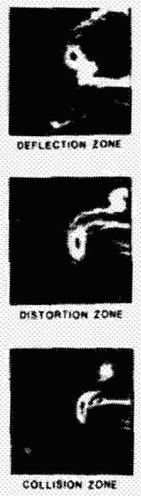

Two-dimensional BVI encounter zones.

a collision zone surrounding the blade stagnation streamline, interaction features vortex core severing by the blade, the so-called direct encounter. Severe BVI, then, features vortex core disruption.

Future work will include measurement of unsteady blade leading-edge pressure during encounter with incident vortices in all encounter zones and measurement of the velocity field of the transverse vortex structures.

(E.R. Booth, Jr., 2645)

Upgraded Aircraft Landing Dynamics Facility Becomes Operational

A $15 million construction project that increases the carriage speed of the Aircraft Landing Dynamics Facility (ALDF) from 110 to 220 knots is nearing completion. This facility has been used extensively to identify and solve problems associated with landing gear systems, tires, wheels, brakes, and runway surface treatments. Some of the earliest research on tire hydroplaning as well as the improvement associated with runway or pavement grooving was accomplished in this facility. The photograph shows the carriage at the end of the acceleration pulse in which the design speed of 220 knots was achieved. The 108,550-lb carriage, on which a landing gear system may be mounted, is accelerated by an 18-in.-diameter high-pressure (3040 psi) jet of water that impinges on a turning bucket at the rear of the carriage to create a force of over 1.8 million lb. This force produces a peak acceleration of 17*g* and accelerates the carriage to top speed in 2 sec and 500 ft. The carriage then coasts through an 1800-ft runway test section and is stopped by an arresting system in 500 ft.

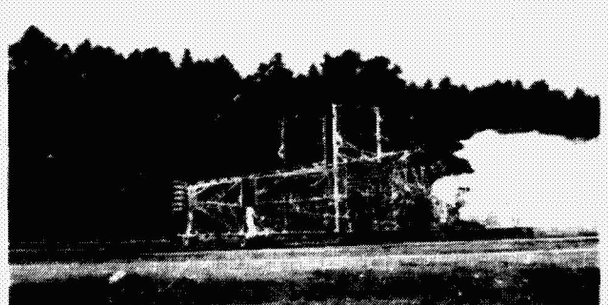

L-85-7803

ALDF achieves 200-knot design speed.

The testing capabilities of ALDF are not found anywhere else in the world. With the increased facility speed, testing of the most advanced aircraft landing gear systems can be accomplished at and beyond operational landing speeds. One of the first test programs will be for the Shuttle orbiter, which has experienced cornering and tire wear problems that have resulted in brake failures. Research programs are also planned which involve tests on radial and H type aircraft tires, runway surface traction tests, and tests to generate data for a National Tire Modeling Program.

(Sandy M. Stubbs, 2796)

Generalized Multilevel Optimization Demonstrated in Structural Applications

In the current state of the art, optimization methods applied to complex structures become very expensive in terms of computer and labor costs because of the large number of design variables and constraints. A new method has been developed to greatly improve the efficiency of these optimization applications through the use of new computer technology that introduces concurrent processing into the engineering practice.

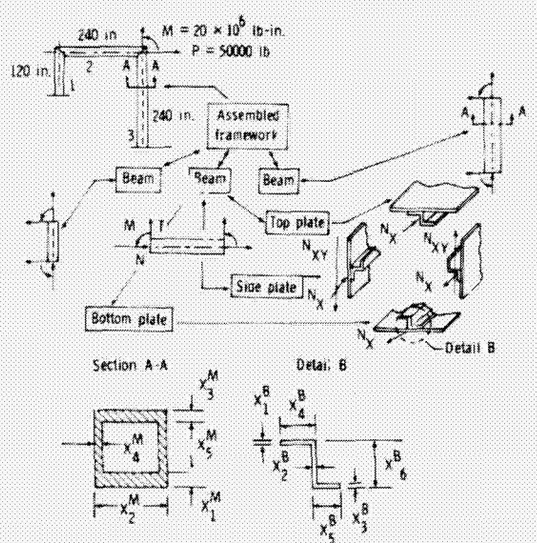

Portal framework used as test case for multilevel optimization and decomposition.

The method incorporates a well-known analytical technique of substructuring augmented with the analysis of the optimum for sensitivity to the problem parameters. These sensitivity data allow the optimizer acting at the assembled structure level to sense the effect of its decisions on every substructure. Optimization for every substructure is treated as a separate operation, and therefore all substructures can be optimized concurrently. The computer technology of concurrent processing allows decomposition of a large structure optimization problem into a number of smaller substructure analysis and optimization tasks which are carried out on separate processors acting in parallel. Thus, an overall compression of the real time needed for analysis and optimization is achieved.

The algorithm of the method has been tested on an example of a highly redundant structure of a framework type, shown assembled and decomposed in the figure. The structure supports a static load and its constraints include displacement, stress, and local buckling. The objective functio.i being minimized for the structure mass and the design variables includes detailed cross-sectional dimensions. Numerical tests have verified the method's accuracy and effectiveness. **(Jaroslaw Sobieski, 2887)**

Study Determines Strength of Thick Composites After Impact

Thin graphite-epoxy composites lose much of their strength when hit by runway debris, dropped tools, and ground equipment, whereas metals do not. Sometimes the damage is not even visible on the surface. A study was conducted at Langley to determine if thick composites were as sensitive to impacts as thin composites. Specimens were cut from a 1.4-in.-thick composite cylinder that was made with a filament-winding process. They were impacted by a free-falling weight and then loaded in tension to measure the residual strength. Indenters of various shapes were affixed to a steel rod and dropped from various heights to determine visible damage and strength loss. The indenters were a ½-in. and a 1-in. ball, a ¼-in. rod, and a 90° corner. The most blunt of the indenters, the 1-in.-diameter ball, was found to be the most critical. It caused nearly as much strength loss as the others but without any visible surface damage. The damage was also relatively invisible to ultrasonic and x-ray analysis.

Results for the 1-in. ball and a 20-lb. impactor are shown in the figure. The ratio of residual strength to original strength is plotted against the kinetic energy of the impactor. Below 25 ft-lbf, the strength is unaffected. The strength falls precipitously between 25 and 50 ft-lbf and then declines gradually up to 400 ft-lbf. The 1-in. ball causes visible surface damage only with energies greater than 400 ft-lbf. Thin laminates, less than 0.1 in. thick, can lose half their strength with impact energies of 1 or 2 ft-lbf. Thus, although impacts reduce the strength of thick composites much less than for thin composites, impacts of thick composites are still quite serious because the damage is invisible and cannot be detected. **(Clarence C. Poe, Jr., 2338)**

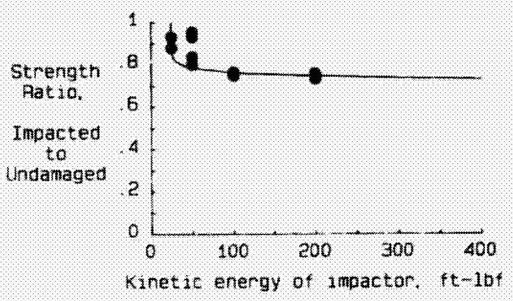

Strength of thick graphite-epoxy after impact.

Three-Dimensional Reinforcement Architecture Improves Mechanical Properties of Thin Carbon-Carbon Panels

Carbon-carbon composites are attractive candidate materials for thermal protection systems and hot structures of advanced space transportation systems because of their strength retention at very high temperatures. Thin carbon-carbon panels are usually fabricated from several layers of graphite fabric with ply directions oriented to develop desirable mechanical properties in the plane of the panel (x and y directions). An emerging material of this type is advanced carbon-carbon (ACC), a two-directional layup of carbon fibers in an eight-harness fabric. A disadvantage

of these two-directional layups is the poor interlaminar strength resulting from the absence of reinforcement in the thickness (Z) direction. A three-dimensional reinforcement architecture can be employed to alleviate this situation; however, some in-plane fiber volume fraction must be sacrificed to place reinforcement in the Z direction. Even though some tensile strength and stiffness may be sacrificed, the proper selection of a t' e-dimensional orthogonal architecture can resu in a significant improvement in flexure strength over that of two-directional layups.

Small panels, 0.07 in. thick, were fabricated from a three-dimensional orthogonal fabric. Flexure, interlaminar shear, and interlaminar tension specimens were machined from these panels and tested. Flexure strength was improved by up to 50 percent and interlaminar properties were improved by 100 to 150 percent of values obtained for ACC.

(Philip Ransone, 4412)

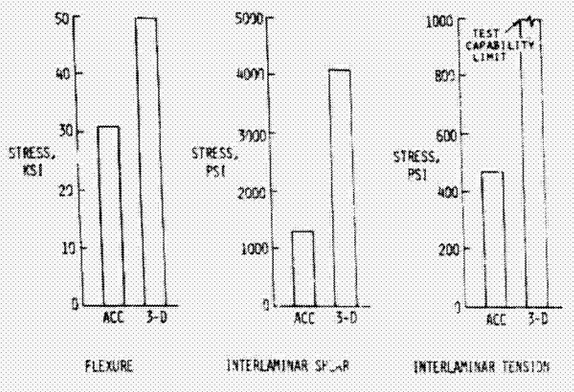

Strength advantages of three-dimensional reinforcement.

Oxygen Barrier Coating for Titanium

Titanium alloys are of prime interest for aerospace applications because of their favorable strength-to-density and high-temperature strength characteristics compared with other aerospace materials. Titanium has been shown to be subject to embrittlement by oxidation and oxygen contamination during high-temperature exposure. Because of the loss in ductility of titanium alloys exposed to oxygen-containing environments at high temperatures, their use over long times has been limited to temperatures below 800°F and short-time uses have generally been limited to temperatures below 1000°F. These limitations on high-temperature applications prevent the realization of the potential of existing and emerging titanium alloys.

Preliminary success in developing an oxygen barrier coating for titanium has been demonstrated. The figure shows a comparison of total weight gain data for uncoated titanium and four approaches to shielding titanium from oxidation. Data for each of the coatings show a significant reduction in weight gain compared to uncoated titanium. Of the coating systems investigated, the aluminum and silica coating, which consists of an electron-beam-deposited submicron layer of aluminum with a top layer of sputter-deposited amorphous silica, is the most attractive approach to shielding titanium from oxygen. The aluminum and silica coating provides an oxygen diffusion barrier that limits surface oxidation of the alloy and oxygen contamination of the substrate alloy. On exposure to high temperatures the titanium alloy interacts with the aluminum and silicon-dioxide layer to form aluminide and silicide compounds, which are impervious to oxygen even on exposure to temperatures as high as 1300°F. This blocking of oxygen diffusion to the alloy substrate restricts oxygen contamination of the alloy in the region near the surface and thus eliminates the source of embrittlement of the alloy.

(Ronald K. Clark, 4557)

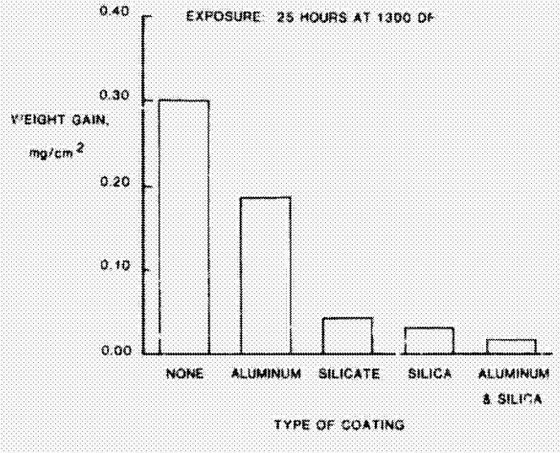

Effect of oxygen barrier coating on weight gain of titanium alloy.

Carbon-Carbon Surface Impact Damage

Carbon-carbon composite materials retain their strength at highly elevated temperatures and are being considered for lightly loaded structural components in future space transportation systems. Material strength at elevated temperatures, however, is dependent on the effectiveness of a protective coating that inhibits carbon-carbon oxidation. Any break in the coating may allow oxidation that would weaken the part so that it cannot fulfill its mission. Thus, tests were conducted to determine the effect of various impact energy levels on surface damage and tensile strength of coated carbon-carbon material. The test specimens contained 6, 12, or 18 plies of T-300 eight-harness satin weave fabric laid up in alternating 0° and 90° orientations. Front and back surfaces of the specimens were coated with a conversion coating of silicon carbide and high- and low-temperature sealer. The specimens were supported as shown and were impacted in the center with a 0.50-in.-diameter aluminum projectile at various velocities.

Front surface damage area is shown as a function of impact energy for the 18-ply material. At the lower impact energy level, front surface damage is characterized by a slight spherical indentation in the material coating with a diameter considerably less than the projectile diameter. At the high-energy level, the front surface damage consists of a spherical indentation and a local loss of coating. At the lower impact energy levels which result in front surface damage for all three thicknesses of material, no back surface damage is evident. Visual detection of impact damage is thus possible in most structural applications. Tests also showed that front surface coating damage due to low energy impacts is contained in a local area, does not result in delamination of the substrate, and does not significantly reduce the tensile strength of the material.

(James Wayne Sawyer, 4201)

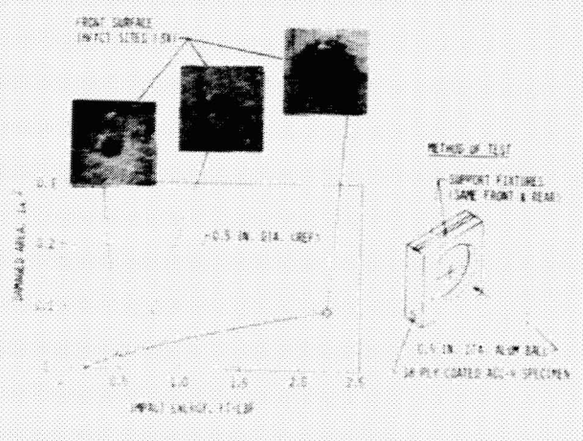

Surface impact damage on 18-ply carbon-carbon.

Ballute Shape Analysis Reveals Potential Instability

The performance of an aeroassisted orbital transfer vehicle (AOTV) is greatly improved when the vehicle is directed through the upper atmosphere and the resulting lift and drag, rather than a rocket propulsion system, are used to dissipate most of the energy necessary to transfer from a high Earth orbit to a lower one. The ballute AOTV concept, which has received considerable study, is a cylindrical vehicle with a large, inflatable, axisymmetric fabric bag attached near the nose. The bag is inflated for the pass through the atmosphere to increase drag and reduce aerodynamic heating. However, the internal pressure of the bag must be varied in order to control its shape and thus control the vehicle's flight path as it encounters the unpredictable atmospheric density variations measured during Shuttle entries. The structure of the bag consists of meridional tapes and fabric which lobes up between the tapes as the radius of the bag is decreased.

A method of predicting the equilibrium position of the meridional tapes (the ballute shape) for various internal pressures was developed. The calculated shapes, which are characterized by the initial angle at the forward attachment point, are shown in the first figure. The turn-down ratio is defined as the ratio of the drag of the 60° design shape, indicated by the solid line, to the drag of a partially deflated shape. A turn-down ratio of between 2 and 3 is required to accommodate the atmospheric density variations. Therefore, a ballute shape with an initial angle of less than 40° would be required. The vehicle must be designed for lateral stability at the lowest anticipated ballute inflation pressure because the center of pressure moves forward as the ballute is deflated, as indicated in the figure. The lobed fabric between the meridional tapes is stabilized by the pressure difference across it. However, this pressure difference is small near the front attachment point and approaches zero over large areas of the windward surface as the ballute is

deflated, as shown in the second figure. The excess fabric between the tapes is therefore unsupported and will be subject to flutter and possible destruction. These results indicate that the ballute, as presently designed, cannot achieve the required turn-down ratio without large areas of the fabric being subject to panel flutter.

(Max L. Blosser, 4295)

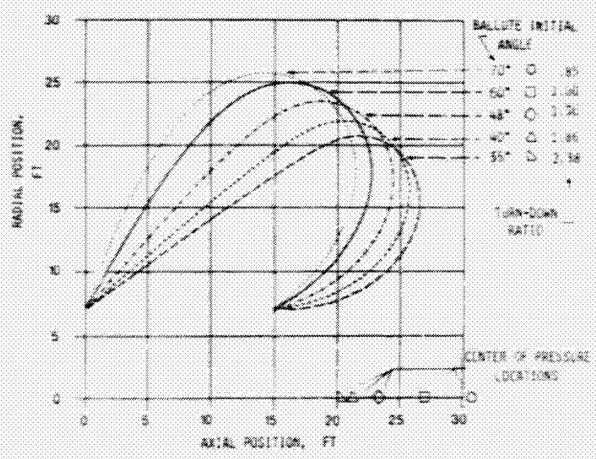

Ballute shapes for various internal pressures.

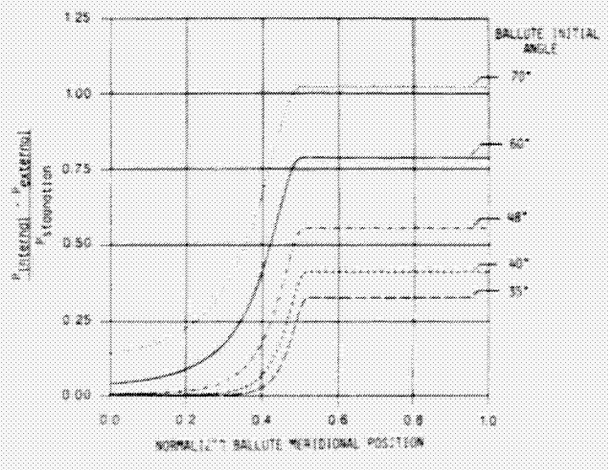

Pressure difference across ballute fabric as a function of meridional position.

Closed-Form Evaluation of Finite-Element Matrices Yields Order-of-Magnitude Savings in Computational Resources

The Taylor-Galerkin algorithm was developed by the University of Wales for compressible flow analysis, although it has application in other disciplines. The algorithm was implemented with triangular elements and included automatic mesh refinement and time domain splitting. Triangular elements were used because the integrals that make up the element matrices can be evaluated in closed form. Quadrilateral elements usually require numerical integration to evaluate element matrices, but they offer a storage advantage in that it takes two triangles to make one quadrilateral. The savings increase in three dimensions, as it takes five tetrahedrons to form one hexahedron.

Each entry in a finite-element matrix consists of one integral. When the compact expression for an integral is expanded for a quadrilateral it contains 27 terms and for a hexahedron it contains almost 19,000 terms. When the Taylor-Galerkin algorithm was implemented with quadrilateral elements it was found that the 27 terms could be simplified algebraically to 4 terms and integrated analytically. In three dimensions, the algebraic simplification of 19,000 terms is impossible. However, closed-form expressions were obtained with the symbolic manipulation program MACSYMA.

The integral evaluation that used the closed-form expressions for the consistent mass matrix (which is used in all transient finite-element analyses) and for matrices unique to the Taylor-Galerkin algorithm is 60 times faster than the usual numerical integration. The computational time for numerical integration can be reduced by reduction of the order

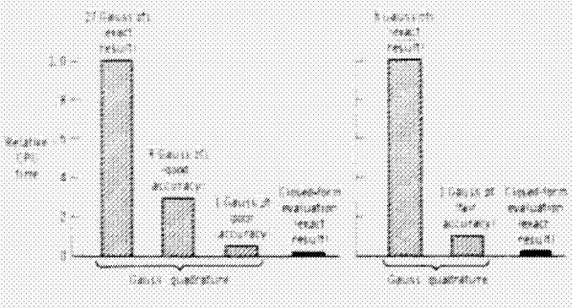

Computational savings from closed-form evaluation of finite-element matrices for Taylor-Galerkin algorithm.

of integration, but this may result in loss of accuracy, which depends on the element shape. For a general-shaped hexahedron, the reduction in order of integration results in a fair approximation to the element integrals with a maximum matrix entry error of 10 percent. Further reduction in the integration order for the mass matrix results in a poor approximation to certain element integrals with a maximum matrix entry error of as much as 200 percent.
(Kim S. Bey, 4441)

Eigensystem Realization Algorithm for Modal Parameter Identification and Model Reduction

An important factor in achieving efficient aerospace structures is the construction of an accurate mathematical model of the structural dynamic behavior. The process of developing or improving this model with the use of test data is called system identification. Although numerous system identification techniques are available, many have limited success when applied to complex structures with high modal density and nonideal behavior.

A new identification approach developed at Langley, called the eigensystem realization algorithm (ERA), has demonstrated consistently high performance with both simple and complex structures. The major steps of the procedure are shown in the flow chart. Beginning with digitized free-response functions, a state space model (called a realization) and a corresponding set of modal parameters are identified. A unique aspect of the method is that it combines minimal realization theory from the controls discipline with modal parameter identification theory from the structural dynamics discipline.

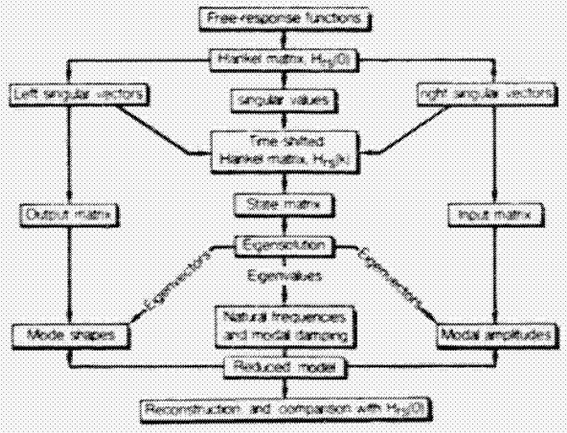

Flow chart of ERA.

One recent successful application of ERA involved the structure shown in the photograph. This is the 105-ft-long OAST-1 solar array, which was extended from the Space Shuttle on mission 41-D under a project managed by NASA Marshall Space Flight Center. It is the largest deployable space structure ever placed in orbit. The dynamic motion of the structure was measured by Langley researchers who used the orbiter TV system to track the white targets shown in the photograph. Subsequent analysis with ERA resulted in identification of the principal vibration modes of the structure.
(Richard S. Pappa, 3196)

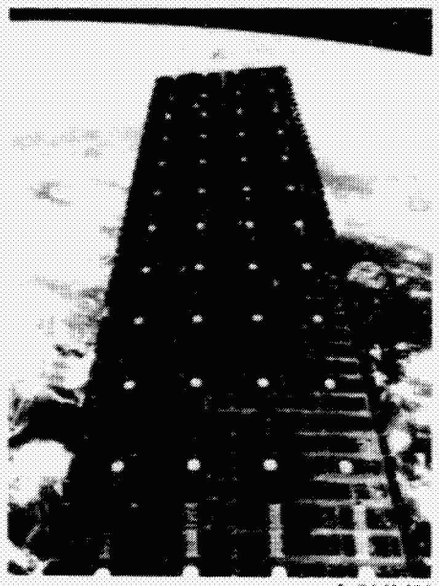

L-84-11,184

Solar Array Flight Experiment.

Analysis Requirements for Large Space Antennas

Large tension-stiffened space antennas operating free of gravity and with close surface accuracy tolerances present difficult problems to the structural

analyst. Many programs developed for conventional Earth structures do not routinely handle these special requirements. Moreover, an increasing reliance on analysis is necessary because testing of full-scale structures on Earth may not be possible. To develop and verify fabrication and analysis procedures for large space antennas, a 15-m hoop/column antenna was designed and built.

Even with precise fabrication templates, the fabricated antenna surface was distorted from the desired paraboloidal surface by an average error of 3.2 mm. The electromagnetic performance of the antenna was poor with this large surface error. To improve the surface accuracy, special analyses were developed to compute adjustments for the surface control cords shown on the figure. Ninety-six cables were adjusted to reduce the surface error 38 percent. This resulted in substantial improvement in electromagnetic performance. This method of using analysis models to compute cable length changes may be used for on-orbit surface adjustment of large space antennas.

Structural vibrations can also degrade the electromagnetic performance of large space antennas and modes, and frequencies must be accurately known to design vibration control systems. The figure shows frequency results for an initial analysis model was refined with more structural detail and better material characterization. A comparison of analysis and test data showed that additional flexibility occuring at deployable joints could significantly affect dynamic response. It will be necessary to establish the stiffness of joints through testing and introduce this effect in the analysis for more accurate predictions to be achieved.

(W. Keith Belvin, 2446)

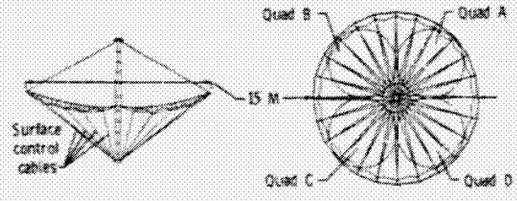

Frequency (HZ)

Mode	Initial Analysis	Test	Refined Analysis
1	0.105	0.068	0.064
2	2.02	0.785	1.00
3	4.73	1.36	1.72
4	—	3.13	3.21

Quad	Fabricated RMS (mm) Measured	Adjusted RMS (mm) Predicted	Measured
A	3.05	1.83	1.91
B	2.72	2.03	2.01
C	3.61	2.46	2.39
D	3.35	1.57	1.55

Vibration and shape analysis of 15-m hoop/column antenna.

Helicopter Interior Noise

A major objective of new helicopter designs is to achieve interior noise levels comparable to those in other commercial transportation systems. Past attempts to reduce the interior noise of helicopters have been only partially successful. One part of the noise reduction methodology under development includes an analytical model of the airborne and structureborne (vibrational) energy paths.

Sikorsky Aircraft, under contract to NASA, has developed an analytical model with the use of the statistical energy analysis (SEA) method. In this analysis each acoustic and structural subsystem is modeled to obtain the power flow and these subsystems are interconnected to obtain an energy balance of the total system. The range of measured noise levels in an S-76 helicopter are shown along with the predicted mean levels for the four speech interference octave bands and the numerical average of the four band levels (SIL-4). The excellent agreement shown in the figure for the interior noise levels, along with the good agreement obtained between measured and predicted vibration levels of the structural subsystems, supports the validity of the SEA model. Based on these results, current efforts are under way to customize noise treatment and vibration isolator designs for installation on the S-76 for further validation of the model.

(William H. Mayes, 3561)

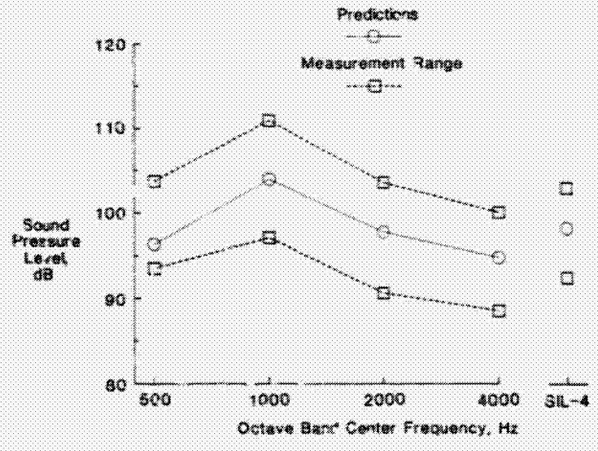

Interior noise of S-76 helicopter at 75 m/sec level flight.

Analysis Predicts Measured Stability Characteristics of V-22 Tilt-Rotor Model

To provide the data base needed for the design development of the V-22 tilt-rotor aircraft, a 0.2-size aeroelastically scaled semispan model of a preliminary design and then an updated version were tested in two separate entries into the Langley Transonic Dynamics Tunnel (TDT). A key objective was to determine aeroelastic stability of the rotor/wing system in the high-speed airplane mode of flight and to correlate these results with analysis. Analytical studies conducted by Langley in support of the tests were based on the Proprotor Aeroelastic Stability Analysis (PASTA) code, a modified version of a computer program originally developed at Langley about 14 years ago to support tilt-rotor tests in the TDT.

The equations underlying the PASTA code are linear and are based on a simple mathematical model of the rotor system. The rotors are assumed to be in axial flow (airplane mode) and to be windmilling (nonthrusting). Quasi-steady strip theory aerodynamics are employed for the blade airloading; the wing unsteady aerodynamic loading is assumed to be zero. A stability derivative representation is employed for airframe aerodynamics associated with aircraft rigid-body motions. A modal representation is employed for the airframe structure. Calculations were made for a wide variety of configurations of the gimballed-hub version of the model. The parameters that were varied included pylon-to-wing locking (on and off downstop), rotor rpm, blade pitch-flap coupling, hub flapping restraint, and wing and blade stiffness distributions. In addition, PASTA was used to analyze several configurations of the model with an updated hub design that had offset flapping hinges in addition to the gimbal.

Results are presented as the variations with airspeed of calculated and measured damping and frequency of the three lowest wing modes (beam, chord, and torsion) which are of importance to stability of the rotor/wing system. Calculated results for the blade lag mode are also shown. The scatter in the experimental damping values for the wing torsion mode is associated with the difficulty of extracting from the response data the high levels of damping characteristics of that mode over the velocity range shown. The wing beam mode (primarily wing vertical bending) is seen to be critical (lowest flutter speed) for the case shown. The degree of correlation shown here is typical of that obtained for all configurations of the model tested.

(Raymond G. Kvaternik, 2661)

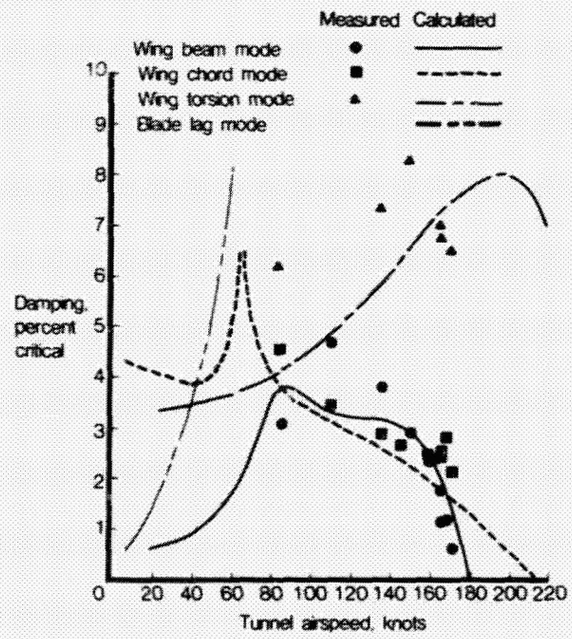

Modal damping.

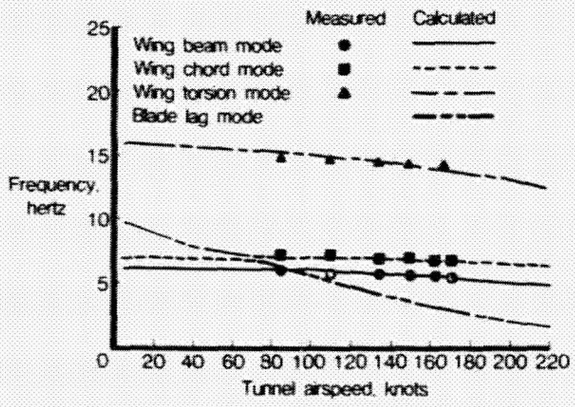

Modal frequency.

Baseline Rotorcraft Noise Prediction Code

Under a joint program with the U.S. helicopter industry, Langley has developed and installed a base-

line rotorcraft noise prediction computer code on the Langley CDC computer system. The existing code is the initial attempt at establishing a computer code architecture to predict full-system helicopter noise. The architecture developed is modular, allows for future expansion, employs standardized interfaces between modules, and is fully documented.

The code structure is divided into four parts: main and tail rotor blade description, rotor performance, noise calculations, and noise propagation. The modular architecture and documented interfaces allow noise predictions to be performed either by description of helicopter geometry or by direct pre-sentation of the data at performance or noise parameters.

The figure shows the results of a comparison of code prediction with experimental main rotor tone noise measured from an Aerospatiale Dauphin 365C helicopter. The prediction and experimental data are for the helicopter blade passing frequency with the helicopter flying directly over an observer at a speed of 150 knots and an altitude of 150 m.

Work has been initiated on a second-generation code that will account for higher harmonic blade loading and blade motion, nonuniform motor inflow, wake distortion, full-surface noise prediction theory, and rotor broadband noise.

(Robert A. Golub, 3842)

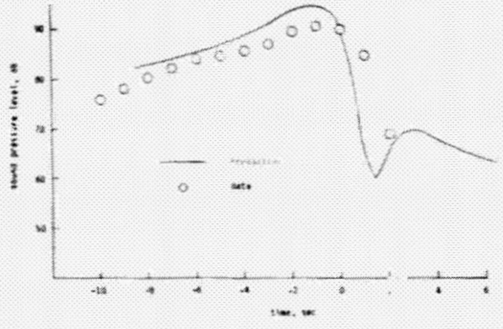

First harmonic of rotorcraft noise for overhead flyover.

Noise Transmission of Composite Panels

Increasing application of composite structural materials in airplane, helicopter, and space vehicle design has motivated an analytical and experimental research program in noise transmission of flat fiber-reinforced composite panels. The theoretical approach uses modal decomposition to find the solution of the differential equation of motion for a specially orthotropic plate with mode shapes that satisfy the simply supported boundary conditions. Experimental modal parameters are used in the prediction to bypass the difficulties of accurate description of the boundary conditions and material properties of the test articles. These modal parameters, frequency, damping, and mode shapes are extracted from frequency response data with an eight-channel computer aided test system.

Included in the study are cross-ply and angle-ply panels of either tape or fabric construction composed of fiberglass, graphite, or aramid fibers embedded in epoxy resin. The predictions are compared with noise transmission measurements conducted in the Langley noise transmission loss apparatus. Good agreement was obtained between theory and experiment, as indicated in the figure. The importance of the modal response to transmission loss is particularly apparent at the frequencies of the first several odd-odd panel modes as determined from the modal analysis. These frequencies are indicated in the figure by arrows with circles enclosing mode numbers. For equal critical shear load, graphite composite panels have a higher fundamental resonance frequency than aluminum panels. Cross-ply panels have a lower fundamental frequency than similar panels with angle-ply configurations. For the tests performed, the fiber orientation does not affect the normal mode behavior of panels composed of four laminae or more with a thickness of at least 1 mm. Application of these results may help preserve the weight saving advantages of composite materials when designing for low interior vehicle noise.

(Clemans A. Powell, 3561)

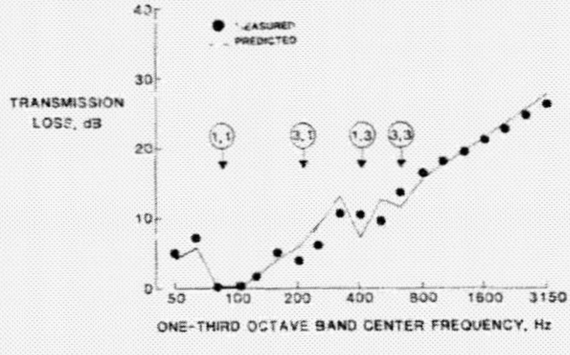

Transmission loss of graphite-epoxy composite panel.

Postbuckling Strength of Graphite-Epoxy Panels

A fuselage or wing panel may be made lighter, may contain fewer parts, and may be of less complex construction if buckling is allowed at loads less than the ultimate design load. The prediction of the ultimate load of metal panels is generally beyond the capability of precise analytical determination, and reliance is on empirical methods based on a large body of test data. Introduction of composite materials with a wide variety of laminate layups and many possible local failure modes greatly increases the difficulty of predicting ultimate load. Great care is required in the design of a composite panel to prevent premature local failures below the potential of the panel.

Three stiffened composite panels 60 in. long and 42 in. wide were fabricated and tested by the Lockheed-Georgia Company under various combinations of shear and compressive loads. The specimens had a 143-in. radius and were stiffened by five J stiffeners spaced approximately 7 in. apart and three frame sections spaced 20 in. apart. The panels had failsafe straps in the skin and skin padding under the stiffeners to suppress the skin-stiffener separation failure mode common to post-buckled stiffened panels. The adequacy of the detail design of the panel is indicated in the graph. Agreement between theory and test is shown for both buckling and ultimate load. Prediction of ultimate load is based on a simple approximate nonlinear modal solution and the relation of maximum calculated strain to test data. Additional testing along with nonlinear analysis is planned to expand the data base for failure of composite panels and provide a fundamental understanding that can be applied to prediction methods.
(James H. Starnes, 2552)

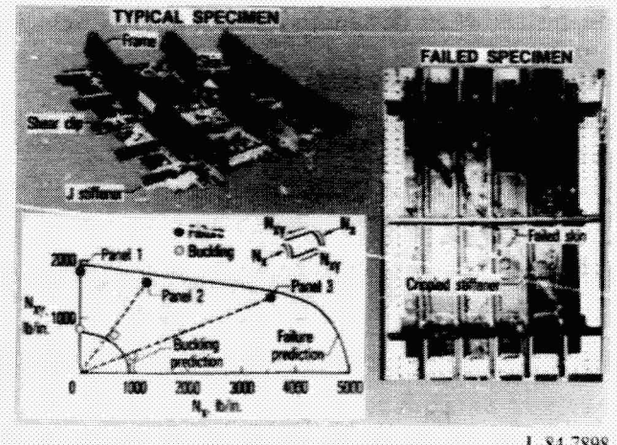

L-84-7898

Shear and compression loaded composite stiffened panels.

Propeller Synchrophasing for Aircraft Noise Control

Continued development of advanced turboprop aircraft will require the development of low-weight innovative noise control treatments. One such concept is the use of propeller phasing to help control the noise entering the passenger cabin. In this ongoing study, an aircraft fuselage is approximated by an infinite cylindrical shell with typical materials and properties. Propeller noise sources are represented by a unique arrangement of simple point sources that reproduce measured exterior fuselage pressure data. The physics of sound transmission and the effects of propeller synchrophasing on the interior acoustic field are examined with the use of this model.

This study points out the role the cylindrical modes play in transmitting low-frequency noise to the interior space. It was shown that the cylinder motion was most dominant in the propeller plane and that this effect as well as the interior acoustic field decayed rapidly along the cylinder axis. Results, correlated with experimental data, showed that the inte-

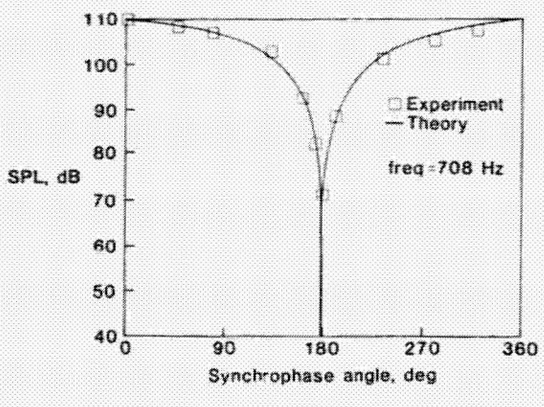

Verification of theory and concept of propeller synchrophasing.

rior noise field was often dominated by just a few modes that efficiently coupled the wall motion to the interior space. The thrust of this work has demonstrated that the use of a properly controlled second propeller may be a very efficient way to control the noise in the aircraft interior with little weight penalty. In the figure, the interior sound pressure level SPL at a point in the source plane on a vertical axis at half the radius is effectively suppressed by 40 dB at a synchrophase of 180°. The theory represents the experimental data very well throughout the range of synchrophase angles and demonstrates the variation of SPL attainable. The experimental data were obtained in a laboratory model of a 20-in.-diameter cylinder two diameters in length. These results suggest that the infinite cylinder model is a reasonable one even for this limited-length model.
(Richard J. Silcox, 3561)

Interaction Between Airborne and Structureborne Interior Noise

A comprehensive analytical and experimental study of the interaction between airborne and structureborne noise radiated by simple structures has been completed. Parameters included in the study were the relative magnitude and phase of the acoustic and vibrational inputs, the path of propagation of the inputs, added structural damping, and material characteristics of the structure.

The results of the study indicate that the interactive effects are much more important than was previously believed. For example, the figure shows how overall dB sound power levels (OAPWL) in the 0- to 1000-Hz frequency range depended on the interaction between the inputs. A 68.6-dB structureborne noise combined with a 82.0-dB airborne noise produces a combined output that can range from 80.7 dB to 83.3 dB depending on the phase relationship between the two inputs. (A 3-dB change in power level is a factor of 2.) This is an extremely important result since previous studies have treated the airborne and structureborne problems as if they were additive (which produces an 82.2-dB result). The implication is that the structureborne component does not have to radiate a significant amount of sound power on its own in order to greatly influence the overall noise radiation of the structure. In fact, the recessive component of the noise need only change the dynamic response of the structure in order to influence the overall noise radiation.

Future plans are to use the results of this study as an aid in the development of a diagnostic tool that would separate the airborne and structureborne components of some unknown combination of the two noises.
(Michael C. McGary, 3561)

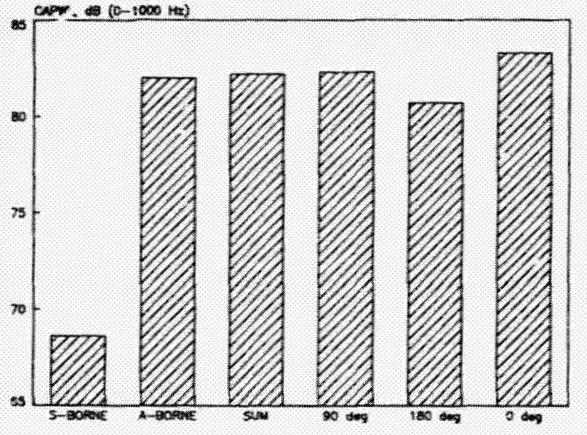

Phase-dependent interaction between airborne and structureborne components.

Mean Surface Approximation to Formulation for Prediction of Supersonic Propeller Noise

Predicting the noise of supersonic propellers is an important subject of research because of the current concern about community annoyance by future advanced turboprop-driven aircraft. Theoretical work on this problem at Langley resulted in two formulations for subsonic and supersonic sources on the blade surface. Several computer codes were developed with highly realistic blade geometry and kinematics, and these have been used successfully for noise prediction. They are known as the full-surface codes. The execution time of these codes on a computer is relatively long for advanced supersonic propellers. The objective of the work reported here was to develop a new noise prediction code to speed up the

computation time without deterioration in the accuracy of the existing sophisticated codes. In the analysis, the sources were assumed to lie on the mean camber surface of the blade. A simple expression for the loading and thickness noise of rotating blades was derived. This formulation is valid in the near and far fields and for blades in supersonic motion.

A new computer code based on the present acoustic formulation was developed to predict the noise of high-speed propellers. Comparison with results from a full-surface code has shown an improvement in execution time by approximately a factor of 2. The new code is also less sensitive to mesh size of integration for numerical evaluation of integrals in the acoustic formulation. The figure shows a comparison of the measured and computed acoustic spectra of an eight-blade propfan (SR-3). The measured data correspond to boom microphone position 4 for the Jetstar operating at design condition at 30,000 ft. The level of each harmonic of the theoretical spectrum is increased by 4 dB to account for scattering by the boom itself, assuming a rigid surface without the boundary layer. It is observed that the agreement between the theoretical and measured data is good. This code will be used for prediction of single-rotor and counterrotating advanced propellers.

(F. Farassat, 2645)

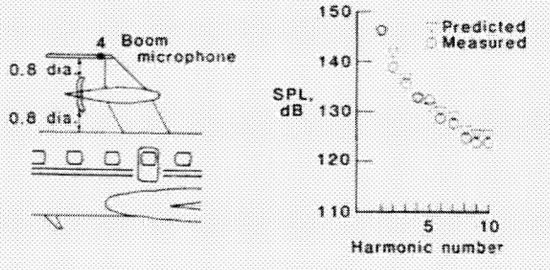

Propeller noise prediction with mean surface code.

Projects Directorate

The Projects Directorate is responsible for the implementation and management of specific tasks related to carrying out Langley's research and technology role in aeronautics and space. These tasks include the following projects or functions: the Earth Radiation Budget Experiment/Stratospheric Aerosol and Gas Experiment (ERBE/SAGE II) Project, the Long Duration Exposure Facility (LDEF) Project, the Control of Flexible Structures (COFS) Project, the Aeronautical Systems Office (ASO), the Space Technology Flight Experiments Office (STFEO), and the Space Flight Experiment Definition and Integration Office (SFEDIO). The Aircraft Energy Efficiency (ACEE) Project was disestablished during FY 1985.

Management responsibilities explicitly include principal decisions concerning program content, scheduling, budgeting, operations planning, contract monitoring, and other aspects of project implementation. Responsibilities for assigned functions or projects include preparation of operating plans; negotiations with NASA Headquarters and other government agencies, universities, and industry; and administration of programs funds and travel and manpower resources.

Advanced Composite Structures Technology

Flight tests were completed July 5, 1985, on the McDonnell-Douglas DC-10 composite vertical stabilizer developed under the NASA Aircraft Energy Efficiency (ACEE) Program. The composite stabilizer met all static and dynamic structural and system interface requirements needed for FAA certification. This application is the largest composite primary structure for commercial transport aircraft to complete flight and ground tests for FAA certification and it weighs 17 percent less than the production metal stabilizer.

As part of the ACEE advanced development program, the capability to repair heavily loaded damage-tolerant wing cover panels was successfully demonstrated. The central stringer and skin of a five-stringer panel were severed and the panel was then repaired with a mechanically fastened patch and tested to failure, which occurred at 126 percent of design limit load. A damage-tolerant design for fuselage skin panels was also developed. Tests showed that the design can withstand flight loads with a 12-in. cut in the panel, and it offers a 23-percent weight savings over metal fuselage structure. The feasibility of filament winding a ring-longeron stiffened fuselage structure was demonstrated by fabrication of a 5.5-ft-diameter by 12-ft-long barrel section. In a joint effort with the three U.S. transport manufacturers, a standard test specification for qualification and acceptance of toughened resin composites was developed and published in NASA RP-1142.
(John G. Davis, Jr., 3081)

Flight test of DC-10 composite vertical stabilizer.

Systems Engineering and Operations Directorate

The function of the Systems Engineering and Operations Directorate is to support ongoing aeronautical and space research at Langley. This work force is divided into four divisions with specific support functions. The Systems Engineering Division is responsible for structural, mechanical, electrical, and aeronautical systems engineering functions required to provide research models and flight hardware for aerospace research, applications, and technology. The Facilities Engineering Division is responsible for engineering and design of aerospace research and development equipment and institutional facilities for aeronautical and space research, such as special handling equipment, model supports, and special test equipment. The Fabrication Division is responsible for developing and fabricating aeronautical and aerospace research hardware related to ground support equipment as well as research facilities test equipment. This division provides developmental manufacturing technology and electronics technical support, including communications systems and instrumented hardware. The Operations Support Division is responsible for providing the technical, mechanical, electrical, and maintenance services for research and institutional facilities. This division operates laboratory equipment and wind tunnels, and collects, records, and interprets test data. In addition to the four divisions, the Facilities Program Development Office and the Systems Safety, Quality and Reliability Office are responsible to the directorate.

Because of the unique requirements of some of the aerospace research performed at the Center, both engineers and technicians are involved in applied research in solving engineering and fabrication problems. These problems relate to the support hardware and software necessary to provide the experimental systems requested by research. The following contributions represent typical engineering and fabrication research and technology development highlights in the Systems Engineering and Operations Directorate.

Automated Fabrication of Secondary Structural Epoxy-Graphite Aircraft Stiffeners

The pultrusion process is being applied to replace labor- and tooling-intensive autoclave methods for the manufacture of graphite-reinforced epoxy aircraft stiffener materials. With this technique, in situ stitched graphite fiber preforms with tailor-made orientations are pulled first through the epoxy resin system for impregnation and then through a heated-cure die which consolidates, compacts, and provides the heat for polymerization. Polymerization occurs as the epoxy-impregnated fiber travels through the cure die at 2 in./min. Fiber orientations of 0°, 90°, +45°, and −45° to the central axis have been used in pultruding "T" and hat shapes. The composite structures emerge continuously at the exit end of the die and are cut to the desired lengths as finished products. This process eliminates the need for large ovens and autoclaves, as well as the requirement for hand layup and vacuum bagging. This ongoing program is conducted jointly by Langley and the Lockheed-Georgia Company to reduce manufacturing cost of aircraft construction. **(Maywood L. Wilson, 2781)**

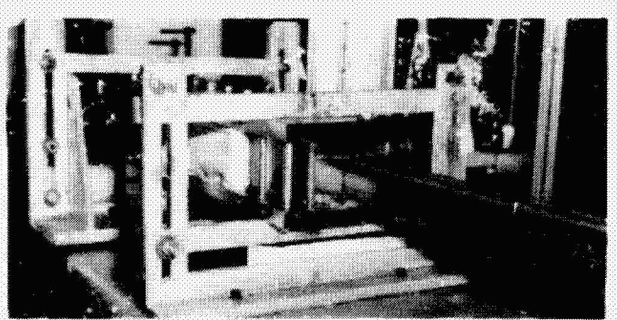

L-85-9982

Pultruded graphite-epoxy aircraft "T" stiffener.

Alternating Surface Segmented Lap Joint

An alternating surface segmented lap joint has been developed to provide an efficient method of attaching removable trailing-edge flaps on thin,

highly loaded wings of high-performance fighter wind tunnel models. This joint design eliminates the need for shear pins and reduces the tensile loading in the attachment screws. The design combines features of both the lap joint and the tongue-in-groove joints to provide a joint that is stiffer and has lower bending stress levels than either of the two conventional joints.

The aft component of the joint resembles an element of a lap joint for which the overlapping portion has been broken into several uniform segments with uniform gaps. Alternating segments are then switched to the opposite surface. This element could also be described as the grooved element of a tongue-in-groove joint for which the groove width was zero and segments of each surface were removed. The mating component has pockets cut into each surface which match each of the segments of the first piece. With proper tailoring of segment and pocket geometry, shear loads due to either beam bending or relative thermal contraction can be accommodated at the segment-edge/pocket-wall interface.

L-84-12,795

Pathfinder II *wing incorporating alternating surface segmented lap joint proof-of-concept specimen.*

The alternating surface segmented lap joint as applied to the NTF (National Transonic Facility) *Pathfinder II* model allows testing under load conditions that would have resulted in unacceptable fastener tensile loads, dowel pin shear loads, and element bending stresses with either of the two conventional joints. Additionally, the two conventional joints would have deformed under loading to produce an unacceptable aerodynamic surface distortion.
(George C. Firth, 4666)

Cryogenic Wind Tunnel Model Filler Materials

Aerodynamic research models require smooth, continuous surfaces to minimize surface-induced flow disturbances. Flaws in surfaces of conventional wind tunnel models have been satisfactorily filled with waxes, plasters, and plastic body filler. However, cryogenic wind tunnels such as the National Transonic Facility, with their unique capabilities and test environments, render such materials unsuitable. Cryogenic facilities typically have high Reynolds number capabilities which require higher surface contour fidelity and finish than are required in conventional facilities. These tunnels also operate at temperatures (−300°F) that cause the conventional filler materials to become brittle, lose contour fidelity because of greater thermal contraction than the primary structure, and suffer bond failure because of thermally induced stresses.

As part of the Cryogenic Model Technology Development Program at Langley, an effort was made to identify and/or develop materials that could be used to fill imperfections on cryogenic wind tunnel models. Candidate filler materials were examined for ease of use, structural and dimensional stability, surface quality, coefficient of thermal expansion, and usage limitations. Various commercial products used by the conventional wind tunnel model community were examined and all were found to exhibit characteristics which severely limit their usage in a cryogenic environment.

A commercial product (Belzona "Super Metal") has been identified and two filler materials have been developed which meet the major criteria for usage in a cryogenic environment. Unfortunately, minor characteristics of each of the materials preclude the use of

any one for all cryogenic wind tunnel applications. "Super Metal" requires about 8 hours to cure and also requires considerable hand work to contour. These characteristics hinder quick model modifications during testing. One of the developed materials consists of a fast-curing epoxy modified with additions of carbon microspheres. This material would be suitable for use during quick model changes. However, due to the slight mismatch of its coefficient of thermal expansion with that of model structural materials, it cannot be used to fill large voids on critical aerodynamic surfaces. The second filler material that was developed, a structural adhesive filled with carbon microspheres, requires about the same cure time as the commercial product but is much easier to hand work. Additionally, this material has demonstrated the best structural properties during dynamic cyclings of specimens at cryogenic temperatures.
(George C. Firth, 4666)

L-85-9179

Grooved wind tunnel model wing specimen used for dynamic testing at cryogenic temperatures.

Rapid Strain Gauge Attachment

A new method of bonding strain gauges has been developed which reduces adhesive cure schedules from a matter of hours to minutes. This procedure, which incorporates the use of inductive heating, is primarily applicable to elevated (204°C) temperature strain gauge requirements. A toroid gun concentrates high temperatures in localized areas according to the principles of induction heating. Gauges can be bonded to test specimens and structures that have high electrical reluctance, low reluctance, or no reluctance (i.e., metals, plastics, and ceramics).

Test data show that strain gauges bonded to structural specimens with the toroid induction bonder produce results equal to those obtained with standard bonding techniques. The advantages of the toroid joining gun over existing methods include low power, rapid bonding, lightweight equipment, localized heat on the strain gauge adhesive, and portability.
(John D. Buckley, 3131)

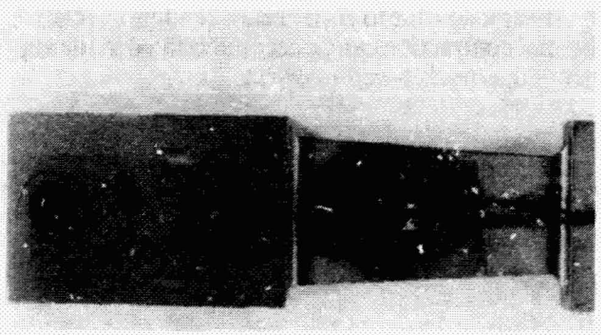

L-83-6914

Strain gauge on metal structure.

Counterweight System for "Zero-G" Simulation of Access Flight Hardware

During the development process of the ACCESS (Assembly Concept for Construction of Erectable Space Structure) experiment, a counterweight system was required. The system was to provide the means of assembling the truss without the effect of gravity on the test object. Because the weight of the erectable structure increases as it is being assembled, due to the parts being added in the process, the balancing force exerted by the counterweight must be constantly changing at any working elevation. The use of a classical system meant manipulation of weights in and out of a counterweight basket until a discrete bal-

ancing force was achieved. This would apply undesirable forces on the test object, and would be a safety hazard.

The basket was replaced with a tank connected to a water supply system. Drainage was provided at the bottom of the tank and controlled at ground level. When a part was added to the structure, the supply valve was opened and regulated until the new part was exactly balanced. When a part was taken off the structure, the forces were balanced with the drain valve. During the course of the test and checkout operation of the ACCESS structure, the system operated without failure and was nearly transparent to the operating technologists.

As the work in the development of erectable structure grows, the use of this counterweight system concept offers a great potential to reduce workplace hazards. Another benefit from this concept will be increased efficiency and the reduction of manpower required to operate the mechanisms.

(William M. Berrios, 4571)

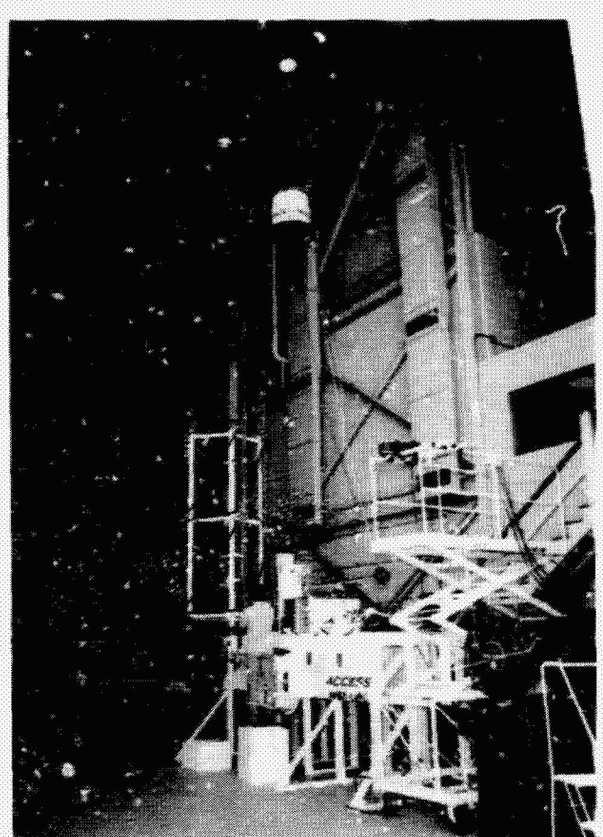

L-85-4121

Water supply counterweight system.

Insulation for Erectable Truss Struts

The thermal design analysis of the ACCESS (Assembly Concept for Construction of Erectable Space Structure) experiment indicated that temperature gradients between truss elements and assembly fixture elements could cause assembly or disassembly difficulties while astronauts were working on the truss over an orbit. A number of coatings were evaluated for use on the aluminum truss structure, including paints and chromic acid anodize. These coatings, however, failed to provide the temperature control necessary. The use of graphite-epoxy was considered for the strut material, but this was ruled out because of schedule and cost considerations.

An insulation concept was developed for individual struts within the truss to reduce the orbital temperature variations. First, a number of "grip rings" were attached to each strut. These were Velcro hook strips applied with an acrylic transfer adhesive. Polyester mesh "bridal veil" material was placed around the struts between rings to separate the aluminized surface of the Kapton from the struts. The Kapton film was then placed around the struts and attached to the Velcro rings with the transfer adhesive. A longitudinal lap joint closed the insulation with the transfer adhesive. Finally, the transfer adhesive was used to place strips of aluminized Kapton on the outside surface over each of the Velcro rings. These final strips and the longitudinal lap joint served as tear stops to preclude the possibility of the insulation being ripped and separated from the struts. The Velcro rings acted to transfer handling forces from an astronaut's hand to the struts and to

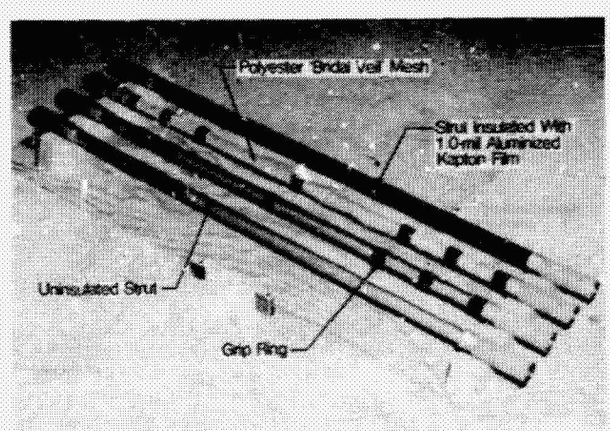

ACCESS strut insulation.

serve as thermal isolator supports for the Kapton film. A manned thermal-vacuum test at the Johnson Space Center showed the insulation to be acceptable for astronaut handling.
(Obie H. Bradley, Jr., 4571)

Totally Confined Spacecraft Separation Joint Evaluation and Improvements

The Lockheed Super•Zip totally confined separation joint is used in several Shuttle applications, such as the configuration shown. A cross section of the "separation ring" is shown in the second figure. Firing either of the two explosive cords causes the tube to expand and fracture the plates at the ligament to achieve separation. The tube contains all the explosive products; the only sound created is that of the metal fracturing. Following a number of ground test failures, an investigation was initiated to determine the effects of system variables and maximize the joint's functional margin. The most obvious system variable, explosive load, was limited by the ability of the tube to prevent rupture. The properties of the material to be fractured are critical to success; the harder, higher-strength conditions of the metal are more sensitive to fracture.

The greatest surprise in the investigation was that the web thickness was more influential than the ligament thickness. Also, 0.025-in.-thick ligaments were more difficult to fracture than a 0.042-in. thickness. Although simple in appearance, the dynamics of the system operation (million psi pressures, microsecond rise times) have eluded understanding through analysis and modeling. As a result of this investigation, the explosive load was increased and significant improvements in quality control were implemented.
(Laurence J. Bement, 4621)

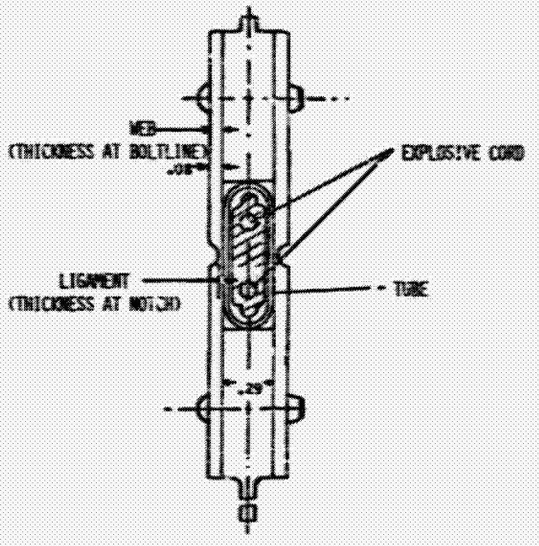

Super•Zip separation joint.

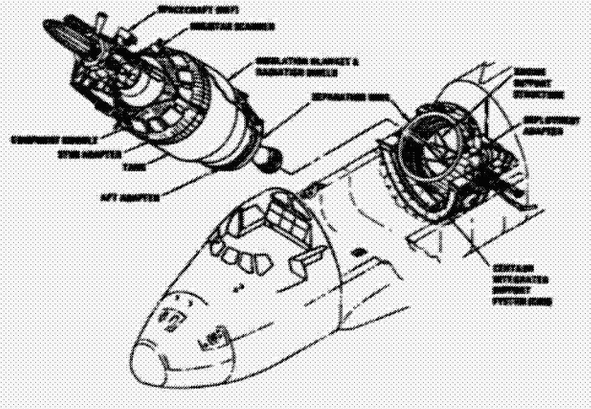

Shuttle/Centaur system summary.

Technology Utilization Program

One of NASA's Congressionally mandated responsibilities is to promote economic and productivity benefits to the nation by facilitating the transfer of aerospace-generated technology to the public domain. NASA's means of meeting this objective is its Technology Utilization Program, which provides a link between the developers of aerospace technology and those in either the public or private sectors who might be able to employ the technology productively.

One important facet of NASA's Technology Utilization Program is its applications engineering projects, which involve the use of NASA expertise to redesign and/or re-engineer existing aerospace technology to solve problems encountered by federal agencies or other public-sector institutions. Applications engineering projects originate in various ways. Some stem from requests for NASA assistance from other government agencies and some are generated by NASA engineers or scientists who perceive possible solutions to public-sector problems through the adaptation of NASA technology. In addition, NASA employs a multidisciplinary applications team which contacts public-sector agencies, medical and public-health institutions, and professional organizations to uncover significant problems in fields such as health care, public safety, transportation, and industrial processes which might be amenable to solution by the application of NASA technology. The projects reported on here are typical of the applications engineering efforts conducted at NASA Langley in support of the Technology Utilization Program.

Infrasonic Array for Detection of Local Meteorological Events

Infrasonic data gathered throughout 1984 on a three-element microphone array in the frequency band from 2 to 16 Hz are found to yield a class of signatures believed to be related to local meteorological events (e.g., low-level wind shear and microbursts). The algorithm for processing the data fulfills two functions: time delay estimation, from which the location of the event as an infrasonic source can be determined, and autospectral and cross-spectral analysis, from which the source can be classified.

The overwhelming bulk of the data can be organized into one of four characteristic signatures. The signature in question features a power law spectrum with a slope generally between −6 and −18 dB/octave and poor average coherence, almost always below 0.35. An example is shown in the figure. It is hypothesized that the microphone signal consists of two components: a large incoherent component due to turbulence generated by the wind at each microphone site, and a small coherent component due to infrasonic emission from a local meteorological event. The algorithm for time delay estimation responds only to the coherent component of the signal and thus permits the location of the emitting event to be determined. The system should prove useful for the detection and location of low-level wind shear.
(Allan J. Zuckerwar, 3446)

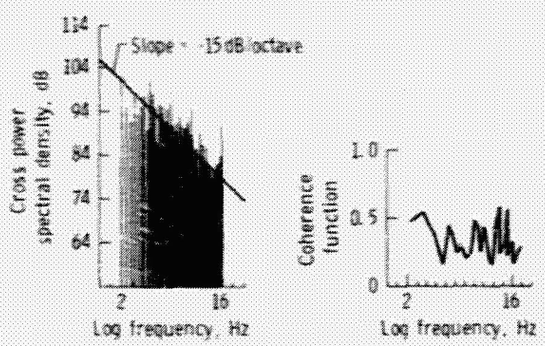

Cross power spectral density and coherence function of infrasonic signal detected at two microphone sites.

Composite Foldable Wheelchair

A cooperative project between Langley and the University of Virginia's Rehabilitation Engineering Center has culminated in 1985 with the production and assembly of two prototype composite foldable wheelchairs. One chair was demonstrated to prospective manufacturers in June 1985 and the other was exhibited to the public at the Paris Air Show and at Health and Human Services Headquarters in Washington, DC.

The composite chair weighs approximately 25 lb and the collapsed width is under 8 in. By contrast, conventional tubular steel wheelchairs weigh at least 50 lbs and are therefore difficult for the elderly or handicapped to manipulate.

The main structural elements of the chair (solid seat, side panels, and foot support) are of skin-stiffened sandwich construction. The core consists of a high-temperature polyimide foam and is covered with a single ply of graphite-epoxy cloth and two plies of Kevlar cloth. The hand rims, used for propelling the chair, are lightweight and are shaped to provide comfort and efficiency, based on ergonomic testing. The padded, vertical panels which form the back can be adjusted with Velcro straps to provide the required comfort and support. Ventilation is permitted between the back panels with this design.

An earlier prototype of the chair has undergone 100,000 cycles on a test carousel at UVA. Further testing, based on ISO and ANSI draft standards, will be accomplished to insure strength and durability.
(Robert M. Baucom, 3043)

On-Line Measurement of Heats of Combustion of Natural Gas Samples

As a technology spin-off of an oxygen monitoring and control system developed for the Langley 8-Foot High Temperature Tunnel, a highly accurate on-line technique has been developed for measuring heats of combustion of natural gas samples. It is based on measurements of the ratio m/n, where m is the flow rate of oxygen required to enrich the carrier air in which the natural gas flowing at the rate n is burned such that the partial pressure of oxygen in the combustion product gases equals that in the carrier air. The ratio m/n is directly related to the heats of combustion of the saturated hydrocarbons present in the natural gas.

Based on a calibration graph relating the m/n values for pure saturated hydrocarbons to their heats of combustion, a measurement of the m/n ratio for the test gas provides a direct means of determining its heat of combustion. The new technique should lend itself readily to on-line measurements at natural gas supply distribution centers where samples from different wells are often mixed to produce a mixture of specified thermal content. The accuracy of the technique is determined solely by the accuracy with which the flow rates m and n can be measured and is on the order of 1 percent.
(Jag J. Singh, 3907)

Hyperthermia Temperature Monitoring Technique

It has been known historically that localized heating of a tumor (greater than 42°C) can be an effective treatment. The performance of chemotherapy is improved and the cancerous cells can be killed. Close temperature monitoring and control of this process, which are essential to prevent damage to the surrounding normal tissue, are extremely difficult. Current methodology involves the insertion of catheters and thermocouples into the tumor and the surrounding area on a repeated basis. The risk of metastasis and infection, as well as the mechanical damage to the tissue of the patient, has limited the usefulness of this treatment. Ultrasonic techniques being developed at Langley offer the potential for a significant improvement in this form of therapy.

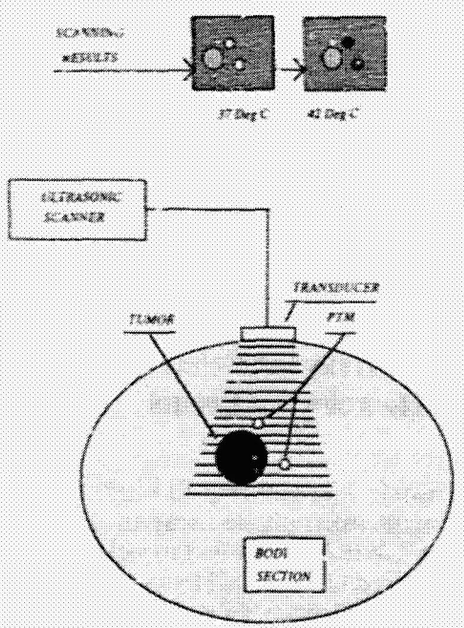

Phase transformation material used to monitor temperature during heat treatment.

The NDE (nondestructive evaluation) Lab at Langley, in concert with the Technology Utilization Office, is transferring a technique wherein small beads of a waxy material (3 to 5 mm in diameter) would be implanted in the immediate vicinity of the tumor. The material used would have a custom-tailored melting point, which would give rise to an ultrasonically measureable alteration in its characteristics. A candidate material has been selected and is being formulated at various melting points in the region of interest. A tissue phantom capable of withstanding in excess of 70°C has been developed. Beads of the phase transformation material (PTM) have been implanted in samples of the tissue phantom and successfully scanned ultrasonically. The technique is being refined prior to clinical tests at Duke University Medical Center. The results of this project will provide the medical community with a considerably enhanced tool for the treatment of cancer.
(Joe Heyman, 3036)

1. Report No.	2. Government Accession No.	3. Recipient's Catalog No.
NASA TM-87623		

4. Title and Subtitle	5. Report Date
Research and Technology 1985 Annual Report of the Langley Research Center	November 1985
	6. Performing Organization Code
7. Author(s)	8. Performing Organization Report No.
	10. Work Unit No.
9. Performing Organization Name and Address NASA Langley Research Center Hampton, VA 23665	11. Contract or Grant No.
	13. Type of Report and Period Covered Technical Memorandum
12. Sponsoring Agency Name and Address National Aeronautics and Space Administration Washington, DC 20546	14. Army Project No.

15. Supplementary Notes

16. Abstract

The role of the Langley Research Center is to engage in the basic and applied research necessary for the advancement of aeronautics and space flight, to generate new and advanced concepts for the accomplishment of related national goals, and to provide research advice, technological support, and assistance to other NASA installations, other government agencies, and industry. This Langley Research Center 1985 Annual Report on Research and Technology contains highlights of our major accomplishments and applications made during the past year. The highlights illustrate both the broad range of the research and technology activities at the Langley Research Center and the contributions of this work toward maintaining United States leadership in aeronautics and space research. For further information about the report contact Jerry C. South, Chief Scientist, Mail Stop 103, Langley Research Center, Hampton, Virginia 23665, (804) 865-3316.

17. Key Words (Suggested by Author(s))	18. Distribution Statement
Research and technology	Unclassified - Unlimited Subject Category 99

19. Security Classif. (of this report)	20. Security Classif. (of this page)	21. No. of Pages	22. Price*
Unclassified	Unclassified	113	A06

*For sale by the National Technical Information Service, Springfield, Virginia 22161

NASA-Langley, 1985